Ground effects and tyre / road contact noise: Influence of the absorption on pass-by noise levels

François-Xavier Bécot, J. Clairet

INRETS/RR/04-531-ENG

François-Xavier BÉCOT, Jean-Michel CLAIRET

Ground effects and tyre / road contact noise

Influence of absorption on pass-by noise levels

Rapport LTE N° 0418
JUNE 2004

François-Xavier BÉCOT, Jean-Michel CLAIRET

Ground effects
And tyre / road contact noise

Influence of the absorption on pass-by noise levels

Report LTE N° 0418
JUNE 2004

The authors :

François-Xavier Bécot
Dr. graduated from INSA-Lyon and from the university of technology of Chalmers (Gothenburg, Sweden).
becot@inrets.fr
Jean-Michel Clairet
is engineer assistant in the physical-acoustic group of the Transport and Environment Laboratory (LTE).
clairet@inrets.fr

This work has been financially supported by the SilVia european project. The study presented here is a contribution from Inrets to the WP 2.
SilVia : Substainable road surfaces for traffic noise control. http://www.trl.co.uk/silvia/
Contract GRD2/2000/30202 (end 2005)

The authors are also grateful to Dr. J-F. Hamet, research director at Inrets-LTE, for the always fruitful exchanges and discussions.

Bibliographic notice

1 Research department (1^{st}author)	2 Project N°	3 INRETS
Transport and Environment Laboratory (LTE)	SILVIA	

4 Title
Ground effects
and tyre / road contact noise

5 Sub-title	6 Language
Influence of the absorption on pass–by noise levels	En
7 Author(s)	**8 Ext. collaboration**
François-Xavier BÉCOT, Jean-Michel CLAIRET	
9 Name, address, financing, co-editor	**10 N° contract, conv.**
European Commission DG TREN - GROWTH	SI2.335701
	11 Date of publication
	June 2004

12 Comments
Technical details on the measurements performed for the present study can be found in "Effet dièdre sur plan réflecteur et sur surface absorbante – Descriptif des mesures", report LTE n°0414 (Fr), by J-M. Clairet and F-X. Bécot.

13 Summary
The present work deals with the influence of the road absorption on the prediction of pass–by noise levels using hybrid methods.
First, the context of the present work is recalled. Objectives and milestones are given.
In a second part, the determination of the acoustic properties of some material is tackled. Two complementary methods are used for this : tube measurements and level difference measurements. Results using the two techniques are compared and discussed.
In a third part, the sound amplification due to the horn effect is characterized experimentally. Situations with a long cylinder and with a single tyre placed over a rigid or an absorbing surface are examined. Measurement results are compared to predictions using two–dimensional models for the tyre radiation. Finally, the horn effect for twin wheels over a rigid surface is measured and discussed.
SILVIA code : SILVIA-INRETS-014-00-WP2-3/9/2004

14 Keywords	15 Distribution
Acoustic, tyre noise, absorption, measures, horn effect, impedance tube, level differences,twin–wheel tyres	**PUBLIC** ISRN: INRETS/RR/04-531-FR

16 Number of pages	17 Price	18 Confidential until	19 Bibliography
136			

Contents

Part I

Background and aims of the study

0.1 Introduction

The work presented here is a part of the SILVIA[1] research program. This work concerns the influence of the acoustical properties of the road surface on the noise radiated by the tyre. The aim of the present study is to improve the relationship between road texture and noise, for road surfaces having substantial absorption properties.

The background of this work is first reminded and the needs for an improved prediction tool are then presented.

0.2 Prediction tools

One early work to stipulate that the road texture and the measured noise levels, e.g. pass–by noise levels, could be related by a simple linear relationship is that presented in [1]. According to this approach, for a given vehicle driving speed, noise spectrum levels L_f are related to the road profile spectrum L_λ according to a relation of the type

$$L_f(dB) \;=\; x \;+\; y \times L_\lambda(dB)$$

the parameters x and y being themselves functions of the frequency f and the roughness wave length λ in consideration. To determine the pair of parameters (x, y), a set of tyre / road combinations as large as possible is required. This type of prediction tools are qualififed as "statistical" because they make use of statistical laws to process the measured data.

Other models, called "hybrid", use both deterministic and statistical representations to build a linear regression. These techniques use a pre–processing of the measured data and establish the statistical laws between texture pre–processed date and noise. In particular, it may be more relevant compared to purely statistical models to relate e.g. the pressure distribution in the contact patch to noise levels than to relate texture to noise levels. By doing so, the non–linear nature of the contact between the tyre belt and the road irregularities is considered.

Obviously, another crucial parameter to include in the data pre–processing is the acoustic properties of the road surface; this latter parameter is known to influence both the generation and the radiation of noise.

0.3 Improvement of the hybrid approach

Results presented in [2] show that purely statistical models are accurate for a large range of standard road surfaces. However, these models fail to predict correct noise levels for road surfaces having a marked texture profile, such as draining or porous surfaces. In these cases, statistical models over–estimate the interaction between the tyre and the road.

To overcome this, the aforementioned study proposes to correct the measured texture profile on the basis of the knowledge of the tyre belt deformation. This technique, called "envelopment", consists in enveloping each measured road profile with a semi–infinite rubber medium having a the tyre belt stiffness. The effect of this correction on the relationship between texture / noise is illustrated in Fig. 1. The resulting texture is somewhat smoother than the measured ones; it corresponds to a horizontal translation in the plane texture / noise.

[1] SILenda VIA – Substainable road surfaces for traffic noise control. http://www.trl.co.uk/silvia/

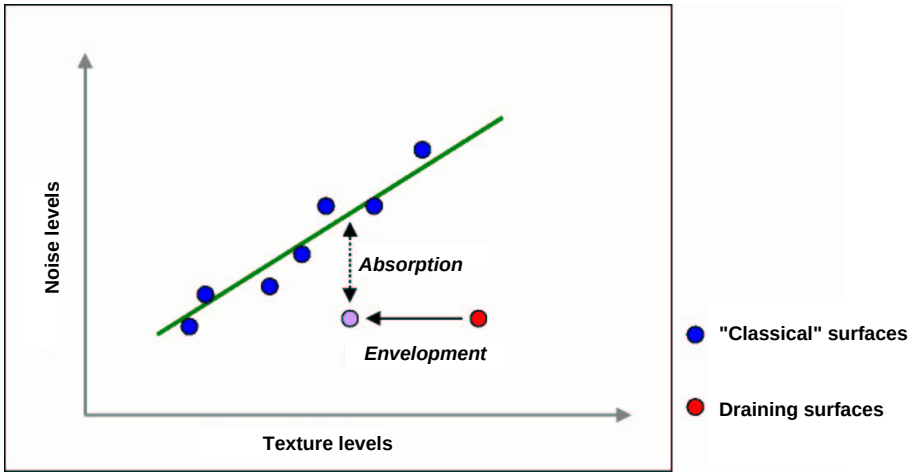

Figure 1: *Illustration of the effect of envelopment technique and expected effect of the absorption correction, for one tyre rolling on different roads (reproduced from reference [2]).*

Nevertheless, as suggested by this figure, the deviation between predicted and measured noise levels may still be substantial after the correction. Information on the absorption properties of the road surface is expected to provide an additional correction term, which would correspond to a vertical translation in the plane texture / noise. The linear regression is then re–calculated according to the new positions of the points in the plane.

At last, the noise levels measured over absorbing road surfaces would be corrected in such a way that they would correspond to noise levels measured over acoustically rigid road surfaces. In this respect, the present work aims at examining the feasibility of the determination of a correction term accounting for the road surface absorption.

0.4 Strategy

As previously mentioned, the correction procedure consists in compensating for the road surface absorption so that measured noise levels would correpond to those measured over acoustically rigid road surfaces. Therefore, a number of modelling tools are needed to predict the influence of the road absorption with respect to the situation where the road is acoustically rigid.

Moreover, the features of these tools must be adapted to the specificities of the measurement procedure. In practical terms, traffic noise assessment is performed using two complementary methods : the SPB[2] technique and the CPX[3] method; their description can be found in [3].

The most common measurement procedure is the *SPB*. According to this procedure, noise levels are measured at specific locations of the road way, at a fixed distance from the lane for a vehicle passing by the microphone. From the modelling point of view, the noise due to a vehicle which passes by the microphone can be reproduced by a using a point source (the discussion on the exact

[2]Statistical Pass–By, ISO 11819-1.
[3]Close–ProXimity, ISO 11819-2

position of this source is far beyond the scope of this work). Given this assumption, a number of methods are available from the literature to include the ground effects depending on the properties of the road surface. If the road surface is homogeneous, ground effects may be introduced by means of a mirror image source, the amplitude of which is multiplied by a reflection coefficient adapted to the geometry considered, *2D* [4] or *3D* [5, 6, 7]. In the case the propagation path occurs over portions of ground having different absorption properties, boundary element–based methods are needed (see for instance the methods proposed in [8] or [9]).

The *CPX* procedure consists in measuring the noise due to the tyre / road contact noise as the vehicle cruises on the examined road. As its name suggests, measurement positions are located very close to the tyre, in a horizontal plane around it. The measurement can be launched at any moment, ensuring a better representativity of the road properties than using the *SPB* method. However, the modelling of the *CPX* situation requires a higher degree of details than for the *SPB* situation. In fact, the complete process of the tyre radiation over an impedance plane must be reproduced in this case; this can be done using works in [10, 11] for *2D* geometries and using [12] for *3D* geometries.

In addition, effects of the road absorption on tyre / road contact noise is suspected to depend greatly on the wheel geometry. Beside different belt stiffnesses, truck tyres have dimensions which are very different from those of light vehicle tyres. Moreover, car tyres are mounted on a single wheel whereas truck tyres are usually mounted on double wheels. Therefore, the influence of these geometrical parameters must be investigated experimentally and numerically using the available prediction tools.

Finally, the experimental determination of the acoustic road properties must consider the specificity of the product which is examined. In particular, it may not be relevant nor accurate to extract a sample of road surface to measure its absorption properties; in–situ methods must be preferred to destructive methods. From a modelling point of view, impedance models must include a sufficient degree of description to correctly predict the acoustic properties of the road surface.

0.5 Work milestones

According to these recommandations, the following six milestones are identified. A time chronology is therefore suggested, but this is suspected to change as work proceeds.

- **Experimental determination of the acoustical properties of the road surface**

  In–situ measurement of the absorption coefficient using impulsion method [13]. In the case specific absorbing material is used, e.g. mineral rock wool, measurement using Kundt's tube (also called plane wave tube) could be performed. Experimental determination of the road impedance from absorption measurement. Experimental determination of the road impedance using the Level Difference Technique [14].

- **Investigation of ground effects on *SPB* measurements**

  Implementation of a prediction tool (use of a mirror image source and adapted reflection coefficient) to quantify the ground effects but also to investigate the sensitivity of the measurement procedure (sensitivity with respect to source position and receiver position, incertainty in road absorption determination, ...).

- **Experimental characterization of horn effect sound amplification over road absorbing surfaces**

Discussion on the validity of the reciprocity principle, which is applied for these measurements. Discussion on the excitation signal to be used (impulsion signal or continuous signal). Discussion on the acquisition process (MLS[4]). Measurements of the horn effect sound amplification, over acoustically rigid surfaces and over sound absorbing surfaces. Measurements for single or double wheels.

- **Numerical investigation of horn effect sound amplification over road absorbing surfaces**

  Discussion on the accuracy of the prediction tools which are available. Sensitivity with respect to geometrical parameters (height of the tyre over the physical reflecting plane of the road, source and receiver positions, ...) and to acoustical parameters (impedance).

- **Numerical investigation of ground effects on predicted tyre / road noise**

  Quantification of the ground effects due to the road surface absorption on the noise due to identified generation mechanisms (mechanical sources, aero–dynamical sources, air–pumping). This implies the coupling of the horn effect prediction tool to a complete tyre / road contact noise prediction tool.

- **Design of an absorption correction procedure**

  According to the results of the previous stages, a correction procedure could be determined. This correction may be different for noise levels obtained from *SPB* or from *CPX* measurements.

[4]Maximum Length Sequence

References for Part I

[1] U. Sandberg G. Descornet. *Road surface influence in tire/road noise – Part I.* In *inter.noise 1980*, Miami, USA, 1980.

[2] P. Klein. *Projet PREDIT "Texture/Bruit" – Etude de la relation bruit / texture sur la base des mesures effectuées dans le cadre de la phase 1.* Technical Report LTE–2033, INRETS, 2000.

[3] J.-F. Hamet J.-M. Clairet P. Klein. *Mesures relatives au bruit de roulement dans les projets 'Texture & Bruit' et SI.R.U.US.* In *Journées d'étude Bruit du trafic routier*, Nantes, France, 2001.

[4] S. N. Chandler-Wilde D. C. Hothersall. *Efficient calculation of the Green function for acoustic propagation above a homogeneous impedance plane.* Journal of Sound and Vibration, 180(5):705–724, 1995.

[5] S.-I. Thomasson. *Reflection of waves from a point source by an impendance boundary.* Journal of the Acoustical Society of America, 59(4):780–785, 1976.

[6] C. F. Chien R W. W. Soroka. *Sound propagation along an impedance plane.* Journal of Sound and Vibration, 43(1):9–20, 1975.

[7] C. F. Chien W. W. Soroka. *A note on the calculation of sound propagation along an impedance surface.* Journal of the Acoustical Society of America, 69(2):340–343, 1980.

[8] D. Habault. *Sound propagation above an inhomogeneous plane: boundary integral equation methods.* Journal of Sound and Vibration, 100(1):55–67, 1985.

[9] F.-X. Bécot. *An efficient application of equivalent sources to noise propagation over inhomogeneous ground.* Acustica - Acta Acustica, 88:853–860, 2002.

[10] P. Klein. *Tyre noise horn effect on an absorbing road surface – Semi–analytical modelling using the multipole synthesis.* In *Forum Acusticum*, Sevilla, Spain, 2002.

[11] F.-X. Bécot W. Kropp. *Modelling of the tyre radiation over absorbing surfaces using the equivalent sources method.* In *Forum Acusticum*, Sevilla, Spain, 2002.

[12] A. Fadavi. *Modélisation numérique des vibrations d'un pneumatique et de la propagation du bruit de contact.* PhD thesis, Ecole Nationale des Ponts et Chaussées, Paris, France, 2002.

[13] F. Anfosso-Lédée. *Les mesures d'absorption acoustique des revêtements de chaussée.* In *Journées d'étude Bruit du trafic routier*, Nantes, France, 2001.

[14] M. Ögren H. Jonasson. *Measurement of the acoustic impedance of the ground.* Technical Report 1998:28, SP, Swedish national testing and research institute, 1998.

Part II

Experimental determination of material acoustic properties

1 – Presentation of the materials

1.1 Introduction

The purpose of this part is to determine the acoustical properties of the material which will be used later in the experiments (see *Section 0.5*).

For this, the following experimental methods are examined :

- 2 microphones impedance tube measurement,
- level difference technique.

Other methods exist but were not used in the present work, such as the Kundt's tube measurement [1], the "extended surface method" [2] or the measurement under grazing incidence [3]. The technique using the two microphones impedance tube is mainly an improvement of the Kundt's tube measurement. These two last techniques are mainly alternatives to the level difference technique and are therefore not used in this work.

These two methods implies two different wave conditions. In the tube, plane waves are propagating and impinge the tested material under normal incidence only. For the level difference technique, a three–dimensional point source is radiating over the tested material surface, towards the microphone ; in this case, the incidence is arbitrary. In addition, the chosen techniques present advantages and inconvenients depending on the type of material which is tested and on the frequency range of interest. For instance, the measure using an impedance tube implies that a sample, the dimensions of which fit to the tube diameter, is available. It is generally difficult to obtain such samples of road surfaces and *in–situ* methods like the level difference technique should be preferred in this case.

Therefore, it was decided to use more common absorbing surfaces. In this respect, two materials were selected to represent situations from little to very absorbent. These materials were also chosen considering their facility of carving in order to be tested in the impedance tube. Within these considerations, were finally selected a fitted carpet (used for instance for corridor or offices carpeting) and panels of mineral rockwool (used for sound and/or thermic insulation). Pictures of these two materials are shown in the following two sections. These materials are then laid on a totally rigid surface so that all the absorption is induced by the material itself. The acoustic materials built in this way can be qualified to be hardbacked absorbing materials.

The acoustic properties of these two materials are determined using the two aforementioned methods in *Chapter 2* and *Chapter 3*. The results are finally gathered and discussed in *Chapter 4*.

Two materials were chosen to have either low or high absorption properties. In addition, their mechanical properties were also taken into consideration to be easy to use and to cut. They are presented in the two following sections.

Figure 1.1: *Fitted carpet of thickness 3.82 mm.*

1.2 Fitted–carpet

The first chosen material is a fitted–carpet, which is typical for carpeting offices or corridors, built for a daily, extensive use. A side picture of this material is shown in Fig. 1.1.

Mechanically speaking, the material is somewhat stiff and the structure is dense and compact. From an acoustical point of view, this carpet is expected to have low absorption properties, particularly at low frequencies, as regards to its small thickness and to its somewhat impervious structure. The carpet is made of very small fibers ; this results in an outer surface which is fairly homogeneous.

The thichness of the carpet is measured to be 3.82 mm. It is provided in one long strip which is 6 meters long and 2 meters wide. There is no major problems in carving this material : cutter, scissors or other standard cutting tools can be used to this effect.

1.3 Mineral rockwool

On the other hand, a mineral rockwool of type Rocksol©2-525 is chosen. It is normally employed for thermic and sound insulation. It was chosen because of its high absorption properties. A side picture of a panel of mineral rockwool is shown in Fig. 1.2.

It is made of compressed fibers and its surface is not as homogeneous as for the carpet. This has for consequence that the acoustic properties measured on small samples may not be representative for the properties of an entire panel of material. Roughly speaking, the acoustical properties of a 10×10 cm^2 are expected to be characteric of the material. On the average, the measured acoustic properties are assumed to be very similar from one panel to another.

The rockwool is provided in panels, the dimensions of which are 1.2 meter long and 0.6 meter wide. The thickness of the panels is measured to be 15.4 mm. Due to the manufacturing process, one of the two faces presents small ripples while the other is rather flat. In the experiments, this latter surface is chosen to be the visible surface of the material.

The carving of the rockwool panels is more problematic than for the fitted–carpet, mainly because of the larger thickness. Particularly for the needs of impedance tube measurements, a fine cutting

Figure 1.2: *Mineral rockwool of thickness 15.4 mm.*

is required. A special tool was built for this, which is shown latter in the text (see Fig. 2.5). When a rough cutting is acceptable, cutters could be used.

From a mechanical point of view, the panels are somewhat stiff. However, they would undoubtedly break if held from one side while the other side is hanging. The manufacturer announces a measured compression of 0.5 mm to 3 mm under a weight of 4 T/m^2 : the surface is rather compact. However, a tyre put on top of it, even with no additional loads, is expected compress the rockwool surface significantly because of the small area of contact. Therefore, heavy objects will preferably be suspended over the rockwool panels to avoid any modifications of the acoustic properties of the material due to compression.

2 – Impedance tube measurement

The principle of the impedance tube measurement is described in [4]. It is briefly reminded in the first section. Limitations, care and possible errors associated with this type of measurement are reviewed in the second section. The equipment used and the results of the measurements are presented in the third, fourth and fifth sections. Finally, the determination of construction parameters, like the flow resistivity, is presented in the last section of this chapter.

2.1 Principle

What motivated the development of this technique was to find an alternate and quicker method than using the Kundt's tube technique to dertermine the acoustical properties of impedance materials. Therefore, the configuration for the two–microphone impedance tube is very similar to the Kunudt's tube.

A stationary wave pattern is driven by a loudspeaker placed at one termination of a closed tube (see Fig. 2.1). At the other end of the tube, a sample of the tested material is placed. The sound field in the tube can easily be calculated by considering the multiple reflection at both ends of the tube. R denotes the reflection coefficient of the tested material and R_l denotes the reflection coefficient at the loudspeaker end. A time dependency in $\mathrm{e}^{+\mathrm{j}\omega t}$ is assumed throughout this work[1]. Hence, the total sound field at a point x of the tube is written

$$\begin{aligned} p(x) \quad = \quad & P_0 \Big[\, \mathrm{e}^{-\mathrm{j}kx} + R\mathrm{e}^{-\mathrm{j}k(2L-x)} \\ & + RR_l \, \mathrm{e}^{-\mathrm{j}k(2L+x)} + R^2 R_l \, \mathrm{e}^{-\mathrm{j}k(4L-x)} \\ & + R^2 R_l^2 \, \mathrm{e}^{-\mathrm{j}k(4L+x)} + R^3 R_l^2 \, \mathrm{e}^{-\mathrm{j}k(6L-x)} + \ldots \Big] \end{aligned}$$

In this equation, L is the length of the tube, that is, the distance between the acoustical centre of the loudspeaker, which provides a pressure P_0, and the reflecting surface of the tested material. Note that the origin of the positions is taken at the loudspeaker. By rearranging the terms, the previous equation can be written

$$p(x) = P_0 \left[\mathrm{e}^{-\mathrm{j}kx} + R\mathrm{e}^{-\mathrm{j}k(2L-x)} \right] \, \left[1 + RR_l \, \mathrm{e}^{-\mathrm{j}k2L} + (RR_l)^2 \, \mathrm{e}^{-\mathrm{j}k4L} + \ldots \right]$$

The second term is a geometrical series, the result of which is well known. Therefore, the total pressure field at the point x is

$$p(x) = P_0 \left[\mathrm{e}^{-\mathrm{j}kx} \; + \; R\mathrm{e}^{-\mathrm{j}k(2L-x)} \right] \frac{1 \; - (RR_l)^N \, \mathrm{e}^{-\mathrm{j}k2LN}}{1 \; - \; RR_l \, \mathrm{e}^{-\mathrm{j}k2L}}$$

[1] An opposite time dependency is used in the ISO standard and in the software provided with the impedance tube, thus giving opposite signs in the propagation functions.

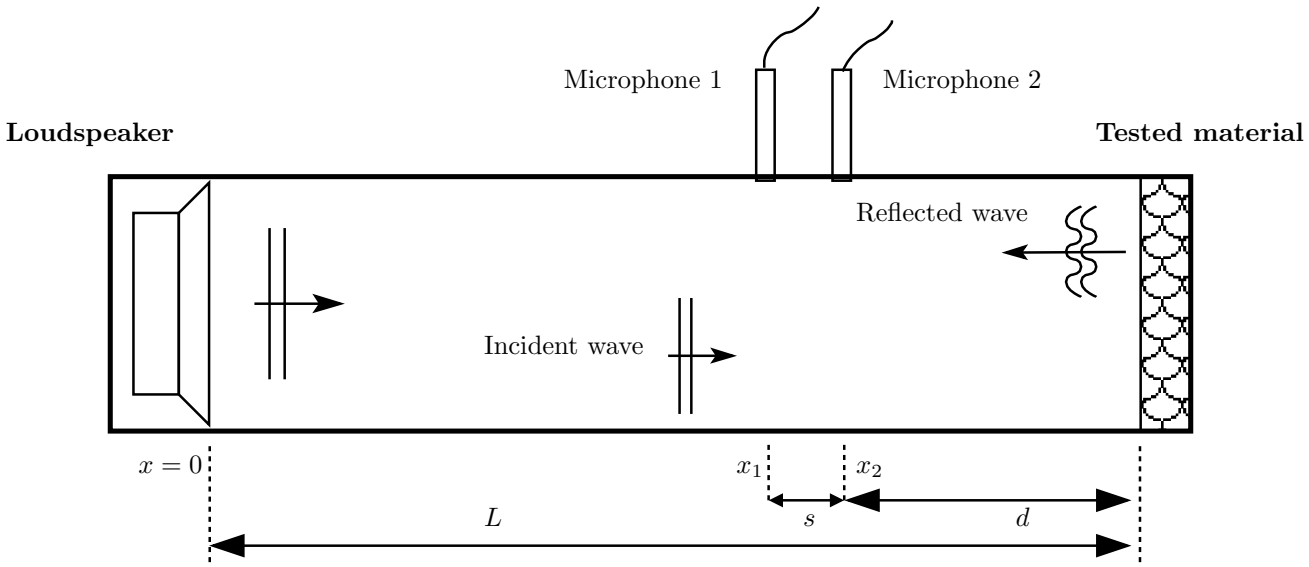

Figure 2.1: *Schematic setup of a two–microphones impedance tube measurement.*

where N is the number of reflections in the tube, including the reflections at the loudspeaker end. This can also be written as

$$p(x) = P_T \left[\mathrm{e}^{-\mathrm{j}kx} \; + \; R\mathrm{e}^{-\mathrm{j}k(2L-x)} \right] \tag{2.1}$$

where the term P_T is a constant regarding the measurement position x. By introducing the transfer function between the two microphones $H_{12} = p(x_2)/p(x_1)$, Eq. 2.1 can be written

$$H_{21} = \frac{\mathrm{e}^{-\mathrm{j}kx_2} \; + \; R\mathrm{e}^{-\mathrm{j}k(2L-x_2)}}{\mathrm{e}^{-\mathrm{j}kx_1} \; + \; R\mathrm{e}^{-\mathrm{j}k(2L-x_1)}} \tag{2.2}$$

Let s, respectively d, denote the distance between the two microphones, respectively the shortest distance between microphones and the material sample (see Fig. 2.1). We have thus

$$x_1 = L - (d + s) \quad \text{and} \quad x_2 = L - d$$

After some manipulations, the reflection coefficient of the tested sample can be written as

$$R \; = \; \mathrm{e}^{2\mathrm{j}k(d+s)} \; \frac{\mathrm{e}^{-\mathrm{j}ks} - H_{12}}{H_{12} - \mathrm{e}^{+\mathrm{j}ks}} \tag{2.3}$$

In the ISO standard [4] and in other works, so–called incident, respectively reflected, transfer functions are introduced by using $H_i = \mathrm{e}^{-\mathrm{j}ks}$, respectively $H_r = \mathrm{e}^{+\mathrm{j}ks}$. This notation, as it might add confusion, will not be used in the following.

The normal impedance of the material can be calculated from the following equation

$$Z \; = \; \rho_0 c_0 \; \frac{1+R}{1-R} \tag{2.4}$$

where ρ_0 and c_0 are the density and the speed of sound in the propagation medium inside the tube (throughout this work, it is air). The absorption coefficient can be determined by

$$\alpha \; = \; 1 - \; \mid R \mid^2 \tag{2.5}$$

or more explicitely

$$\alpha \;=\; 1 \;-\; \left| \frac{\mathrm{e}^{-\mathrm{j}ks} - H_{12}}{H_{12} - \mathrm{e}^{+\mathrm{j}ks}} \right|^2 \tag{2.6}$$

In conclusion, once the transfer function between the two microphones is measured, the determination of the acoustic properties is straightforward. Of course, a number of limitations entail the accuracy of the measure ; they are presented in the next paragraph.

2.2 Robustness of the technique

Besides the errors in the distance measurement, limitations and errors inherent to the method are reviewed below. Note that some of the topics below are not treated in the ISO standard in spite of their practical aspects. When needed, some of the topics below are illustrated with preliminary measurements.

2.2.1 Mean flow

The previous derivation understood that there is no mean flow in the tube. This is generally true since the impedance tube is closed at one end by the loudspeaker and at the other end by the material sample.

2.2.2 Attenuation and losses in the tube

The second assumption in the previous derivation is that there is no attenuation during the sound propagation, except that due to the absorption from the tested material. Parasite attenuation could be due to sound leakages at the tube terminations, but this is not expected to be relevant unless heavy defaults in the tube manufacturing are found out. In contrast, losses at the tube walls due to viscousity and thermoconductivity may affect significantly the measurements.

The ISO standard [4] recommends that this mechanism of energy dissipation is accounted for, by writing

$$k \;=\; k_0 - \mathrm{j}k_{loss} \quad \text{with} \quad k_{loss} \;=\; 0.0194\, \frac{\sqrt{f}}{c_0 D} \tag{2.7}$$

where D is the tube diameter[2]. This formula has been first developped by Lord Rayleigh and then modified by Beranek. It predicts a larger attenuation with tubes of smaller diameters. Fig. 2.2 shows the calculated attenuation in the large and small tube setups used in the present work. Note that the values shown here do not overlap because of the different diameters for different tube setups. This predicts very low values of the attenuation for both the large tube and the small tube setup.

However, these values are ideally discussed in terms of the influence of the attenuation on the accuracy of the measurements. The calculation was proposed in [6]. The error estimate for the

[2]If the tube section is square, the equivalent diameter equals four times the cross section area divided by the tube perimeter as precised in [5]

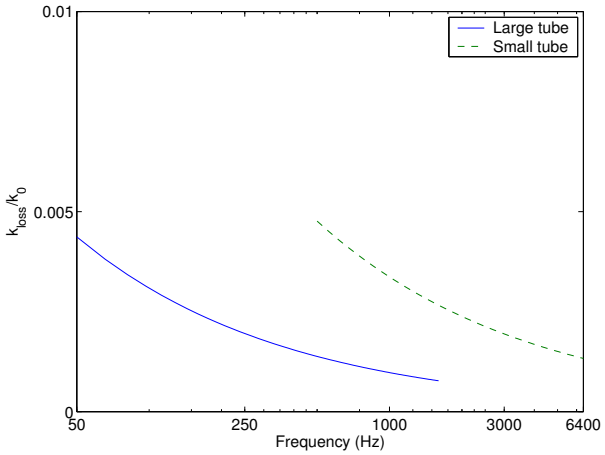

Figure 2.2: *Attenuation in the large and the small tubes (see Eq. 2.7).*

calculation of the absorption coefficient is straightforward :

$$\frac{d\alpha}{\alpha} = \frac{-2|R|\ d|R|}{1-|R|^2}$$

where $d|R|$ is expressed as $e^{2k_{loss}(d+s)}$ (see Eq. 2.3). By varying the value of the module of R, one obtains a good picture of the effect of the attenuation on the determination of the absorption coefficient. The estimations of the error in percentage are in shown in Fig. 2.3(a) for the large tube and in Fig. 2.3(b) for the small tube. The error values are shown for the frequency range of validity of the corresponding tube setup.

It is observed that, for both setups, the error is less than 10 % on the most range of R values. It decreases with increasing absorption value. As a matter of fact, when the tested sample has high absorption properties, the error induced by the effect of viscosity is very little. To the contrary, when the material is close to acoustically rigid, the error is very high and tends to infinity in theory.

An important fact is that the Pulse© software neglects this parameter, probably because the tube walls have been treated especially to minimize the effects of viscosity. Facing the lack of informations concerning this parameter, this question is left for further investigations.

2.2.3 Position of the microphones

The choice of the microphone positions inside the tube is subject to a number of limitations, which are inherent to the sound propagation in tube.

First, it is important that the microphone is not placed in the near field of the loudspeaker. The ISO standard recommends that the microphones are placed at a distance larger than 3 tube diameters, and in any case, at distance larger than one tube diameter.

Secondly, the tube diameter and the distance between the microphones are also connected. From Eq. 2.3, we note that e^{-jks} and e^{+jks} should not equal 1 or -1. If this happens, the reflection coefficient takes on a constant value, whatever the material of the tested sample.

$$R = e^{2jk(d+s)}\ \frac{\pm 1 - H_{12}}{H_{12} - \pm 1} = -e^{2jk(d+s)}$$

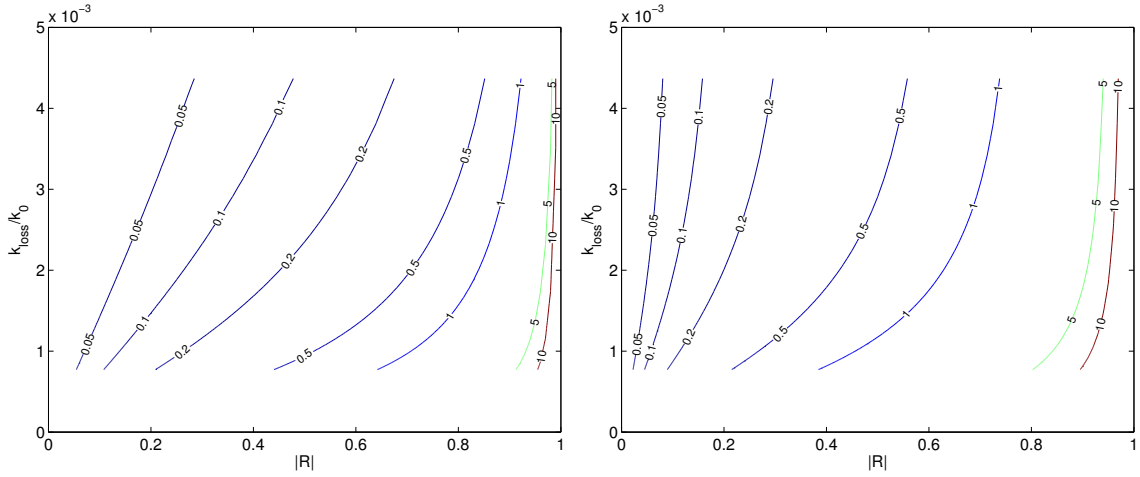

(a) Large tube setup

(b) Small tube setup

Figure 2.3: *Error estimate due to viscosity on the measurement of absorption coefficient : values as a function of R in percentage.*

To overcome this, we should choose the position between the microphones such that

$$ks \neq n\pi \quad \text{with} \quad n = 1, 2, \ldots$$

On the other hand, when the distance between microphones is fixed, e.g. for practical reasons, measurements will be corrupted at frequencies

$$f_n = \frac{c_0}{2s} n \quad \text{with} \quad n = 1, 2, \ldots$$

Moreover, the frequency range of usage of the tube is limited at high frequencies by the cut–off frequency inherent to the propagation of plane waves inside the tube. Above this frequency, the propagating waves are no longer plane. According to [7], for circular tubes, the first cut–off frequency is found at

$$f_{c.o.} = \frac{\alpha_{10} c_0}{D} \quad \text{with} \quad \alpha_{10} = 0.5861$$

where D is tube diameter. α_{mn} are such that $J'_m(\pi\alpha_{mn}) = 0$, where J'_m is the derivative of the Bessel function of order m. This value determines the upper frequency limit at which plane waves can be formed inside the tube. Therefore, it is also the limit of validity for the measurements.

A smart solution to get the largest frequency range of validity possible consists in setting the forbidden frequencies f_{limit} beyond the first cut–off frequency. This gives a condition on the distance s between the microphones, which can be written as

$$f_{c.o.} < f_1 \quad \text{which gives} \quad s < \frac{D}{2\alpha_{10}} \quad \text{for } n = 1. \tag{2.8}$$

The resulting values of s for the tube setups are given in *Section 2.3*.

2.2.4 Microphone mismatch

For the measure of the pressure field at two different points, the tube used in the present experiments is built in such a way that two microphones can be mounted flush with the tube walls. The pressures at the two positions are recorded simultaneously using two different channels. Thus, the determination of the acoustic properties only needs one measure. This has for consequence that the measurement will be subject to a possible mismatch between the two measurement channels.

To overcome this, a correction factor is calculated by performing one measure with a given material sample, which is not necessarily the one the user wants to test. In this case, the measured transfer functions are denoted with a star $(*)$. If H_1^* is the transfer function measured with the microphones in position say 1 (see Fig. 2.1), let H_2^* be the transfer function measured when the microphones exchange positions. By doing so, a correction factor is calculated according to

$$H_c \;=\; \sqrt{H_1^*\; H_2^*} \;=\mid H_c \mid\; \mathrm{e}^{\mathrm{j}\varphi_c} \tag{2.9}$$

The corrected transfer function $\tilde{H}_{12}$ is then obtained by

$$\tilde{H}_{12} \;=\; \frac{H_{12}}{H_c}$$

It should be underlined that the correction influences both the magnitude and the phase. In fact, it is the corrected transfer function $\tilde{H}_{12}$ which is used in Eq. 2.3, Eq. 2.4 and Eq. 2.5.

Moreover, the correction measurement should be done in the presence of a rather absorbing material. By doing so, strong reflections in the tube are avoided and the possibility that a node of pressure coincides with one of the microphones' position is reduced.

Another way to overcome a possible mismatch between the microphones is to use the same microphone and to move it to the different measurement positions. Hence, no correction is needed anymore. However, this procedure takes longer time than using two microphones, a parameter which may be of importance when a series of material are to be tested.

2.2.5 Calculation of H_{12}

The transfer function is ratio between the two complex pressures measured at position 1 and 2. From linear theory [8] and as described in [4], H_{12} may be determined by using one of the following relations :

$$\text{a) } H_{12} = \frac{S_{12}}{S_{11}} \quad \text{or} \quad \text{b) } H_{12} = \frac{S_{22}}{S_{21}} \quad \text{or} \quad \text{c) } H_{12} = \left[\frac{S_{12}}{S_{11}}\frac{S_{22}}{S_{21}}\right]^{1/2} \tag{2.10}$$

where S_{12}, respectively S_{21}, is the cross–spectral density between $p(x_1)$ and $p(x_2)$, respectively between $p(x_2)$ and $p(x_1)$. S_{11}, respectively S_{22}, is the auto–spectral density of $p(x_1)$, respectively $p(x_2)$. These quantities are defined as

$$\begin{aligned} S_{11} &= \frac{1}{T}p(x_1)\tilde{p}(x_1) \quad \text{and} \quad S_{22} = \frac{1}{T}p(x_2)\tilde{p}(x_2) \\ S_{12} &= \frac{1}{T}p(x_1)\tilde{p}(x_2) \quad \text{and} \quad S_{21} = \frac{1}{T}p(x_2)\tilde{p}(x_1) \end{aligned}$$

where $\tilde{p}$ is the complex conjugate value of p and T is the length of the recorded signals (it is supposed here that the same sampling frequency is the same for the measurement using microphone 1 and for that using microphone 2).

According to [4], Eq. 2.10c) will preferably be used in cases of unwanted noise both at the input and the output of the measurement chain, Eq. 2.10b) in cases of noise only at the input. Finally, Eq. 2.10a) will be used in cases of noise at the output, situation most encountered in practice.

2.2.6 Fitting of the material sample

The measurement technique is clearly independent on the shape of the tube. Mainly rectangular or circular cross sections are used for impedance tubes.

As a rule of thumb, the material sample should best fill the tube cross section. The question arises then on how tight the fitting of the sample should be. This is a practical matter of importance because carving tools adapted for a straight–line carving are numerous, but more seldom are the ones adapted for circular carving. The ISO standard [4] does not mention this problem. It is expected however that a default, the size of which is small compared to the wavelength, should not affect strongly the measurement. This may also depends on the shape and the position of the default.

To the contrary, the sample may be merely too large for the tube so that, by pressing gently on it, the user manages to fit the sample in the tube. This situation is however not recommended. Both measurements and finite–element predictions presented in [9] show that fibrous materials placed in an impedance tube exhibit shearing modes if they are constrained at their edges. These modes are associated to minima of transmission losses, which correspond to minima in absorption values. This may be overcome in practice by adjusting the sample in order to make it slightly loose in the tube.

2.3 Measurement equipment

The experimental setup used in the present work is based on a commercially available impedance tube of circular cross section shown in Fig. 2.4. This impedance tube is ideally used with an FFT analyser from the same manufacturer. The properties of this equipment are presented below.

2.3.1 Tube configuration

The experimental setup used is presented in Fig. 2.4. It consists in two tubes, one housing the loudspeaker and the microphones (on the right hand side of these pictures) and the other one where the sample is placed called the sample holder (on the left hand side of the pictures). As seen previously, the tube diameter determines the highest frequency of validity of the measurements. Therefore, two sample holders with different diameters are available, one for the low frequency range and another one for the high frequency range. The characteristics of each tube are summarized in the table below, as well as the limiting values given by theory.

One can note that all parameters respect the theoretical recommandations, except for the position of the closest microphone of the large tube setup. Moreover, this criteria is the same for the large tube and for the small tube, because the sound is always generated in the same tube extension of 0.1 m diameter. This can be seen in Fig. 2.4.

2.3.2 Carving tool

A special carving tool was needed to obtain samples of material to the shape and size of the tube. For this, two templates made of brass were used, the dimensions of which correspond to the two tube diameters. These templates were attached to the two jaws of a vice held vertically. The

Parameter value	Large tube	Small tube
Diameter	0.1 m	0.029 m
Distance loudspeaker / sample surface	0.3 m	0.425 m
x_1 (measured value)	0.2 m	0.39 m
Validity range	*> 0.3 m*	*> 0.3 m*
s	5 cm	2 cm
Validity range	*< 8.53 cm*	*< 2.47 cm*
d	0.1 m	0.035 m
f_{min}	50 Hz	500 Hz
f_{max}	1600 Hz	6400 Hz
Cut–off frequency ($f_{c.o.}$)	*1992 Hz*	*6871 Hz*

Table 2.1: *Geometrical characteristics for the large and small tube (see Fig. 2.4).*

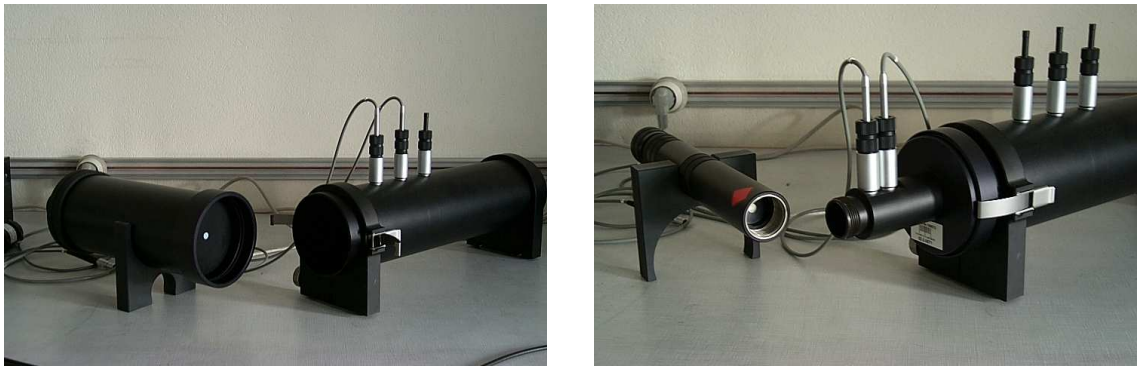

(a) Large tube setup (b) Small tube setup

Figure 2.4: *Two–microphones impedance tube Brüel & Kjær Type 4206.*

apparatus is shown in Fig. 2.5 for a template having 10 cm diameter. A similar setup is used with an aluminium template of 0.29 cm diameter. This apparatus allows to cut out material samples of thickness up to around 5 cm. After this first cut, the sample was adjusted so that it slipped softly into the tube ensuring that the tube walls exert neglectable constraints on the sample edges.

The sample is put against the sample holder so that the outer surface of the material comes into the recommended position inside the tube. For this, a piston can be moved inside this part of the tube to fit to the thickness of the material. Note that this allows to have an additional air layer behind the sample to reproduce the situation of hanging ceilings.

2.3.3 FFT analyser

Sound pressures are measured using two identical microphones, which were mounted flush with the tube walls. For this, sites are built in the tube, which has for consequence that the microphones can occupy only a limited number of pre–determined positions. The reader will note that these

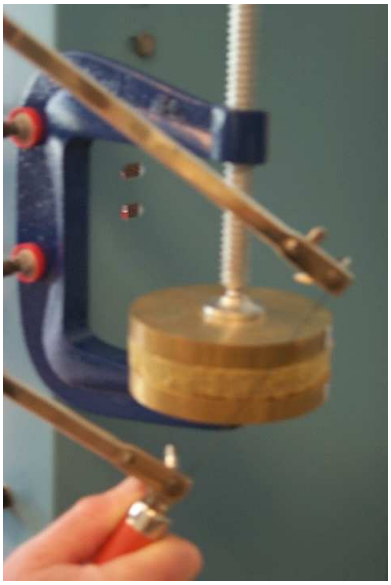

Figure 2.5: *Carving system for large tool samples. The wire–saw used for this is seen at the foreground.*

positions are different for the large and the small tube setup.

The results are analysed and stored using the Pulse© FFT analyser also from Brüel & Kjær. Besides standard features of an analyser, it has a series of scripts specially dedicated to the measurement using the impedance tube Type 4206. The correction transfer function is directly available and the main acoustic properties of the sample are computed (reflection coefficient, absorption and acoustical impedance). In particular, the calculation of these quantities depends on the position of the microphones, the position of the sample in the tube, etc. Therefore, the scripts used to calculate these quantities should contain the correct values of these parameters according to the tube configuration.

A final remark concerns some special requirements from the software. The manufacturer recommends that at least 110 dB are measured at the microphones. This ensures that exterior noise could be omitted. In addition, the difference of sound levels between the two microphones should be at most 40 dB. In the experiments presented here, it was found difficult to respect this criteria and to maintain a level of at least 110 dB. Instead, if the first criteria is respected in priority, level differences from 45 dB to 60 dB at most were obtained depending on the type of material. Note that moving away the sample from the loudspeaker end did not help decreasing the observed level difference. Moreover, when the level difference criteria was respected, no significant differences in the acoustic properties were observed compared to when this criteria was violated. Moreover, the acoustic properties of the *B&K* material samples measured when this criteria was violated correspond very well with those given as templates. Therefore, according to these experiments, this criteria was not considered as crucial ; instead a sufficient high sound pressure level should be maintained in the tube.

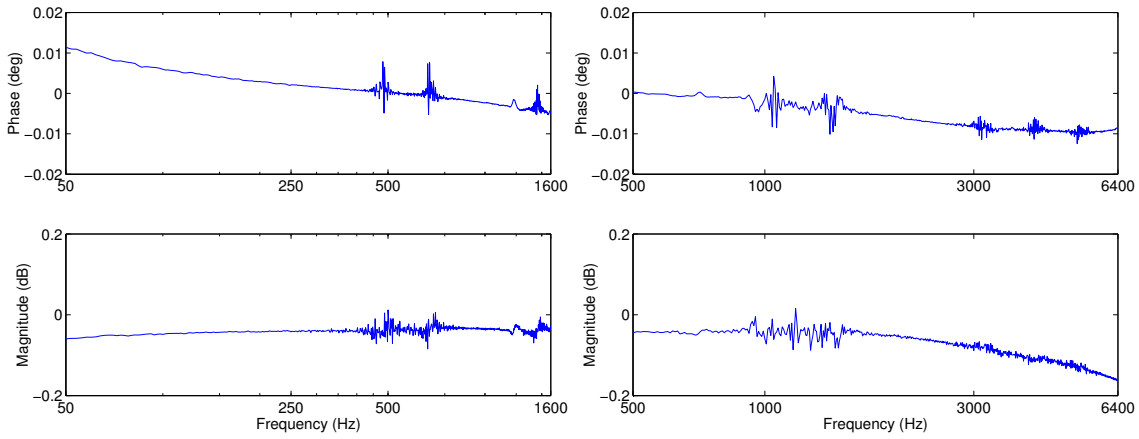

(a) Large tube

(b) Small tube

Figure 2.6: *Phase and magnitude of H_c. Material sample provided by B&K.*

2.4 Preliminary measurements

According to the limitations and pitfalls mentioned above, a series of preliminary measurements have been made using various material samples to check the accuracy of the measurement setup.

2.4.1 Correction transfer function

The purpose of this measurement is to compensate for an eventual microphone mismatch, acting both on the phase and on the magnitude. The procedure used is described in *Section 2.2*. In order to validate the correction measurement, the impedance tube manufacturer recommends that the phase variations of H_c should be comprised between -2° and +2°. For the magnitude of H_c, the maximum authorized variations should lie within 2 dB.

The material sample used for this should be rather absorbing. For this, the manufacturer provides two material samples for the large tube and the small tube. Note however that a correction transfer function may be obtained with any material sample which respects the recommended maximum variations. Results for the samples provided by the manufacturer are shown in Fig. 2.6(a) for the large tube and Fig. 2.6(b) for the small tube. The criteria are respected since the maximum variations obtained, whithin 0.02° for the phase and around 0.2 dB for the magnitude, are well below the maximum threshold. This means that the measured transfer functions can be used for correcting the microphone mismatch. If the criteria are not respected, another material should be sought. The effect of the correction is discussed on the next paragraph.

2.4.2 Typical absorption measurements

Once the correction obtained, it is proposed to perform a standard measurement on the provided material samples, the absorption of which is provided by the manufacturer. Hence, the effect of the correction for the microphone mismatch can be investigated. The absorption coefficients obtained

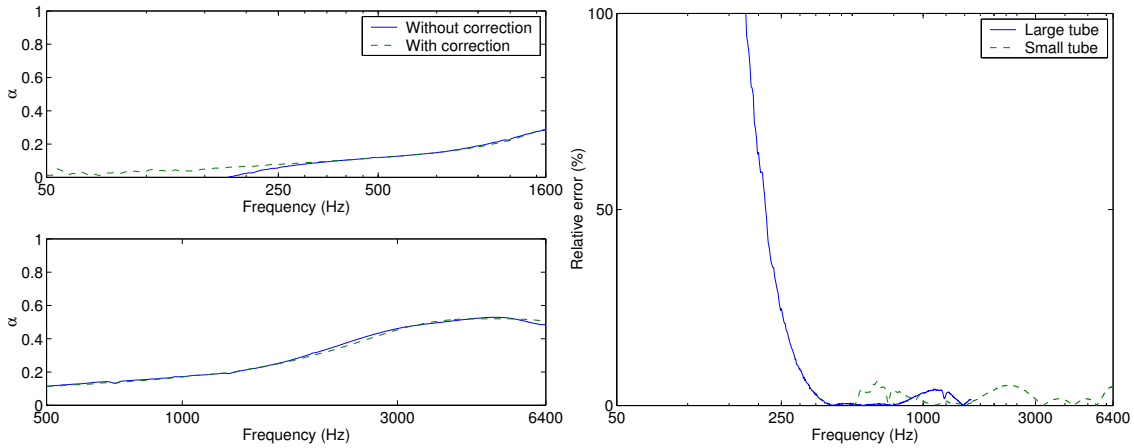

(a) Measured absorption coefficient. Top : large tube – Bottom : small tube

(b) Error on the absorption coefficient

Figure 2.7: *Effect of the mismatch correction on the absorption coefficient. Material sample provided by B&K.*

with or without correction are shown in Fig. 2.7(a). For the large tube setup, significant deviations are observed between the values calculated with or without correction below 250 Hz. The error, as shown in Fig. 2.7(b), largely exceeds 100 % due to the very low absorption values of the sample at the frequencies (see §*2.2.2*). At higher frequencies, the error becomes very low, which means that calculated values correspond well with and without the correction. For measurements using the small tube setup, the absorption values correspond well in both cases. The relative error does not exceed 15% in this case, which is however still significant.

Finally, it is recommended that the correction procedure is always applied to avoid large errors in the frequency range where the tested material has low absorption properties.

Moreover, it is interesting to compare the results obtained using the different tube setups. Fig. 2.8 shows values of the absorption coefficient which were obtained after correction for the microphone mismatch. The absorption values correspond well on the frequency ranges of validity common for the two setups, i.e. from 500 Hz to 1600 Hz. For information, results using the small tube setup have been plotted for frequencies as low as 50 Hz, at frequencies at which the measure should not be trusted. Though, the values obtained with the small tube are in fair agreement with those obtained using the large tube down to around 100 Hz. Therefore, a fairly good overlapp may be expected between measurements obtained using the two different setups. Finally, these results correspond well with the values provided by the tube manufacturer.

2.4.3 Sample carving quality

In *Section 2.2*, the tool for carving circular samples has been presented. As the size of the sample is suspected to bias the measurement, two "default" situations are examined and compared to a "ideal" situation : first, the sample size is too small and secondly, the sample size is too large.

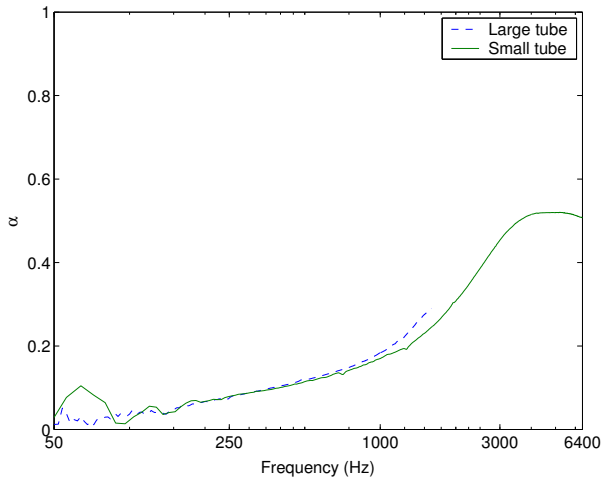

Figure 2.8: *Measured absorption coefficient for the material sample provided by B&K. Compared results obtained with the large and the small tube setup – Mismatch correction included.*

Fig. 2.9(a) shows two samples which are to be used in the large tube setup. One fits well to the tube geometry (right hand side sample) and the other one (left hand side) presents a coarse carving default. The reader should note that the two different samples are shown to compare the size of the default. From a practical point of view, measurements were performed on the same sample before and after the default was made to avoid any additional sources of deviations.

The length of the default edge is around 4.5 cm ; it may be considered as the largest relevant default dimension, thus giving an estimate of the lowest sensitive frequency. The frequency having a one–quarter wavelength in the order of the edge length is above 1800 Hz, thus out of the range of validity of the measurement. This may seems inappropriate for our purpose. However, defaults of larger dimensions are even less realistic.

The obtained absorption values for both samples are shown in Fig. 2.9(b). It is observed that these values correspond well with each other on a large frequency range. It should be emphasised that the correspondance is achieved even at frequencies where the absorption is high. At frequencies above around 1000 Hz, small deviations are observed. As the the default characteristic wavelength does not fall in this frequency region, it may be hazardous to conclude on the influence of the default.

The picture changes if the sample size is merely too large for the tube section (see §*2.2.6*). The dimensions of the corrupted sample are such that it enters the tube with a gentle compression on its edges. As a matter of fact, the distinction between this sample and a sample without any constraints cannot be made visually.

To test the sensitivity of measurements to this parameter, the following procedure has been adopted. The material samples are cut using the carving tool shown in Fig. 2.5. Measurements are performed once on this sample. Then, the sample size is adjusted by proceeding as follows. The sample is placed in the tube and the piston which hardbacks the sample is removed in order to get the tube open at both ends. When looking at a source of light through the tube, it is possible to localise the discrepancies in the carving. The region of defaults are then trimmed little by little until rays of light pass all around the sample circumference. At the end, the adjusted sample moves slightly inside the tube under its own weight.

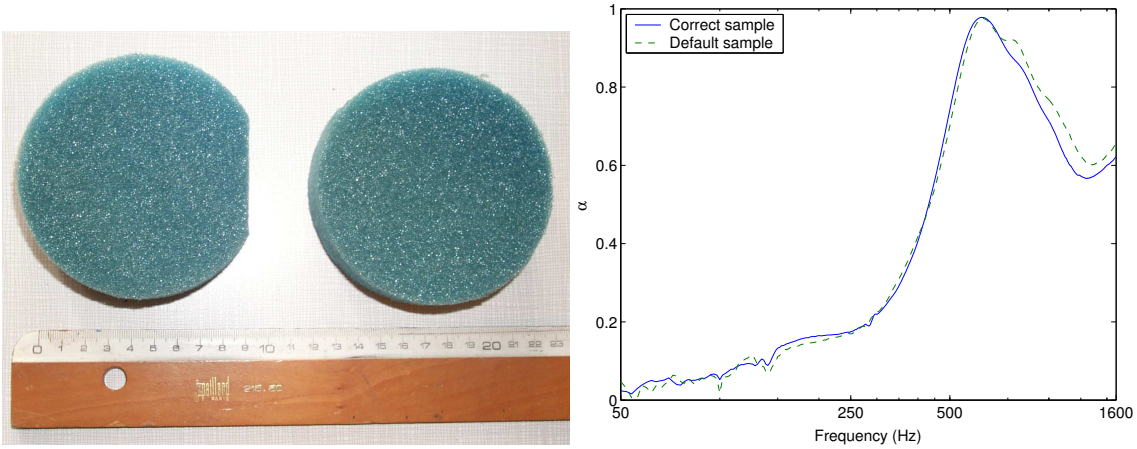

(a) Samples used for the test : default sample (left) and well–fitted sample (right)

(b) Absorption coefficient

Figure 2.9: *Effect of a default in the carving of the sample. Material : expansed foam used for packing protection.*

Absorption values obtained using the small tube setup are compared when the sample is first cut out and after the same sample has been adjusted to the tube size. Results are shown for a non–fibrous Fig. 2.10(a) and a fibrous material Fig. 2.10(b). For the two types of materials, significant deviations are observed. For the expansed foam, the "step" observed around 1500 Hz for the first–cut material sample is shifted towards lower frequency and becomes very little marked when the sample size is adjusted. For the mineral wool, the sharp dip around 1300 Hz is also shifted downwards ; its amplitude also decreases substantially. Measurements, not shown here, performed on the mineral wool with the large tube setup (low frequency range) show the same tendency.

These results thus confirm and extend those presented in [9] for fibrous materials. It appears that the range of materials, which can be excited in shearing in an impedance tube, is broad enough to pay a special attention to the carving quality of the samples. For this, the carving tool presented in previous section needs to be improved to account for this requirement. However, due to the lack of time, this tool was kept througout the experiments and a special care was taken to adjust the sample size to the tube according to the procedure described above.

2.4.4 Sample size versus material acoustic properties

As mentioned in *Chapter 1*, the measured properties of mineral rockwool may vary substantially from one sample to another. This is clearly illustrated in Fig. 2.11, which shows the absorption coefficients measured using the large tube setup and the small tube setup. Note that the different samples were all cut out of the same rockwool panel.

The values obtained using the large tube setup are fairly coherent. Very small deviations are observed between 250 Hz and 500 Hz, which may be due to carving defaults in one of the samples. On the rest of the frequency range observed here, the correspondance between the measured values is good.

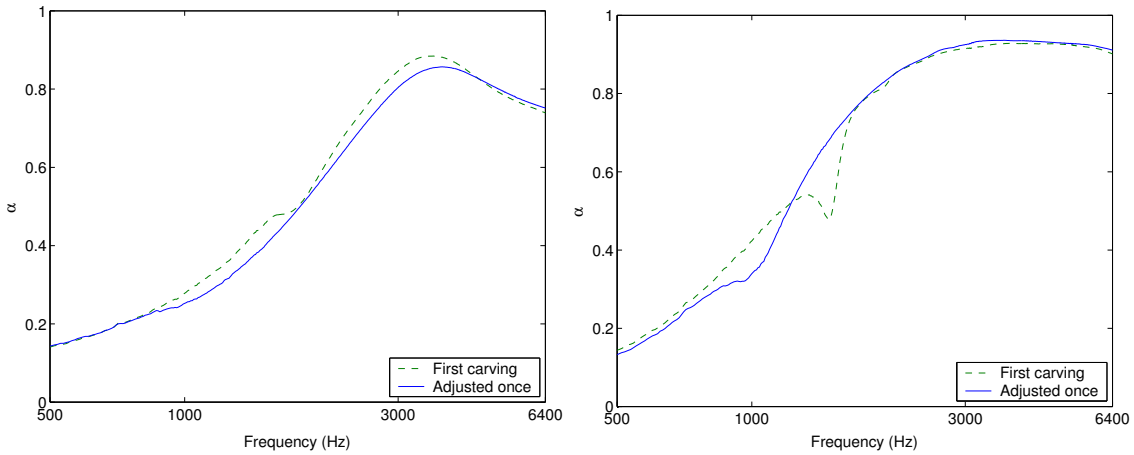

(a) Non–fibrous material : expansed foam used for packing protection (different sample from that of Fig. 2.9). Thickness = 20.8 mm

(b) Fibrous material : mineral rockwool shown in Fig. 1.2

Figure 2.10: *Effect of the tube edge constraints on the absorption on fibrous and non–fibrous materials. Small tube measurements.*

The picture changes drastically when measuring the absorption of two different samples using the small tube setup. As expected, the properties of the rockwool vary significantly from one sample to another. Besides the fact that both absorption coefficients show a dip, which is certainly due to edge constraints, the frequency range where the two measurements correspond well is rather narrow, approximately between 1500 Hz and 2000 Hz. This gives an error around 15 % below 1500 Hz and around 5 % beyond 2000 Hz, which is quite substantial.

Therefore, ideally, the acoustic properties this type of material will be measured on several samples if the small tube setup is used. Then, the measurement giving the best overlap with the large tube measurements will be kept to predict the material properties at higher frequencies. With a view to modelisation, the predictions, using for instance a given impedance model, will preferably fit to the measurements using the large tube setup. The acoustic properties can be predicted then at any frequencies.

2.5 Measurements results

The section presents the acoustical properties of the materials chosen in this work, measured using the impedance tube previously described. The materials are described in *Chapter 1.*

The acoustic quantities of interest are : the reflection coefficient, which is the first quantity available from measurements, the absorption coefficient, which gives a measure the absorption power of the material, and the normalised acoustical impedance, which is the input to most sound propagation models.

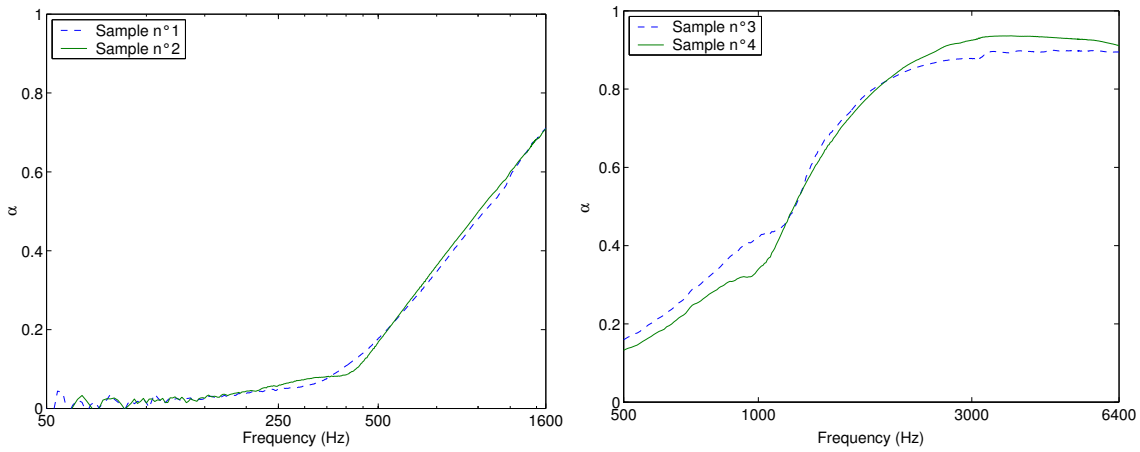

(a) Large tube setup

(b) Small tube setup

Figure 2.11: *Coherence of the measured acoustical properties with respect to the sample size – Absorption coefficient of the mineral rockwool Fig. 1.2.*

The results obtained using the large tube setup and the small tube setup are shown in the same figure and in the frequency range of validity of each measurement setup, i.e. from 50 Hz to 1600 Hz and from 500 Hz to 6400 Hz respectively.

2.5.1 Fitted–carpet

The acoustic properties of the fitted–carpet are shown in Fig. 2.12.

First of all, the overlap is reasonable for all measured and deduced acoustical quantities ; this tends to show that the measurements are reliable.

The reflection coefficient is almost purely real up to 1000 Hz ; its value is very close to one from 50 Hz to 1000 Hz. This means that the carpet is acoustically very close to rigid in this frequency range. At higher frequencies, the real part and the imaginary part decrease uniformly. With increasing frequencies, the imaginary part becomes negative, which is typical for an absorber.

This is more clearly seen on the values of the absorption coefficient (see Fig. 2.12(b)). From 0.1 around 2000 Hz, it increases up to over 0.4 at 6400 Hz. Actually, this value represents a significant absorption. Note also the very good overlap for the absorption value obtained using the two setups.

Finally, the impedance values are shown in Fig. 2.12(c). In the low frequency range below 200 Hz, impedance values are not relevant because of the too low absorption properties of the carpet in this frequency range (see Eq. 2.4). Besides these numerical difficulties, the impedance values in the cross–over frequency range correspond well for the two measurements. The impedance has a very high positive real part and a high negative imaginary part. This corresponds to a highly reflecting material. With increasing frequencies, the real part and the imaginary part takes on lower values. However, the decay is more rapid for the real part than for the imaginary part. Therefore, at higher frequencies, the imaginary part is larger in absolute value than the real part, which is typical for a spring–like character.

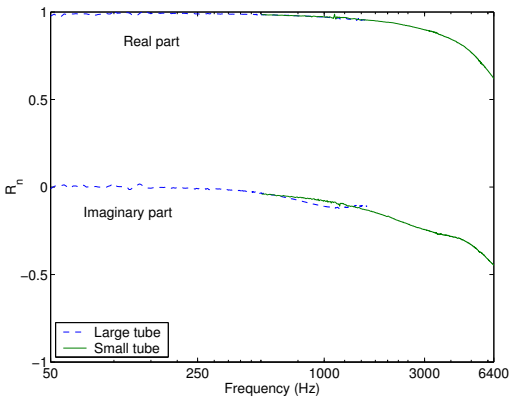

(a) Reflection coefficient

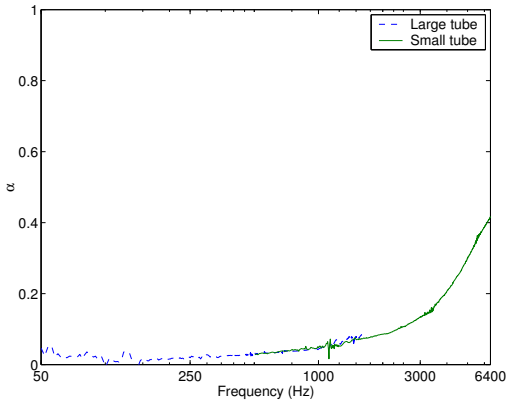

(b) Absorption coefficient

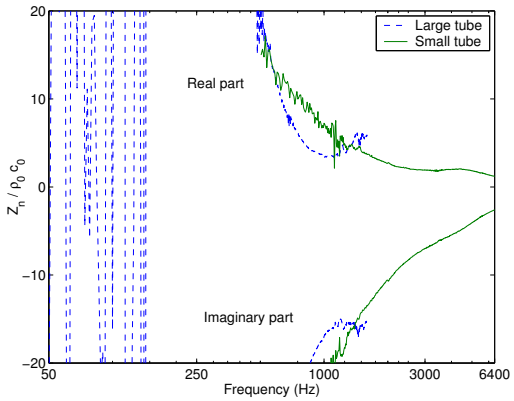

(c) Normalised acoustical impedance

Figure 2.12: *Acoustical properties of the fitted carpet Fig. 1.1.*

Therefore, the impedance tube measurements give a complex acoustical behaviour for the fitted–carpet. Below 1000 Hz, the behaviour is that of an acoustically rigid material. Beyond 2000 Hz, it has a spring–like character and its absorption power is significant (around 0.4 at 6000 Hz). In total, the carpet represents well the "little" absorbing material needed in this work.

2.5.2 Mineral rockwool

The mesured reflection coefficient of the mineral rockwool is shown in Fig. 2.13(a). The overlap between the two frequency range measurements is reasonable[3]. Under 250 Hz, the real part of the reflection coefficient is close to one, whereas the imaginary part takes on small, decreasing,

[3]The overlap was good for most of the measurements ; however, only the small tube measurement which gives the best overlap is shown here.

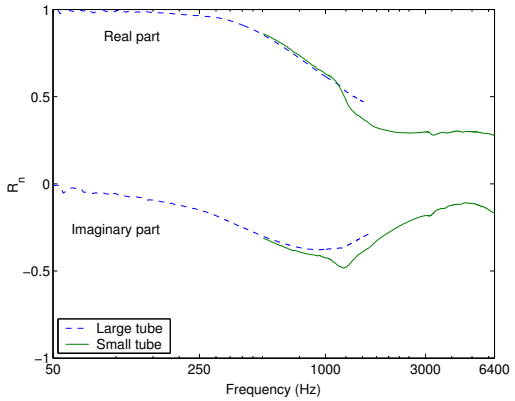

(a) Reflection coefficient

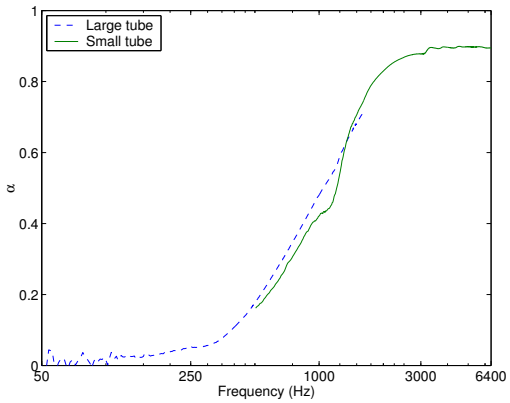

(b) Absorption coefficient

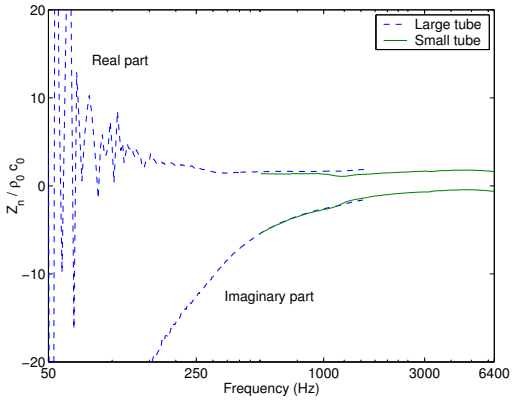

(c) Normalised acoustical impedance

Figure 2.13: *Acoustical properties of the mineral rockwool Fig. 1.2.*

negative values. This corresponds to a low absorbing material. As the frequency increases, the real part decreases to reach a constant value. On the other hand, the imaginary part has larger negative values with increasing frequency up to around 1000 Hz. At this point the tendency is reversed and the imaginary part tends to zero.

This has for consequence that the absorption coefficient levels out at higher frequencies, as can be seen in Fig. 2.13(b). The threshold value lies around 0.9 from 2500 Hz and at higher frequencies. It is also observed that below 250 Hz, the absorption power of the rockwool is low, being less than 0.1.

The deduced values of the impedance, which are shown in Fig. 2.13(c), are substantially lower than those obtained for the carpet, for both the real and the imaginary part. Actually the real part is almost constant on the whole frequency range, whereas the imaginary part takes on lower values as the frequency increases. Again, the rapid varitions of the values at frequencies belwow 100 Hz are due to the fact that the reflection coefficient is close to one at these frequencies.

In conclusion, the rockwool used in the experiments has an absorption power which increases with frequency. At frequencies above 3000 Hz, the absorption properties of the rockwool is very high. Hence, the rockwool represents well the high absorbing material necessary for the following of the tyre noise experiments.

2.6 Determination of the material acoustical properties

For prediction purposes, the acoustical quantity of interest is the impedance distribution as a function of frequency. However, for a better understanding of the acoustical phenomena and in order to design optimal properties of the acoustical material, it is of interest to access directly the construction parameters : flow resistivity, acoustical thickness of the material, porosity, tortuosity.

This section presents a method to determine the input parameters of a given impedance model from the measurements performed using a two–microphones impedance tube. The procedure, which consists in fitting some measured data to some predicted values, is fully presented in *Appendix 11*. The propagation model used is presented and the properties of the quantities available from measurements are discussed. A number of examples of optimisation runs are finally given.

2.6.1 Propagation model

For measurements using an impedance tube, plane sound waves impinge the surface of the tested sample under normal incidence. In these conditions, it is safe to assume that the impedance value at one point of the material surface is independent on the value of the impedance at neighbour points, and that the material is locally reacting.

Therefore, two parameters are sufficient to fully described the propagation of sound in a medium : the propagation constant and the wave impedance. In the present work, these quantities are given by the model proposed in [10]. Although this latter model was especially designed for fibrous materials, it has been shown in numerous works that this model was suitable for a large range of non–fibrous material. Therefore, this model was chosen for the optimisations concerning the fitted–carpet and the mineral rockwool. Of course, the procedure described here also holds for other impedance models which includes more construction parameters like the porosity or the tortuosity.

As a reminder, the model proposed in [10] gives the following expressions for the propagation constant and the wave impedance in the material :

$$\begin{aligned} Z_{mat} &= 1 + 9.08\ {F_\sigma}^{-0.75} + \mathrm{j}11.9\ {F_\sigma}^{-0.73}, \\ k_{mat} &= k_0 \left[1 + 10.8\ {F_\sigma}^{-0.70} + \mathrm{j}10.3\ {F_\sigma}^{-0.59}\right] \\ \text{with} \quad F_\sigma &= \frac{1000 f}{\sigma} \end{aligned}$$

In these equations, k_0 is the wave number of sound in air, f is the frequency and σ is the flow resistivity of the material (given in N.s.m^{-4} or kg.m^{-3}.s^{-1}).

For the tube measurements, the material is placed direcly on an acoustically, rigid piston. The examined impedance material is then a hardbacked layer of material. The acoustical impedance measured at the surface in the normal direction is then a function of the layer thickness l as :

$$Z_l \;=\; \mathrm{j}Z_{mat}\;\cot(lk_{mat})$$

assuming a $\mathrm{e}^{-\mathrm{j}\omega t}$ time dependence. Therefore, one has to take the complex conjugate of this value to get the same time dependence as for the measurements.

Once the normal acoustical impedance is known, the other acoustical quantities can be calculated using Eq. 2.3, Eq. 2.2 and Eq. 2.6.

2.6.2 Measurements data

The measurement data available from tube measurements are :

- The transfer function between the two microphones (see Eq. 2.2). It is a set of complex values. This is very first measured data. All other quantities are deduced from this set of data. Therefore, it is natural to perform an optimisation based on these values, which are *a piori* not corrupted by eventual numerical difficulties.
- The reflection oefficient. It takes on complex values. It is deduced from the transfer function values according to Eq. 2.3. This quantity is explicit in terms of absorption power.
- The absorption coefficient. It is the only real set of data of all acoustic quantities available. This quantity, deduced from the reflection coefficient (see Eq. 2.5), is the parameter mainly used to quantify the absorption power of materials.
- The normal acoustical impedance. It takes on complex values. Determined from Eq. 2.4, it is the quantity used as input in outdoor propagation models.

According to *Appendix 11*, the function to be optimised should not present strong extremum values nor rapid variations. Therefore, the optimisation upon transfer function values may be difficult in most cases. For the transfer function presents two extrema, more or less marked depending on the absorption power of the tested sample. These extremum values correspond to a constructive and a destructive interference between the incident wave and the reflected wave inside the tube. For very absorbing materials however, the extrema are somewhat smoothened and the optimisation upon transfer function values may be possible. To the contrary, reflection and absorption coefficient are slowly varying functions in most cases.

The last factor of influence on the success of the optimisation is the frequency range considered. Quite naturally, this range will be at most the frequency range of validity of the measurements, i.e. 50 Hz to 1600 Hz for large tube measurements and from 500 Hz to 6400 Hz for small tube measurements. Moreover, according to the discussion of §*2.2.2*, the low frequency range, where the absorption is in general weak must be avoided. In addition, the frequency range where shearing modes are suspected must be eluded (see §*2.2.6*), because the propagation model does not include this phenomenon. However, a special attention is paid to the carving of the samples so that shearing modes may be very little visible.

2.6.3 Optimisation initial values

The results of this procedure are the optimal values of the model parameters, that is in our case the material thickness l and the flow resistivity σ. Given the cost function chosen (Eq. 11.1), the optimal values give the best correspondence between the measured and the predicted quantity, i.e. transfer function, reflection coefficient or absorption coefficient.

It is important to note that in the present case, the value of one optimised parameter, i.e. the material thickness, can easily be measured. This has two consequences. The first one is that there is a certain confidence in one of the initial values ; this reduces the risk to end up with only a local minimum of the function. The second consequence is that the optimal thickness value found by the optimisation process can be compared to the measured one. Therefore, the validity of the second parameter value, i.e. the value the flow resistivity, may be addressed to the validity of the thickness optimal value. One thus has a sort of measure of the error made in the optimisation.

At last, one could even perform an optimisation upon the flow resistivity only. This was however avoided for two reasons. First, it was found difficult to measure accurately the thickness of the materials used in the present study because of their structure. Moreover, the thickness value found by the optimisation process is the distance between two acoustical reflecting planes, the positions of which may not coincide exactly with the actual outer surfaces of the material. Therefore, the material thickness was left as an input parameter.

2.6.4 Examples of optimisation runs

In this paragraph, three examples of optimisation runs are given and discussed. Conclusions are addressed to the method functionning and typical difficulties. The final results and the conclusions concerning the experimental determination of impedance model parameters are given in the next section.

The examples are presented as follows[4]. The top figure compares the measured and predicted values for the optimised quantity. In the three lower figures are shown the predicted and measured values for the other quantities. The values of the optimal material thickness and the optimal flow resistivity are given in the legend of the figure. Finally, in all figures, the frequency range used for the optimisation is indicated by a gray strip. For large tube measurements, the frequency range spans from 200 Hz to 1000 Hz, and for small tube measurements, the frequency range spans from 1000 Hz to 5000 Hz.

Fig. 2.14 and Fig. 2.15 presents examples of optimisation performed on large tube measurements. In the first figure, optimisation is performed upon transfer function values and in the second figure, optimisation is performed upon absorption coefficient values.

One should note that the same set of measurements data are used for the two runs. Therefore, the main difference between the two optimisation runs consists in the different shapes of the functions to be fitted : the transfer function vary more rapidly than the values of the absorption coefficient.

In the case transfer function values are optimised (see Fig. 2.14), the correspondence is good for all quantities. The overall good agreement with the measurements in this case would argue for the reliability of the predictions. The picture changes when the optimisation is performed upon

[4]The same layout is used for the exhaustive results presented in *Appendix 12*.

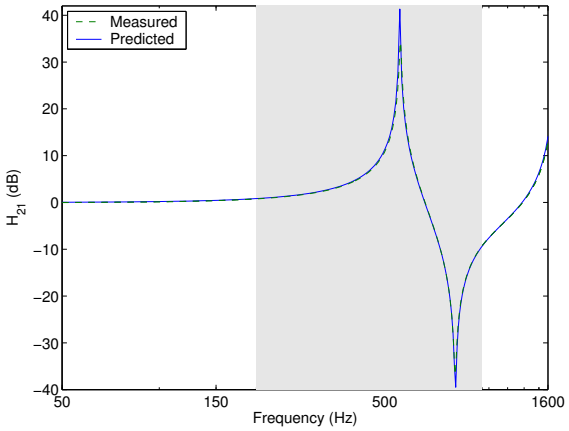

(a) Transfer function

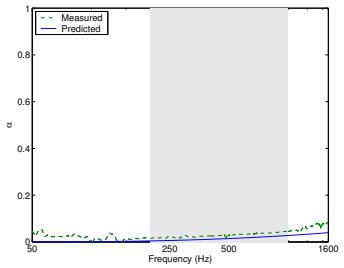

(b) Absorption coefficient

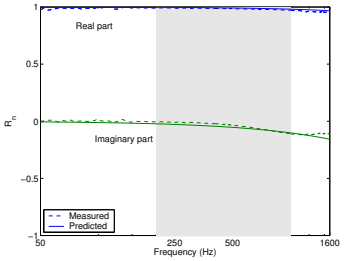

(c) Reflection coefficient

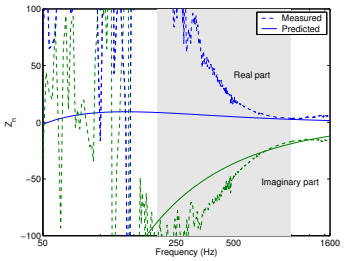

(d) Acoustical impedance

Figure 2.14: *Example of optimisation for large impedance tube measurements. Tested surface is fitted–carpet. Optimised quantity is transfer function : $l(mm) = 2.50$; $\sigma(kNsm^{-4}) = 4.9$.*

absorption coefficient values (see Fig. 2.15). Even though the correspondence is good for the optimised quantity, i.e. the absorption coefficient, predictions and measurements for the other quantities is very poor. In this case, the optimisation process fails, yielding unreliable predictions (e.g. the largely over–estimated value of the material thickness). This may be due to the fact that the absorption coefficient takes very low values on the scanned frequency range.

A last example is given in Fig. 2.16 where the optimisation is performed upon small tube measurements. The optimised quantity is the absorption coefficient. For this quantity, as expected, measurements and predictions are in good correspondence in the frequency range of the optimisation. Below and above this frequency range, small deviations are observed. However, for the other quantities, the predictions do not fit well to the measurements. Even though the optimal value of the material thickness coincides well with the measured value, the poor correpondence between predictions and measurements tends to discard the results of the optimisation.

In conclusion, the optimisation upon absorption coefficient values seems to be more delicate than the optimisation upon transfer function values. This is somewhat unexpected and it is still not

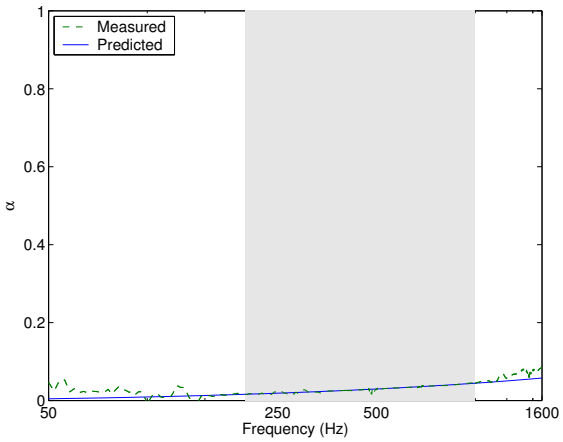

(a) Transfer function

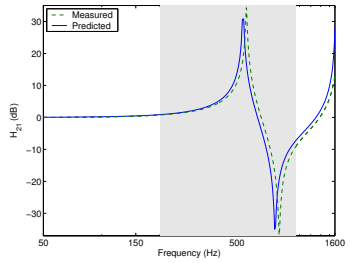

(b) Absorption coefficient

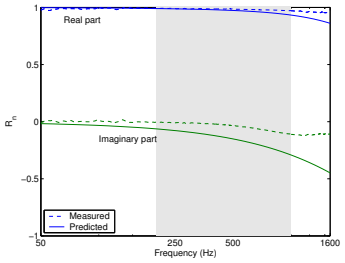

(c) Reflection coefficient

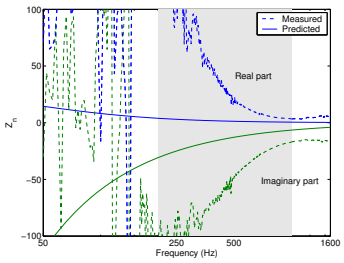

(d) Acoustical impedance

Figure 2.15: *Example of optimisation for large impedance tube measurements. Tested surface is fitted–carpet. Optimised quantity is absorption coefficient : $l(mm) = 7.94$; $\sigma(kNsm^{-4}) = 0.6$.*

explained. Fortunately, this paragraph illustrates the main difficulties found during the optimisation procedure. The other configurations give results which are more coherent and more reliable ; they are presented in the coming paragraph.

2.7 Material acoustic properties

The optimisation process was performed as desribed previously for measurements obtained using the two–microphone impedance tube setup.

As aforementioned, for measurements using the large tube, the frequency range of optimisation spans from 200 Hz to 1000 Hz. For measurements using the small impedance tube, the frequency range spans frequencies from 1000 Hz to 5000 Hz. These ranges were used for measurements on the fitted–carpet and on the mineral rockwool. Different frequency ranges for different materials were tested without showing relevant differences provided a sufficiently large range was included. Taking a too short frequency range indeed may give only a partial picture of the material behaviour.

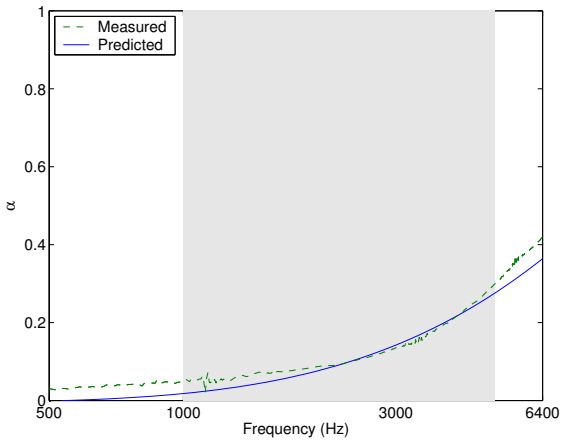

(a) Absorption coefficient

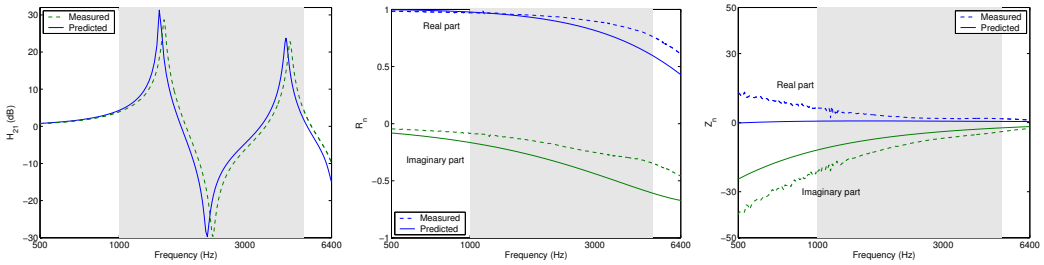

(b) Transfer function (c) Reflection coefficient (d) Acoustical impedance

Figure 2.16: *Example of optimisation for small impedance tube measurements. Tested surface is fitted–carpet. Optimised quantity is absorption coefficient : $l(mm) = 3.69$; $\sigma(kNsm^{-4}) = 56$.*

The initial values given in the next paragraphs result from a series of preliminary "blind" runs performed with arbitrary initial values. From a practical point of view, a larger freedom was left for the initial value of the flow resistivity than for the initial value of the material thickness. Hence, the initial values indicated below are the ones giving the most coherent values of the optimal parameters for both large tube and small tube measurements. They are given in millimeters (mm) for the material thickness and in $kNsm^{-4}$ ($= 1000\ Nsm^{-4}$).

Results are synthetised in Table 2.2 and Table 2.3 below, while extensive results are given in *Appendix 12*. In these tables, the mean value of one set of measured data is calculated. In addition, the ratio of the standard deviation to the mean value is given as a measure of the coherence between the different optimisation runs : the smaller the value, the better the coherence. This quantity is dimensionless.

Finally, given the optimal parameters kept for the rest of the study, the acoustical impedances for the two materials are plotted in the complex plane as a function of frequency.

Optimised quantity	Fitted–carpet		Mineral rockwool	
	Large tube	*Small tube*	*Large tube*	*Small tube*
Transfer function	2.50	2.09	17.8	18.3
Absorption coefficient	7.94	3.69	17.9	18.1
Reflection coefficient	2.41	2.13	17.7	18.6
Acoustical impedance	2.20	2.20	17.3	18.5
Mean value	*3.76*	*2.53*	*17.7*	*18.4*
STD / mean	*0.74*	*0.31*	*0.015*	*0.012*

Table 2.2: *Optimal values of the material thickness l (in mm).*

Optimised quantity	Fitted–carpet		Mineral rockwool	
	Large tube	*Small tube*	*Large tube*	*Small tube*
Transfer function	4.9	22	115	88
Absorption coefficient	0.6	56	110	92
Reflection coefficient	4.9	26	117	88
Acoustical impedance	2.6	17	119	88
Mean value	*3.25*	*30*	*115*	*89*
STD / mean	*0.64*	*0.58*	*0.033*	*0.022*

Table 2.3: *Optimal values of the flow resistivity σ (in kNsm^{-4}).*

2.7.1 Fitted–carpet

For the fitted–carpet, the initial values of the impedance model parameters were : 3 mm for the thickness and 30 kNsm^{-4} for the flow resistivity.

The optimisation process predicts a mean thickness of 3.76 mm using large tube measurements whereas a 2.53 mm mean thickness is predicted using small tube measurements. A closer look at the results for both the large and the small tube measurements reveals that the optimal values found using the absorption coefficient data seem to deviate significantly from the values obtained using other quantities. If this value is excluded from the set of large tube datas, the mean is found to be 2.37 mm and the measure of the coherence falls to 0.065 ; if this is done for small tube measurements, the mean becomes 2.14 mm and the measure of the coherence falls to 0.026. The deviation for the large tube measurements is certainly due to the fact the absorption coefficient takes on rather small values. The optimisation using such low values may be delicate in this case. For small tube measurements, the explanation is still not clear.

Even with this new value of the material thickness, the optimal values are smaller than the measured one, which is 3.82 mm. The deviation between the measured and the optimal value of the material thickness can be explained by the construction properties of the fitted–carpet. The carpet consists indeed in an impervious layer of glue, the surfaces of which gathers the material fibers. Therefore, the acoustical thickness may be smaller than the distance between the outer surfaces of the material.

Moreover, the optimal values of the flow resistivity are found to be 3 kNsm^{-4}, respectively 30 kNsm^{-4}, for large tube measurements, respectively for small tube measurements. Again, the value obtained using absorption coefficient seem to be out of range of the values obtained using other quantities. If this value is excluded, the mean for the large tube measurements becomes

4.13 kNsm^{-4} and the measure of the coherence falls to 0.32 instead of 0.64. For small tube measurements, if this value is excluded, the mean is found to be 21.6 kNsm^{-4} with a coherence which falls to 0.21 instead of 0.58.

Therefore, for the calculation of the final values of the impedance model parameters, it seems more reliable to exclude the values obtained using the absorption coefficient datas. The values of the parameters kept for the following are the mean of the values obtained from large tube and small tube measurements. Therefore, the optimal thickness is found to be $l = 2.25$ mm and the optimal flow resistivity is 12.9 kNsm^{-4}.

2.7.2 Mineral rockwool

The initial values for the mineral rockwool were : 15 mm for the thickness and 100 kNsm^{-4} for the flow resistivity.

For this material, the value of the ratio between the standard deviation and the mean is rather small for all set of measurements. This indicates that the results are substantially coherent, and thus reliable in all configurations, for both values of the impedance model parameters.

The optimal value of the material thickness is found to lie around 18 mm, which is a slightly larger than the actual measured value which is 15.4 mm. This difference is certainly due to the fact one surface of the rockwool samples presents small ripples. The amplitudes of these ripples may vary substantially from one sample to another. Thus the acoustic distance between the two frontiers of the material may differ from the material distance measured on one sample.

Moreover, the flow resistivity for mineal rockwool is found to lie between 115 kNsm^{-4} for large tube measurements and 89 kNsm^{-4} for small tube measurements. These values correspond very well with values obtained in [11] for a similar material[5]. The difference obtained between large tube measurements and small tube measurements is not significant as suggested in [12] where classes of flow resistivity are proposed (see *Chapter 3* for more details).

Finally, the values of the impedance model parameters kept for the rest of the study are taken to be the mean value between the values found using large tube and small tube measurements. The optimal thickness of the mineral rockwool is thus $l = 18$ mm and the optimal flow resistivity is $\sigma = 102$ kNsm^{-4}.

2.7.3 Summary

Fig. 2.17 shows the value acoustical impedance as a function of frequency plotted in the complex plane, which is obtained using the optimal values of thickness and flow resistivity. Impedance values for the domain of validity of the tube measurements, i.e. up to 6400 Hz, are plotted as thick line. Values computed up to 100 kHz are indicated with a dotted line. on these figures are also plotted the curves of equal absorption, which correspond to circles in the complex impedance

[5]The values were obtained in the mentionned work using the level difference technique (see *Chapter 3*).

plane. The value of total absorption (Z real and equal to Z_{air} is indicated with a cross located inside the 0.9 equal–absorption curve.

These representations of the impedance clearly reveal the distinctive behaviour of the two tested materials. The impedance for the fitted carpet turn around the point $Z = Z_{air}$ without reaching it. This corresponds to a low absorbing material. On the other hand, the impedance for the rockwool goes almost straight toward this point and reaches it at the very end of the examined frequency range. This is typical for a high absorbing material.

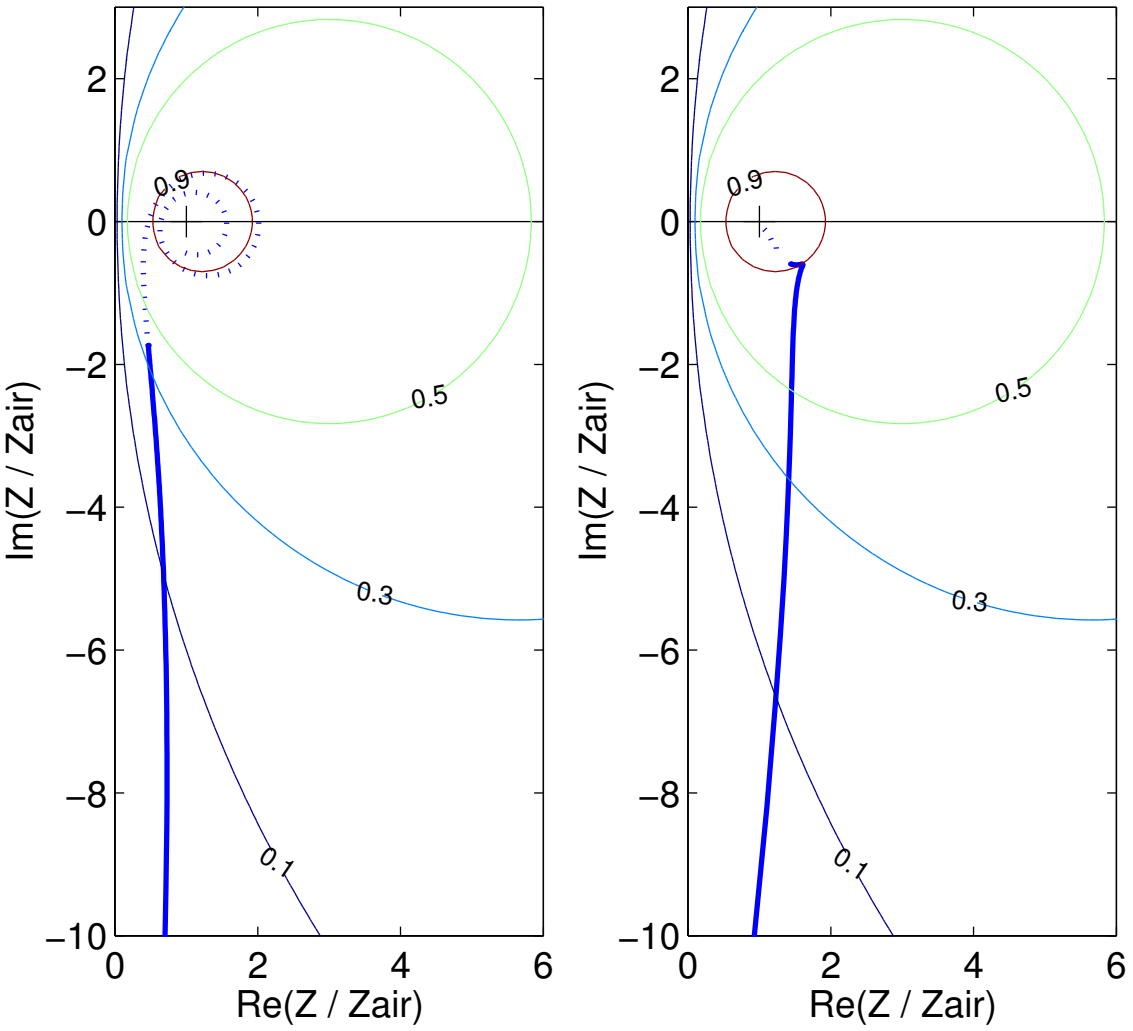

(a) Fitted–carpet : $l(\text{mm}) = 2.25$; $\sigma(\text{kNsm}^{-4}) = 12.9$

(b) Mineral rockwool : $l(\text{mm}) = 18$; $\sigma(\text{kNsm}^{-4}) = 102$

Figure 2.17: *Acoustical impedance of the tested materials obtained from tube measurements – Values plotted in the complex plane.*

3 – Level difference technique

Methods to determine the acoustic properties of impedance materials can be classified in two categories : the destructive methods and the non–destructive ones. Methods of the first type are mainly "laboratory" techniques ; so–called "impedance tube" measurements belongs to this category. To the contrary, non–destructive methods are often associated with the adjective "in–situ" because they can be implemented on the site where the tested material is supposed to be laid. The advantages of the techniques of the second type compared to destructive methods are evident when dealing with road surfaces.

This chapter presents a non–destructive method, the level difference technique, as an alternate to impedance tube measurements for the determination of the chosen surfaces' acoustical properties. This method is fully presented in [12]. It is mainly used in scandinavian countries where it has been elaborated. It gives access to the same material parameters as the previous tube measurements : the thickness and the flow resistivity.

The chapter is organized as follows. The level difference technique is described in the first section ; influencing parameters are reviewed in the second section and measurement results are given in the third section.

3.1 Basis of the technique

3.1.1 Method principle

The level difference technique holds on the fact that a number of accurate numerical tools are now available for the simulation of outdoor sound propagation. In particular, the field radiated in a homogeneous medium by an omnidirectional sound source placed over an impedance plane can be modelled with a good accuracy in two–[13, 14, 15] or three–dimensional geometries [16, 17, 18, 19]. At this point arises the idea that these models could be used to reproduce the measure. Therefore, the field of investigation could be extended to the inner properties of the materials, whereas these properties are not directly the objects of the measurement. The measuring effort is then replaced by the modelling and the computational effort.

Therefore, important parameter values, like the flow resistivity or the porosity, could be determined from an elementary measure of the sound field above that surface. By fitting the measured sound pressure levels to the predicted ones, the values of the model input parameters can be estimated. Hence, the number of material properties deduced from the measurements depends only on the degree of description of the chosen propagation model. For instance, for one set of measured data, several models could be tested in order to extract several parameters separately.

The advantage of this method is that no particular equipment but a sound source and a microphone, is required compared to impedance tube measurements. This has for consequence that

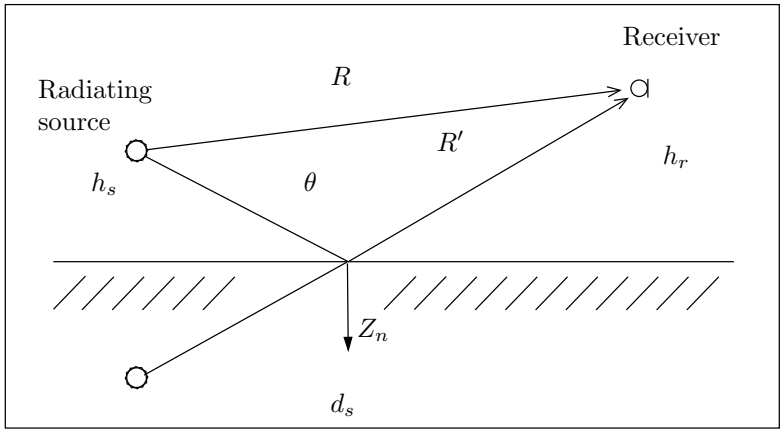

Figure 3.1: *Source radiating over an impedance surface.*

measurements may be carried out quite easily in almost all sites[1]. The only restriction is the degree of correspondence between the propagation model chosen and the experimental conditions. This implies either that the experiments should reproduce the best the model assumptions or that the model should include the experimental restrictions.

In conclusion, the implementation of the level difference technique requires the use of a propagation model including the description of the source together with an accurate description of the surface properties. These two aspects are presented in the two next paragraphs.

3.1.2 Propagation over an impedance plane

As previously mentioned, the choice of a propagation model is highly connected to the conditions under which the experiments are conducted. For practical reasons, a three–dimensional, omnidirectional sound source is prefered to an omnidirectional line source. The details on the realisation of this source are presented in *Appendix 14*.
The situation to be modelled is the following one : a three–dimensional point source radiating over a homogeneous impedance plane. The geometry is schematised in Fig. 3.1.

In this case, according to [18, 19], the total sound field above the impedance plane can be written as

$$p(R) \;=\; \frac{\mathrm{e}^{\mathrm{j}kR}}{R} \;+\; Q_s \;\frac{\mathrm{e}^{\mathrm{j}kR'}}{R'} \tag{3.1}$$

where k is the wave number and R, respectively R', is the length of the direct sound path, respectively the reflected sound path. Finally, Q_s is the so–called spherical reflection coefficient ; its expression is given in the next paragraph.

In order to study only the effect of the impedance plane, one should get rid of the geometrical spreading which is due to the nature of the sound source. For this, the value relative free–field is

[1]This also holds for the extended surface method as it is mainly a special case of the level difference technique.

used instead of the pressure p

$$p_{rel}(R) \;=\; \frac{p(R)}{\mathrm{e}^{\mathrm{j}kR}/R} \;=\; 1 + Q_s \frac{R}{R'} \mathrm{e}^{\mathrm{j}k(R'-R)}$$

By writing $Q_s = |Q_s|\mathrm{e}^{\mathrm{j}\varphi}$, the previous equation becomes

$$p_{rel}(R) \;=\; 1 + \frac{R^2}{R'^2}|Q_s|^2 + 2\frac{R}{R'}|Q_s|\cos(\; k(R'-R) + \varphi)$$

The sound pressure level in decibel is then obtained by

$$\mathrm{Lp}_{rel}(R) \;=\; 10\log_{10}\left|p_{rel}(R)\right|^2$$

which finally gives

$$\mathrm{Lp}_{rel}(R) \;=\; 10\log_{10}\left(1 + \frac{R^2}{R'^2}|Q_s|^2 + 2\frac{R}{R'}|Q_s|\cos(\; k(R'-R) + \varphi)\right)$$

Without free-field normalisation, as in the measurements, the sound pressure level in decibels writes :

$$\mathrm{Lp}(R) \;=\; 10\log_{10}\left(1 + \frac{R^2}{R'^2}|Q_s|^2 + 2\frac{R}{R'}|Q_s|\cos(\; k(R'-R) + \varphi)\right) - 10\log_{10}(R^2)$$

As using only one receiver may lead to identify only a particular property of the sound field at this position, it is more accurate to qualify the ground effects by using two or more receivers. If two receivers, referenced by R_1 and R_2, measure the sound pressure delivered by the same sound source, the level difference is expressed as the difference of the sound pressure levels recorded at these two positions :

$$\Delta\mathrm{L} \;=\; \mathrm{Lp}(R_2) - \mathrm{Lp}(R_1)$$

3.1.3 Characterization of the surface reflexion

The spherical reflection coefficient in Eq. 3.1 is expressed as a function of the reflection coefficient for plane waves R_p as

$$Q_s \;=\; R_p \;+\; (1 - R_p)\; F(w)$$

where $F(w)$ is an error function, which can be seen as compensating for the error made when considering that spherical waves are reflected as if they were plane. If θ is the angle of reflection with the surface normal, R_p can be written according to [7] as

$$R_p \;=\; \frac{Z_n - \cos\theta}{Z_n + \cos\theta}$$

where Z_n is the normal acoustical impedance of the surface. Note that this expression has already been used to calculate the value of the impedance from the value of the reflection coefficient obtained with impedance tube measurements (see Eq. 2.4).

To be able to compare the results obtained using the level difference technique to those obtained from impedance tube measurements, it seems natural to choose the same model for the sound propagation in the material, namely that proposed in [10] (see §*2.6.1* for the governing equations). For these measurements too, the materials are laid on an acoustically rigid plane.

Unlikely tube measurements, the incidence can take on any values from grazing to very steep depending on the source and receiver positions. Therefore, it would be more adapted in this case that the value of the impedance is calculated according to the angle of incidence of the sound waves. This can be done fairly easily as shown in [20]. However, it is chosen to consider only the impedance value in the normal direction to the surface to have exactly the same set of data as for impedance tube measurements. One may observe that the extended surface method, making use of a source and a microphone which are vertically aligned, do not present this bias when using normal impedance values.

3.2 Implementation of the method

This section presents the practical application of the method. In particular, the sensitivity of the technique to geometrical and acoustical parameters is discussed in the first and the second paragraph. In the third paragraph, the general procedure together with some use recommendations are given.

3.2.1 Level difference measurements

The optimisation procedure used for level difference measurements is the same as for impedance tube measurements. The reader is thus referred to *Appendix 11* for full details on the optimisation.

The main difference between optimisation upon tube measurements and level difference measurements concerns the type of the optimised quantity. The present method uses the difference of sound pressure levels measured at two receivers positions for a unique radiating source. In other words, one estimates the value of the transfer function between two receivers. Therefore, the optimised quantity presents an interference pattern, the shape of which will be more or less pronounced depending on the absorption properties of the surface.

In this case and unlikely tube measurements, the optimisation results were found to be less sensitive to change in the initial values. Thus, a very few number of "blind tests" (see §*2.7*) were needed to obtain the initial values kept for the input parameters.

3.2.2 Sensitivity to measurement positions

Another parameter of influence is the measurement accuracy of the source and receiver positions. Mainly three distances have to be measured : the height of the source, the height of the receiver and the horizontal distance between the source and the receiver.

Numerical tests presented in the reference document [12] demonstrate that placement errors are not critical as long as they can be kept under 1 cm error. In our case, it is reasonable to consider that the microphone and the source positions are measured with an uncertainty at most equal to their sizes. Since sound pressure levels are recorded using quarter inch microphones (1 inch $\approx$ 2.54 cm), the uncertainty for the measurement of the microphone position falls to around 0.6 cm. As described in *Appendix 14*, the acoustic source has a diameter of 6 mm yielding a measurement error far below the 1 cm required. Therefore, the measurement errors are not expected to influence significantly the level difference measurements.

3.2.3 Other influencing parameters

The impedance materials chosen for this study can be used indoors quite easily. This allowed to perform the measurements in laboratory conditions. Therefore, parasite effects of wind or temperature gradient with height could be neglected for the present experiments. If outdoor measurements were to be performed, e.g. for road surfaces, these effects may not be neglected so easily. If this case, measurements conditions must be controlled and / or these phenomena must be included in the propagation model.

A drawback of laboratory measurements is the vincinity of walls which may introduce parasite reflexions on the recorded signals. To avoid this, objects in the proximity of the source / microphone were treated to minimize the sound reflexions. In addition, small range geometries were used which allowed to filter out corrupted parts of the signal. A last care was taken by recording both time signals and frequency spectra (see below).

Concerning the values of the measurement positions, no specific recommandations are given in the reference document [12]. However, extreme positions should be avoided, like very steep or near to grazing incidences. For rather steep incidence, either the source and the microphone are very close to each other, which may induce perturbations from the equipment or from the near field of the source. At grazing incidence, the measured reflection coefficient is always -1, whatever the ground impedance, which corrupts the measurement data.

3.3 Measurement setup

3.3.1 Preliminary measurements

The propagation model assumes that the materials are laid on an acoustically rigid support. Practically, the fitted–carpet is laid on the floor of the laboratory, which is made of Gerflor© linoleum flagstones of dimension $0.3\times0.3\ m^2$ and the mineral rockwool is laid on a $2.5\times1.22\ m^2$ wooden plate (see [21] for details). To test the acoustical properties of these floors, a series of measurements are performed. Sound pressure levels are recorded for a given geometry when the source and receiver are above the floor and when they are in "free–field" conditions.

Sound pressure levels relative to free–field are then compared with predictions obtained with a two–dimensional model and a three–dimensional model for the sound propagation over a rigid surface. These models use the respective free–field Green functions for two– or three–dimensional geometries. The Green functions include a mirror image source to account for the presence of a infinite rigid plane. Using the notations of Fig. 3.1, relative sound pressure levels are expressed as :

$$\begin{aligned} \mathrm{Lp}_{rel,2D} &= 10\log_{10} \mid 1+\frac{\mathrm{H}_0^{(2)}(kR')}{\mathrm{H}_0^{(2)}(kR)} \mid^2 \\ \mathrm{Lp}_{rel,3D} &= 10\log_{10} \mid 1+\frac{R}{R'}\ \mathrm{e}^{\mathrm{j}k(R'-R)} \mid^2 \end{aligned}$$

Results shown in Fig. 3.2 for the linoleum and the wooden plate shows a very good correspondence between the measured and the predicted values. Other measurements not shown here for other geometries show the same degree of correspondence. Therefore, it is safe to consider that these floors are acoustically rigid and that the materials laid directly on the ground of the floor can be considered as hardbacked.

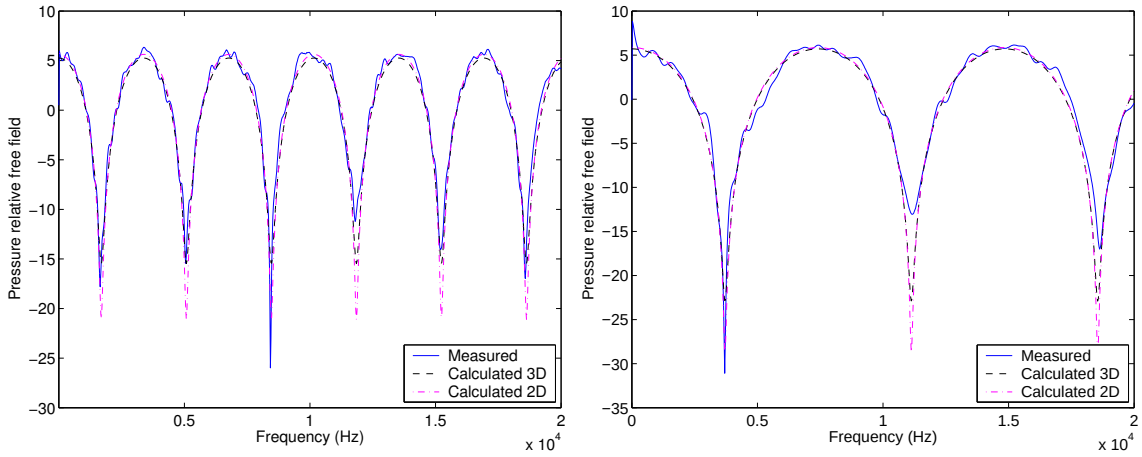

(a) Linoleum floor : $h_s = h_r$=0.16 m and d_s=0.5 m.

(b) Wooden plate : $h_s = h_r$=0.12 m and d_s=0.6 m.

Figure 3.2: *Test of the acoustical properties of the floor backing the absorbing materials.*

3.3.2 Experimental procedure

The measurement setup is that schematised on Fig. 3.1 and showed on Fig. 3.3. That is, a source and a microphone are positioned over the surface to be tested, at a given distance d_s apart from each other. The height of the source and of the microphone are respectively h_s and h_r. The measurement is repeated for three different microphone heights for the same position of the source, which yields three sets of level differences. The optimisation procedure is finally performed upon each set of level differences giving three pairs of optimum parameter values.

Given the size of the laboratory, typical measurements positions are : h_s =0.2 m, d_s =0.6 m and h_r =0.2 ±0.1 m, which gives three microphones positions. Angles of incidence are comprised between 50° and 63°, which is in accordance to the measurement specifications. Practically, only one microphone is used at once to avoid parasitical sound reflexions on the microphone holders.

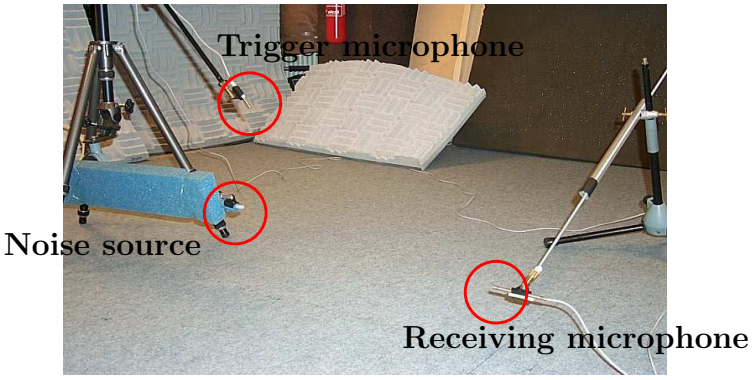

Figure 3.3: *Picture of level difference measurement over fitted–carpet.*

The source position is checked and adjusted if needed after the position of the microphone is changed.

The acquisition settings are adapted to the measurements setup and the desired frequency range. Mainly, given the short distances used in the experiment, the sampling frequency should be high enough so that the different impulses can be distinguished.
The very short duration time of the acoustic impulse requires that the highest sampling rate available is chosen, namely 100 kHz. This allows to describe the main peak of the impulse on 4 to 5 points (see Fig. 3.4), which is a minimum. Therefore, a special attention should be paid to the capacities of the analyser to be used with this acoustic source. For instance, at 50 kHz, the impulse is described on 2 to 3 points. This leads to a hazardous truncation of the main peak which may false the nature of the signal[2].
For the analyser used in this experiment, the sampling rate for the time record is 2.56 times the highest frequency in the spectrum. This gives a time increment of $dt = 1/(2.56 f_s) = 3.90\ \mu s$. Moreover, for the measurement positions of Fig. 3.4, the difference of arrival times of the direct pulses are at minimum 9.7 μs. This has for consequence that the different impulses are separated by 2 to 3 points minimum, as shown in Fig. 3.4(b). Therefore, for a horizontal distance of around 0.6 m, the microphones should be at least separated by around 0.1 m.

Given these parameters, three different types of signals are recorded : the averaged spectrum ('SU' signals below), the averaged time signal ('AV' signals) and the linear spectrum computed from the averaged time signal ('SC' signals). Even though the final considered quantity is the sound spectrum, the interest of taking time signals is that one can filter out unwanted sound reflexions, which may corrupt the recorded signals. Another advantage is that one can artificially increase the frequency resolution by over–sampling the recorded signal. Note that this does not help separate the different impulses on the original time signal. However, this procedure has been tested without significant changes on the optimisation results ; it has not been used further in the present work.

The optimisation is finally performed on the three different types of signals giving three sets of optimum parameters for each microphone position.

3.3.3 Example of measurement results

An example of measurement data and optimisation results is shown in Fig. 3.5. It shows the recorded averaged spectrum on the left hand side figure for the three receivers' positions. The measurement positions are also recalled on the left hand side of the figure. On the same part of the figure are indicated the initial values of thickness and flow resistivity used for the optimisation. The resulting optimum parameters are finally given for each transfer function. On the figures the frequency range of optimisation is indicated in gray.

It can be observed that the optimisation gives three pairs of parameters having coherent values. Moreover, the predicted transfer function fits well the measured one on a frequency range which is larger than the range of optimisation.

Similar observations can be made on Fig. 3.6 where the recorded measurement data is the frequency spectrum calculated from the averaged time signal. As expected, the frequency spectrum is very similar in both cases, thus giving very similar pairs of optimum parameters.

[2]For instance, on the tested signals at 50 kHz, the peak corresponding to the direct pulses had a lower amplitudes than the pulses corresponding to the reflected field.

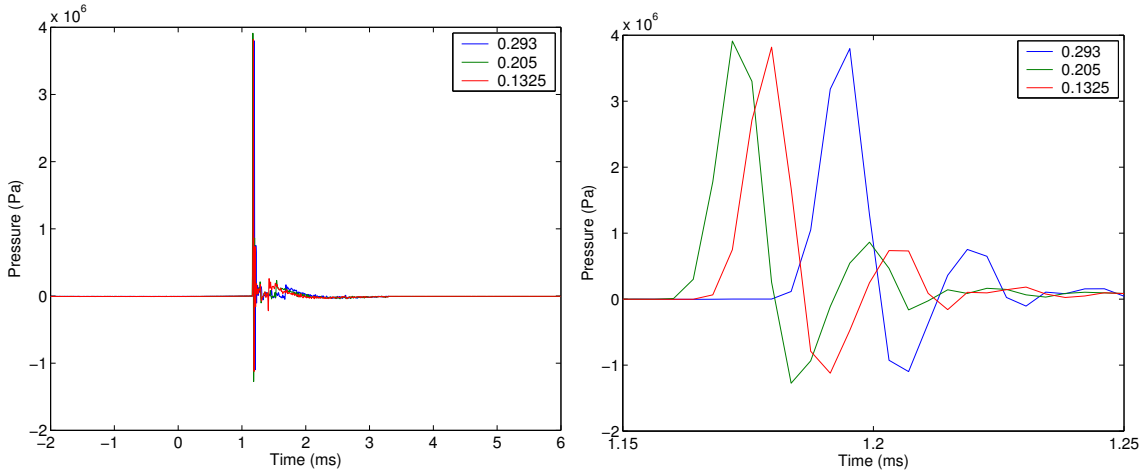

(a) Full record (b) Close–up on the direct impulses

Figure 3.4: *Example of an unfiltered time signal recorded at f_s =100 kHz. Source at d_s =0.6 m, h_s =0.2 m ; three receivers at h_r =0.132 m, 0.205 m, 0.293 m*

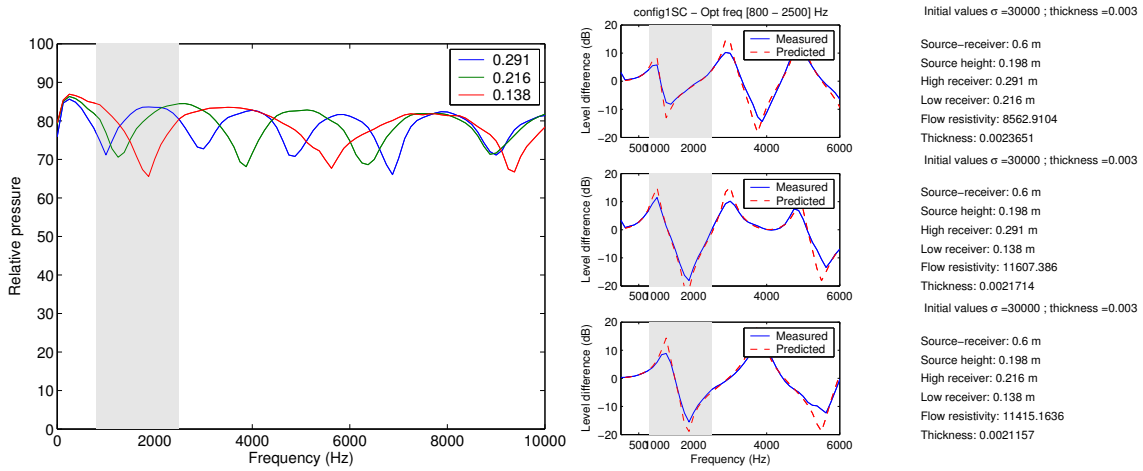

(a) Measurement data (b) Optimisation results

Figure 3.5: *Example of optimisation results from level difference measurements. Surface is fitted–carpet – h_s =0.2 m, d_s =0.6 m, h_r =0.291 m, 0.216 m, 0.138 m – Signal is spectrum from averaged time signal.*

Finally, the frequency range of optimisation is chosen to include the first interference, as recommended in [12]. Hence, this range may change with the geometry of the source / receiver. Other ranges, in particular larger frequency ranges, were tested without significance influence on the results. At most, taking a too large frequency range, e.g. up to 5000 or 6000 Hz, leads to poorer

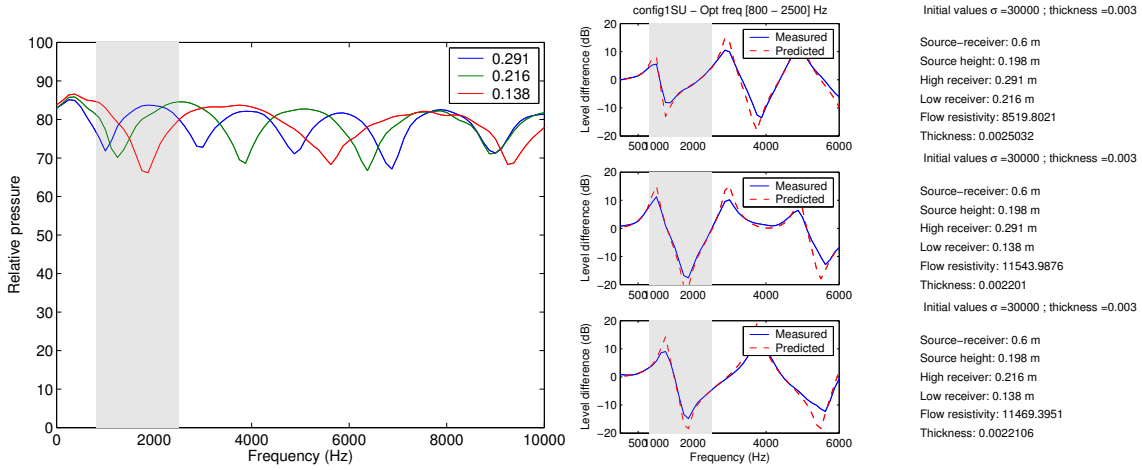

(a) Measurement data (b) Optimisation results

Figure 3.6: *Example of optimisation results from level difference measurements. Surface is fitted–carpet – h_s =0.2 m, d_s =0.6 m, h_r =0.291 m, 0.216 m, 0.138 m – Signal is averaged spectrum.*

optimisation in the sense that the disparity between the resulting parameter values is larger.

3.4 Measurement results

This section presents results of optimisation runs for all measurement configurations which have been tested. Exhaustive results of optimisation upon level difference measurements are shown in *Appendix 13*.

For all the runs, the optimisation is performed for frequencies between 800 Hz to 2500 Hz for the carpet and for the mineral rockwool. Initial values given for the minimisation search are the same as for tube measurements. Moreover, measurement results are presented in a similar manner as for tube measurements, in Table 3.1 for the fitted–carpet and in Table 3.2 for the mineral rockwool. For each measurement data, three pairs of parameter values are obtained corresponding to the three possible pairs of microphones used. The positions of the microphones are indicated in the left column of the tables as *High*, *Medium* and *Low* ; the exact positions are given in the text.

The discussion which follows only concerns the results from level difference measurements. Results are compared to those obtained with tube measurements in *Chapter 4*.

3.4.1 Fitted–carpet

For measurements over the carpet, the initial values given in the optimisation process are : 3 mm for the thickness and 30 kNs/m^4 for the flow resistivity.

Two measurement configurations are examined for the fitted–carpet. In the Table 3.1, the index '1' understands the following source and receiver positions : h_s =19.8 cm, d_s =60 cm and h_r =29.1

cm, 21.6 cm, 13.8 cm. For the measurement files having the index '2', the following positions are used : h_s =19.8 cm, d_s =75 cm and h_r =29.1 cm, 20.6 cm, 14.0 cm. One can observe that the angles of incidence are more important for the second set of measurements than for the first one, but they are still in the acceptable range of incidences (from 56° to 65°).

Type of signal	SU 1		AV 1		SC 1		SU 2		AV 2		SC 2	
	t	σ	t	σ	t	σ	t	σ	t	σ	t	σ
High / Medium	2.50	8.51	1.32	8.45	2.36	8.56	2.00	10.0	2.15	10.5	2.04	10.0
High / Low	2.20	11.5	1.95	12.3	2.17	11.6	2.37	13.5	2.20	14.4	2.35	13.4
Medium / Low	2.21	11.5	1.87	11.9	2.11	11.4	2.35	13.6	2.24	13.9	2.32	13.5
Mean value	*2.31*	*10.5*	*1.71*	*10.9*	*2.21*	*10.5*	*2.24*	*12.4*	*2.19*	*12.9*	*2.24*	*12.3*
STD / mean	*0.07*	*0.16*	*0.20*	*0.19*	*0.06*	*0.16*	*0.09*	*0.16*	*0.02*	*0.16*	*0.08*	*0.16*
Global mean *(STD / mean)*	Thickness t =2.15 *(0.09)*						Flow resistivity σ =11.6 *(0.10)*					

Table 3.1: *Optimal parameter values for the fitted–carpet. Thickness t in millimeter and flow resistivity σ in kNsm^{-4}.*

The predicted values of the material thickness are very coherent since the measure of the coherence (*STD / mean*) is at most 0.20. All optimisations but one predict a material thickness around 2.3 mm, which is somewhat smaller than the measured value (3.82 mm). Only one set of measurements, the set denoted 'AV 1' predicts lower values of the thickness around 1.71 mm. This deviation is not due to the nature of the signal because the other time signal yields predictions similar to the other measurement data ; it was not clearly explained.

For the predictions of the flow resistivity, all measurement data are in very good correspondence. The measure of the coherence is either 0.16 or 0.19, which is a satisfactory value. As a matter of fact, the disparity in the results is only due to the predictions using the highest two microphones. However, the averaged value are in good coherence with most of the predictions.

As a result, it seems safe to consider that the averaged values are representative of all the predictions. Therefore, for the fitted–carpet, the values kept are : t =2.15 mm for the thickness and σ =11.6 kNs/m^4 for the flow resistivity.

3.4.2 Mineral rockwool

Results for the mineral rockwool are given in Table 3.2. As for the fitted–carpet, time signals, averaged spectrum and linear spectrum from averaged time signals are used. Only one measurements configuration is used for this material. The positions of the source and of the receivers are : d_s =60 cm, h_s =20.2 cm and h_r =29.3 cm, 20.5 cm, 13.2 cm. The initial values of the minimisation search are : 15 mm for the thickness and 100 kNs/m^4 for the flow resistivity.

For all the thickness predictions, the measure of the coherence is 0.04, which is good. Predicted values of the material thickness lie around 15 mm for a measured value of 15.4 mm.

The predicted values of the flow resistivity are also in a very limited range, the coherence being 0.02 at most. This set of measurement data predicts a value around 138 kNs/m^4.

Type of signal	SU 1		AV 1		SC 1	
	t	σ	t	σ	t	σ
High / Medium	15.6	139	15.9	137	15.9	137
High / Low	14.5	139	14.7	140	14.7	141
Medium / Low	14.5	136	14.9	135	14.9	135
Mean value	*14.9*	*138*	*15.2*	*137*	*15.1*	*138*
STD / mean	*0.04*	*0.009*	*0.04*	*0.02*	*0.04*	*0.02*
Global mean	Thickness		Flow resistivity			
	t =15.1		σ =138			
(STD / mean)	*(0.01)*		*(0.004)*			

Table 3.2: *Optimal parameter values for the mineral rockwool. Thickness t in millimeter and flow resistivity σ in $kNsm^{-4}$.*

Given the very good coherence obtained for these predictions, it is safe to keep the averaged values of all predicted parameters. Therefore, the kept values for the mineral rockwool are : t =15.1 mm for the thickness and σ =138 kNs/m^4 for the flow resistivity.

3.4.3 Summary

As for tube measurements, the impedance value obtained using the kept parameters is computed using the model in [10]. Values are plotted in the complex plane in Fig. 3.7(a) for the fitted–carpet and in Fig. 3.7(b) for the mineral rockwool. The thick blue line holds for the frequencies between 200 Hz and 6000 Hz and values up to 100 kHz are indicated with a dotted line. On these figures, the point of maximum absorption ($Z = \rho_0 c_0$) is indicated with a black cross.

The impedance for the fitted–carpet turns around the point of maximum absorption without getting closer. The absorption value for the fitted–carpet levels out at a value of 0.5. To the contrary, the impedance for the mineral rockwool tends rapidly to the point of maximum absorption, almost reaching 0.9 at 6000 Hz. In total, this represents two materials with very different absorbing properties.

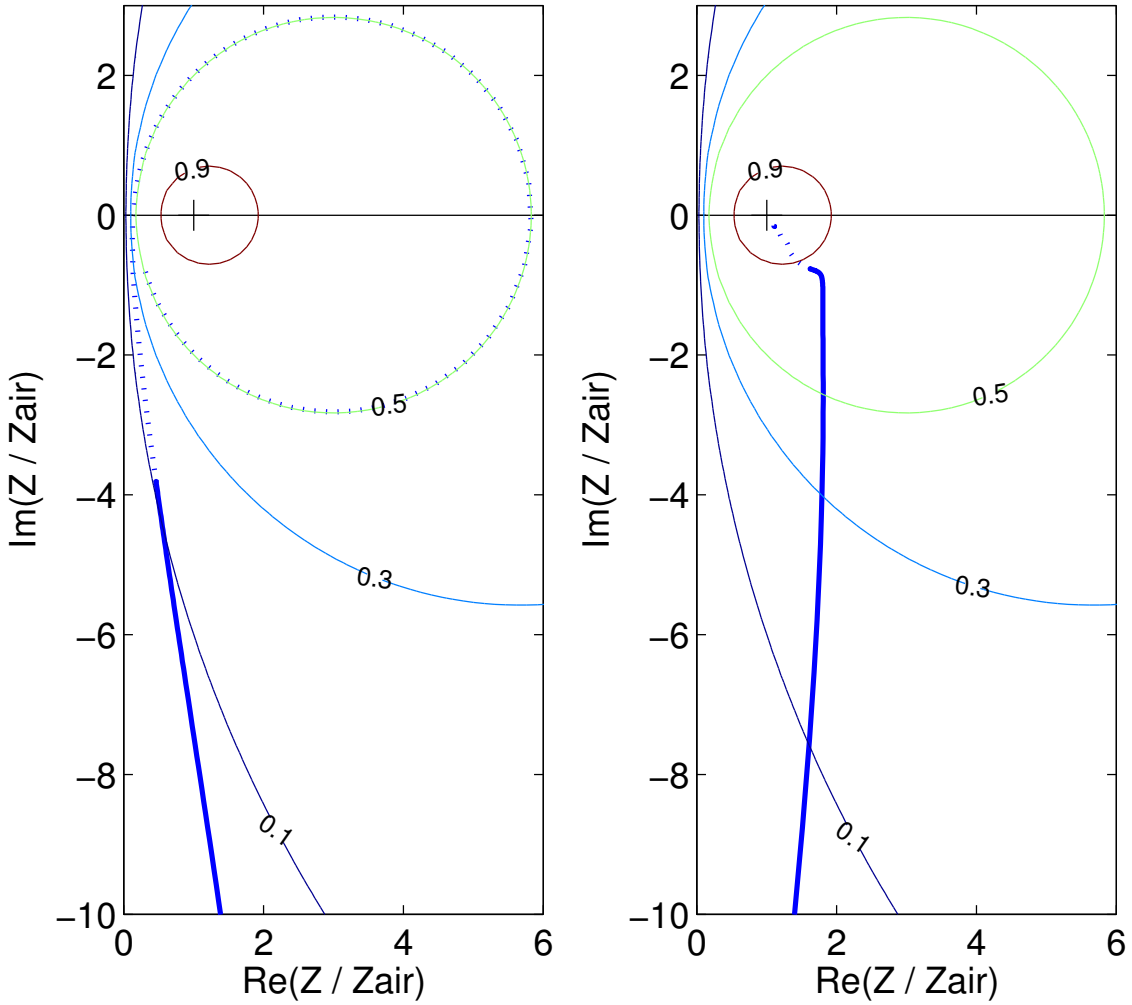

(a) Fitted–carpet : $l(\text{mm}) = 2.15$; $\sigma(\text{kNsm}^{-4}) = 11.6$

(b) Mineral rockwool : $l(\text{mm}) = 15.1$; $\sigma(\text{kNsm}^{-4}) = 138$

Figure 3.7: *Acoustical impedance of the tested materials obtained from level difference measurements – Values plotted in the complex plane.*

4 – Summary and discussion

This part presents two methods for the determination of material acoustic properties.

Firstly, the procedure using tube measurements was presented. A detailled study of the functionning of the method has been conducted, which reveals the main difficulties of the method implementation and in particular that a special car should concern the cutting of the material samples. This makes it difficult for the determination of real road properties, which is a well–known drawback of the method. However, the use of a model for the sound propagation inside the tube allows to determine the material construction parameters. In the present study, the quantity of interest are the material thickness and the flow resistivity but other material parameters could be sought.
Secondly, the so–called level difference technique has been implemented. The recommandations and the limitations of use were discussed. The implementation of this technique requires the use of a propagation model. Hence, it gives access to the desired construction parameters left as varying parameters. The ease of implementation of this technique makes it very interesting for outdoor and in–situ measurements.
According to this, the two methods implemented in the present study are complementary.

Concerning the values of the construction parameters, they are in a satisfactory correspondence for the two techniques. They are summarised in the table below.

Material	Fitted–carpet		Mineral rockwool	
	t	σ	t	σ
Tube meas.	2.25	12.9	18	108
LVD meas.	2.15	11.6	15.1	138
Final values	**2.20**	**12.25**	**15.1**	**138**

Table 4.1: *Comparison of optimal parameter values obtained from tube measurements and from level difference measurements. Thickness t in millimeter and flow resistivity σ in $kNsm^{-4}$.*

As expected for the carpet, the obtained material thicknesses are somewhat lower than the measured ones (3.82 mm for the carpet). Since the values are very coherent, the final values are the mean of the obtained values. As shown in Fig. 4.1(a), this gives values of the absorption coefficient which are somewhat lower than the measured one using the tube.
For the mineral rockwool however, tube measurements give a value which is larger than the measured one, which is 15.4 mm. In order to simulate the same global absorption properties, the flow resistivity obtained from these measurements is lower than the one obtained from level difference measurements. Therefore, it seems more reasonable to keep the values obtained with the level difference measurements. With these values, the predicted absorption coefficient value is in good agreement with the measured one, as shown in Fig. 4.1(b).

In conclusion, measurements using the level difference techniques seem more reliable for the prediction of the properties of the tested materials. Due to a simple application, this technique is less

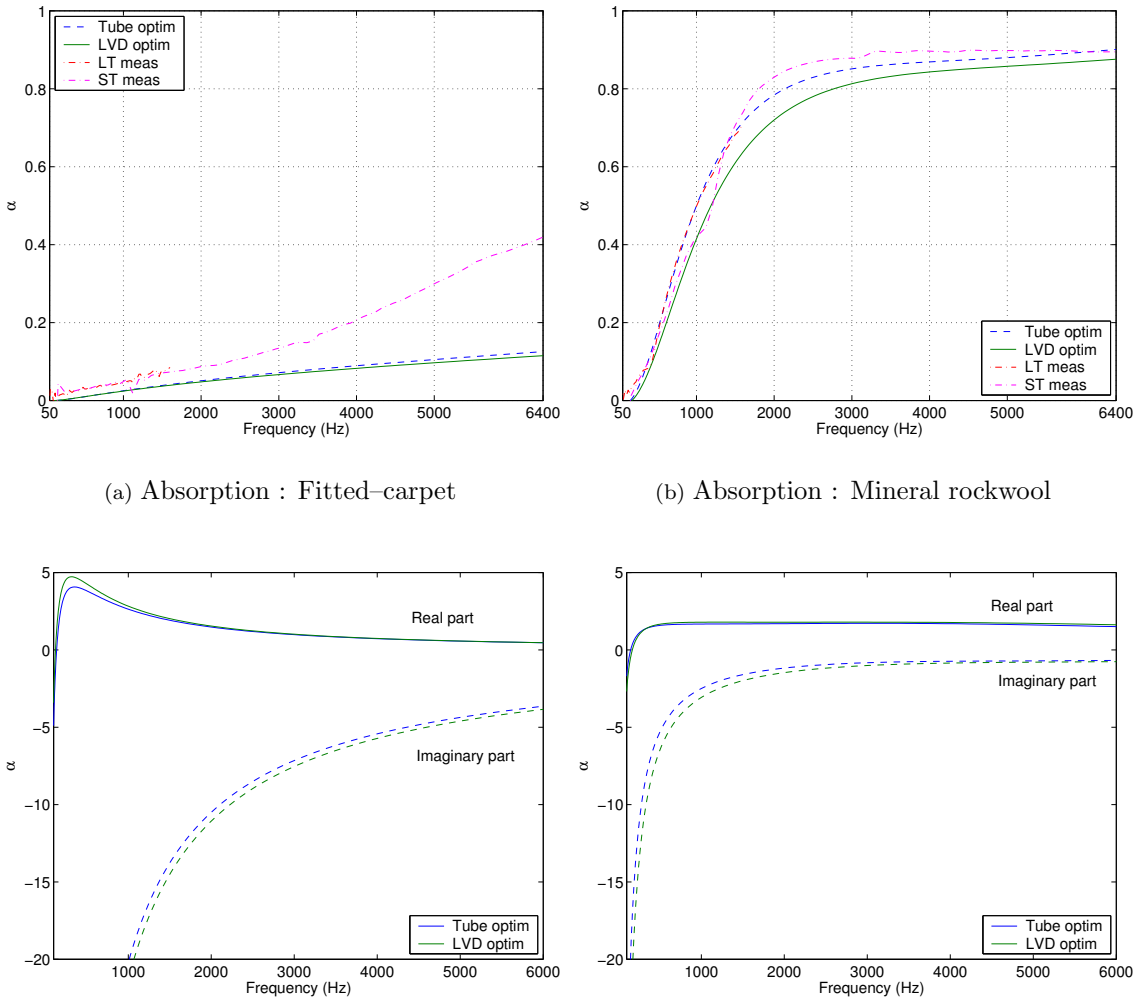

(a) Absorption : Fitted–carpet

(b) Absorption : Mineral rockwool

(c) Impedance : Fitted–carpet

(d) Impedance : Mineral rockwool

Figure 4.1: *Results for the final parameter values obtained with tube measurements or with level difference measurements. Results are compared to small tube and large tube measurements.*

subject to measurement errors. However, this requires the design of an accurate acoustic source, as the one available at the department.
With a view to prediction purposes, the resulting impedance values correspond well for the two techniques. Comparisons shown in Fig. 4.1(c) and (d) proove that the deviations observed in the parameter values do not affect strongly the value of the impedance.

References for Part II

[1] AFNOR. *Determination of sound absorption coefficient and impedance in impedance tubes – Part 1: Method using standing wave ratio.* Technical Report NF EN ISO 10534-1, 2001.

[2] AFNOR. *Mesurage in situ des propriétés d'absorption acoustique des revêtements de chaussées.* Technical Report NF EN ISO 13472-1, 2002.

[3] M. Bérengier M. Garai. *A state-of-the-art of in–situ measurement of sound absorption coefficient for road pavements.* In *17th I.C.A. Proceedings*, Rome, Italy, 2001.

[4] AFNOR. *Determination of sound absorption coefficient and impedance in impedance tubes – Part 2 : Transfer–function method.* Technical Report NF EN ISO 10534-2, 2003.

[5] ASTM. *Standard test method for impedance and absorption of acoustical materials using a tube, two microphones, and a digital frequency analysis system.* Technical Report C 384–98, 2001.

[6] W. T. Chu. *Extension of the two–microphone transfer function method for impedance tube measurements.* Journal of the Acoustical Society of America, 80(1):347–348, 1986.

[7] P. M. Morse K. U. Ingard. *Theoretical acoustics.* Princeton University Press, Dec., 1986.

[8] A. F. Seybert D. F. Ross. *Experimental determination of acoustic properties using a two–microphone random–excitation technique.* Journal of the Acoustical Society of America, 61(5):1362–1370, 1977.

[9] B. H. Song J. S. Bolton. *Investigation of the vibrational modes of edge–constrained fibrous samples placed in a standing wave tube.* Journal of the Acoustical Society of America, 113(4):1833–1849, 2003.

[10] E. Delany E. N. Bazley. *Acoustical properties of fibrous absorbent materials.* Journal of the Acoustical Society of America, 3:105–116, 1970.

[11] F-X. Bécot. *Tyre noise over impedance surfaces – Efficient application of the Equivalent Sources method.* PhD thesis, Chalmers university of technology & Insa–Lyon, 2003.

[12] M. Ögren H. Jonasson. *Measurement of the acoustic impedance of the ground.* Technical Report 1998:28, SP, Swedish national testing and research institute, 1998.

[13] S. N. Chandler-Wilde D. C. Hothersall. *Sound propagation above an inhomogeneous impedance plane.* Journal of Sound and Vibration, 98(4):475–491, 1985.

[14] S. N. Chandler-Wilde D. C. Hothersall. *Efficient calculation of the Green function for acoustic propagation above a homogeneous impedance plane.* Journal of Sound and Vibration, 180(5):705–724, 1995.

[15] Y. L. Li M. J. White and M. H. Hwang. *Green's functions for wave propagation above an impedance ground.* Journal of the Acoustical Society of America, 96(4):2485–2490, 1994.

[16] K. U. Ingard. *On the reflection of a spherical sound wave from an infinite plane.* Journal of the Acoustical Society of America, 23(3), May 1951.

[17] S-I. Thomasson. *Reflection of waves from a point source by an impendance boundary.* Journal of the Acoustical Society of America, 59(4):780–785, 1976.

[18] C. F. Chien W. W. Soroka. *Sound propagation along an impedance plane.* Journal of Sound and Vibration, 43(1):9–20, 1975.

[19] C. F. Chien W. W. Soroka. *A note on the calculation of sound propagation along an impedance surface.* Journal of the Acoustical Society of America, 69(2):340–343, 1980.

[20] J-F. Hamet. Modélisation acoustique d'une chaussée drainante - Coefficient d'absorption en incidence oblique d'un système multicouches. Rapport MMA 101 INRETS, Institut National de Recherche sur les Transports et leur Sécurité, 1989.

[21] J-M. Clairet F-X. Bécot. Effet dièdre sur plan réflecteur et sur surface absorbante – descriptif des mesures. Report LTE n°0414, Institut National de Recherche sur les Transports et leur Sécurité, june 2004.

Part III

Horn effect measurements

5 – Study background and measuring procedure

The present study is supported by a number of works, both experimental and theoretical, which are presented in the first section. The second section is dedicated to modelling purposes and reviews the existing models for the tyre noise emission. The models used in the present work, which have been partially developed at INRETS, are finally described.

5.1 Presentation of the horn effect

The so–called *horn effect* was explained by Ronneberger in [1]. It consists in the adaptation of the radiation impedance of the sources located close to the contact zone, to the wave impedance in air. The horn formed by the tyre surface and the road surface in the contact region leads to an amplification of the radiation efficiency of the sources placed in this region. This effect has been illustrated for instance in [2] an in [3]. Therefore, the tyre, which in the free–field is a bad radiator, becomes a very efficient radiator in the proximity of the road surface.

Experimentally, the horn effect is illustrated by measuring on the one hand the pressure field radiated by the tyre in the free–field due to a given excitation and on the other hand the pressure radiated by the same tyre in the presence of the road due to the same excitation. By taking the ratio of both pressure fields, amplification factors are formed which qualifies the horn effect for the given tyre and the given excitation.

Practically, it is difficult to excite tyre vibrations and to measure the sound due to these vibrations. Instead, it is usually admitted that the horn effect could be measured by using an omni–directional point source located in the contact region between the tyre and the road. For the measurement of the reference pressure field, that is when removing the tyre, it is more practical to measure the sound field radiated by the noise source when removing the road. It is this second definition of the horn effect which is used in the present work.

Furthermore, the principle of acoustic reciprocity applies in this case (see for instance [4] for the validity of the principle). This implies that the pressure field is the same if the source and the microphone exchange positions. This means that the noise source can be placed in front of the tyre and that the microphone can be placed inside the contact region. This usually results in measurement setup which are more handy due to the fact that the noise source, which usually requires a bit of space, is placed away from the contact zone. It is this type of arrangement which is used in the present work.

5.2 Review of existing models

There has been a large research effort for few decades now to model the horn effect. One of the earliest work is that presented in [5], which model the contact region as the space between two

infinite rigid planes. The multiple reflexions of sound inside this apex are calculated by using a series of image sources. This simple model has also been studied experimentally and theoretically in [6] and in [7].

One of the first model to use an approached geometry of the contact zone is the model proposed by Kropp in [8]. This model has been implemented more recently in [2] and in [3]. It is this model which is used in the present work ; it is described in §*5.3.1.*

Two models presented in [9], in [7] and in [10] should finally be mentioned because they use the exact geometry of the tyre / road interface. They are based on the boundary element method, which allows to take any shape of the tyre. This method is also suited to include the effect of the ground absorption as shown in [9].

5.3 Models used in the present work

Among the existing models, two models are for the tyre radiation are used in the present work. One is for the tyre radiation over rigid surfaces and the second one holds for the tyre radiation over absorbing surfaces.

5.3.1 Model for a rigid surface

The model for the rigid surface is based on the works of [8] and is described more in details in [11]. It is used in the present work for comparisons with measurements of *Chapter 6* and *Chapter 7*.

This model, two–dimensional, assumes the tyre to be an infinitly long cylinder. This assumption is valid as long as the wavelength in air is small compared to the tyre width.

For this representation of the tyre, the method of equivalent sources [12], also called source simulation technique, is used to implement the calculations. For this, a multipole source is placed on the axis of the cylinder to give the pressure field radiated by the tyre. To account for the presence of an acoustically rigid ground, the mirror image of the multipole source is introduced which has the same amplitude. The key point of the method is that both multipole amlpitudes are tuned so that a velocity boundary condition is best reproduced on the tyre surface. Once this is done, the radiated pressure field can be calculated at any point outside the tyre body and above the ground.

In our case, the velocity boundary condition is due to a *2D* monopole source, placed in front of the tyre. The field is calculated for a receiver placed inside the contact region, between the tyre and the road. It should be mentioned that the present implementation of the method does not allow the tyre and the road to be in contact. Instead, a small gap is introduced between the tyre and the road.

Moreover, the model is implemented for a circular cylinder or a deformed cylinder to simulate the effect of a load on the wheel axle. For this, all points placed on both sides of the contact zone centre, on a length corresponding to the contact length, are given the minimum height above the road, i.e. the gap value. The problem is then solved as for a circular cylinder using a standard pivot method.
The effect of the tyre deformation on the accuracy of the problem solving is shown in Fig. 5.1. In this figure, the conditionning number of the equation system to be solved is given as a function of the frequency, for a circular tyre and for a deformed tyre. As expected, the effect is negligible at low frequencies. Above 1500 Hz however, the conditionning number significantly increases by about 40 %. For a too large conditionning number, above a few hundred, the system becomes ill–posed

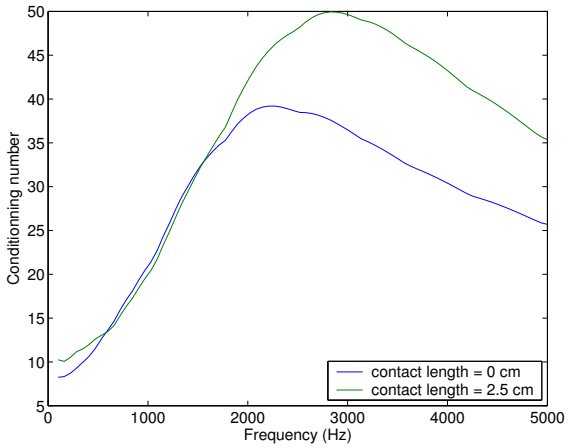

Figure 5.1: *Effect of the tyre deformation on the accuracy of the problem solving.* N_{max} *=64, collocated equation system, gap =1 mm.*

close to singular. This has for consequence that the amplitudes of the sources are determined with less accuracy. However, the values shown here are still acceptable and the solving is still expected to be numerically reliable.

5.3.2 Model for an absorbing surface

The model for absorbing surfaces is based on the previous model for rigid surfaces. It combines this latter model to a model for the sound propagation over an arbitrary impedance plane, which is also based on the equivalent sources method [13]. It results in a model for the tyre radiation over surface of arbitrary acoustic impedance. Details on this model can be found in [11].

This model, also two–dimensional, considers the tyre as an infinite cylinder. A multipole source is placed on the cylinder axis to reproduce the sound radiated by the tyre. The sound reflexions are given by a series of monopole sources placed directly on the ground surface. Hence, the sources control the value of the acoustic impedance on a small portion of ground. This method is mainly an alternative to standard integral equations.

For an absorbing surface, two boundary conditions have to be fulfilled : a velocity boundary condition on the tyre surface and an impedance boundary condition on the ground. The amplitude of the sources are tuned in an iterative process so that both boundary conditions are simultaneously fulfilled. Once it is done, the pressure field can be calculated at any point outside the tyre and above the ground.

Predictions obtained with this model are compared with measurements of the horn effect over absorbing surfaces in *Chapter 8*. For all calculations, the tyre is assumed to be perfectly circular. This corresponds to the actual measurement conditions as indicated on the desription of the experiments below.

5.4 Measurement procedure

The procedure for measuring horn effect amplification factors is described in this section.

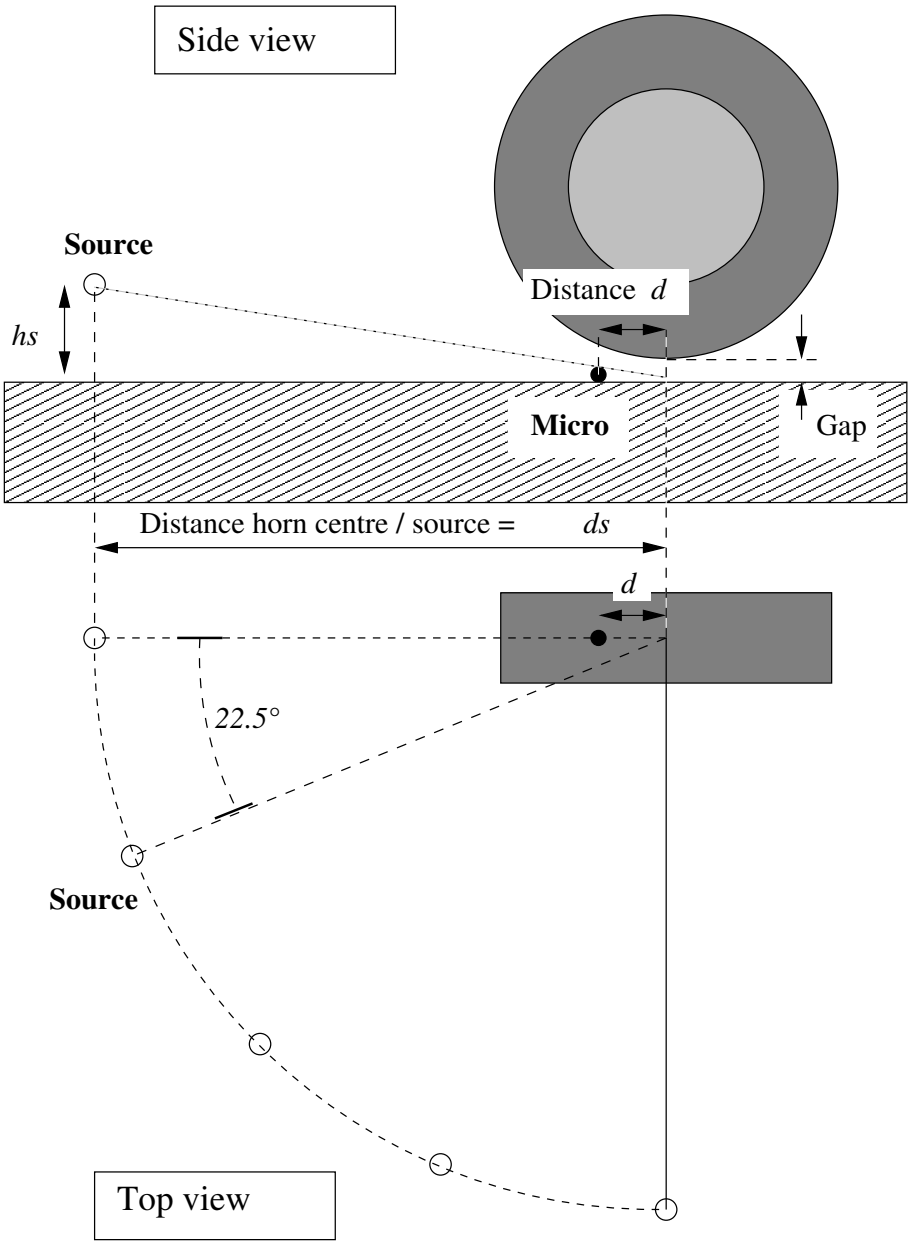

Figure 5.2: *Positions used for horn effect measurements.*

5.4.1 Source and receiver locations

For all measurements shown below, a 20 kHz sampling rate is used. This range is largely beyond the frequencies of interest, i.e. 6000 Hz.

The experimental setup is shown in Fig. 5.2.
As previously mentioned, the measurement of the horn effect amplifications is performed using the acoustic reciprocity. Therefore, the acoustic source is placed in front of the tyre, outside the horn, while the microphone is placed inside the horn region.
The acoustic source used for this experiment is that already used for level difference measurements (see *Appendix 14* for a full description of the source). The chosen positions of the source are scaled positions of pass–by noise measurement positions.

1/10-th scaled position : h_s =0.12 m and d_s =0.75 m.
1/15-th scaled position : h_s =0.08 m and d_s =0.5 m.

Two microphone locations are kept for the measurements. The positions are given as the distances from the horn centre (see Fig. 5.2).

d =0.08 m and d =0.1 m.

Due to the size of the microphone, it was chosen to put the microphone perpendicularly to the wheel plane (see Fig. 5.3(a)). The extremity of the microphone is placed at the centre of the belt (on the picture, the black line on the ground correspond to the axis of the wheel). Moreover, with this arrangement, it was not possible to put the microphone closer to the horn centre without closing the horn.

(a) Microphone inside the horn (b) Global view of the experimental setup

Figure 5.3: *Pictures of the experimental setup used for horn effect measurements.*

Measurements are performed in the plane of the tyre ("in–plane" measurements in the text below) and around the tyre ("directivity" measurements).

5.4.2 In–plane measurements

For in–plane measurements, the two positions of the source and the two positions of the microphone are used, which gives four measurement configurations. For the "directivity" measurement, only one position of the source and of the receiver are used, giving only one measurement position.
The receiver positions are summarized in the paragraph below.

5.4.3 Directivity measurements

For the directivity measurements, azimutal positions from 0° to 180° by steps of 22.5° are examined, as in the early measurements of [5]. This gives 9 measurement positions around the tyre.
Practically, it is easier to move and ajust the position of the microphone instead of moving the source (see Fig. 5.3(b)). Therefore to examine all azimutal positions, the acoustic reciprocity is used. This means that, for a position of the microphone in the front side of the contact zone, azimutal positions from 0° to 90° are measured. To measure the positions from 112.5° to 180°, the microphone is moved on the back side of the contact zone and the source is moved from 67.5° to 0°.

5.4.4 Summary of measuring positions

The measurement positions used for the in–plane and measurements for the directivity measurements are summarized in the tables below.
The cross indicates that the corresponding positions is actually used, while the line indicates that these positions are not used.

IN–PLANE	d =0.08	d =0.1
d_s/h_s =0.75 / 0.12	×	×
d_s/h_s =0.5 / 0.08	×	×

DIRECTIVITY	d =0.08	d =0.1
d_s/h_s =0.75 / 0.12	×	–
d_s/h_s =0.5 / 0.08	–	–

Table 5.1: *Source and microphone positions used for in–plane and directivity measurements.*

Real directivity angles	**0°**	**22.5°**	**45°**	**67.5°**	**90°**
Azimutal source positions	0°	22.5°	45°	67.5°	90°
Microphone position d =	+0.08	+0.08	+0.08	+0.08	+0.08

...	**112.5°**	**135°**	**157.5°**	**180°**
...	67.5°	45°	22.5°	0°
... d =	-0.08	-0.08	-0.08	-0.08

Table 5.2: *Azimutal source positions and microphone positions used for directivity measurements.*

6 – Cylinder over a rigid surface

This chapter presents measurements of horn effect amplifications for a cylinder over a rigid surface. The experimental setup is first described and measurements results are given. Comparisons to predictions using a *2D* model for the tyre radiation are finally presented and discussed.

6.1 Principle of the measurements

6.1.1 Experimental setup

(a) Inside view

(b) External view with the source and the microphone

Figure 6.1: *Experimental setup of the cylinder used for the measurements.*

Measurements are performed over a rigid surface. This latter is the wooden plate described in §*3.3.1* (see [14] for construction details).

The cylindrical structure, which is shown in Fig. 6.1(a), is laid directly on the surface with no additional load than its own weight. It is made of four identical tyres mounted on the same axle to give a circular shape to the structure and to stiffen it up. The dimension of these tyres is 165/65 R13.
The surface of the cylinder is made of a Kelco© sheet, of 1.5 mm thickness and of dimensions 1.26×2.50 m^2. This sheet is semi–rigid and is assumed to be acoustically rigid. The resulting structure has a length of 1.26 m and a diameter of 0.2738 m. For obvious reasons, only in–plane measurements are performed (see *Section 5.4*).

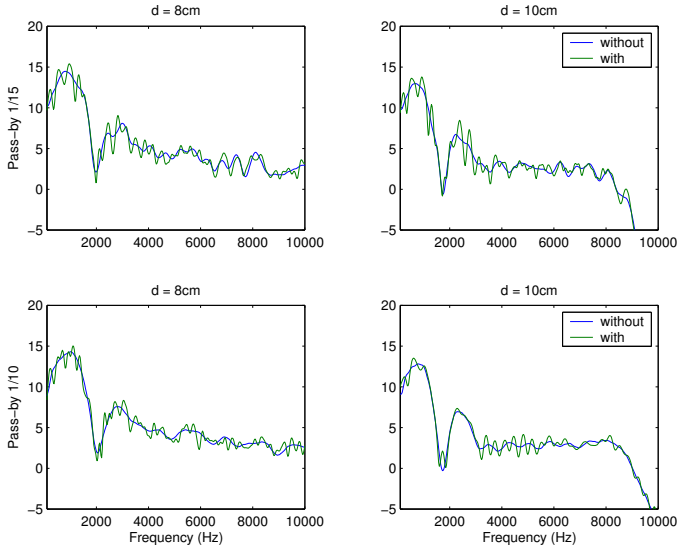

Figure 6.2: *Horn effect for a cylinder over a rigid surface : all results.*

6.1.2 Recorded signals

The cylinder structure built in this way has a finite length. With a view to compare the measurement results with predictions from a two–dimensional model, it may be of interest to remove the diffraction occuring at the end of the cylinder structure. This is done by adjusting the length of the weighting window (force window in this case) applied to calculate the frequency spectrum.

Therefore, two measurements are performed with the cylinder and without the cylinder for the reference measurements, each time, including or excluding the diffraction at the edges. This gives in total four measurements.

6.2 Measurement results

Measurements are shown in Fig. 6.2 for all measurement positions, with and without edge diffraction. The effects of diffraction are more visible as the source gets closer to the cylinder. Moreover, these effects decrease as the microphone moves away from the horn centre. Removing these effects correspond to consider the cylinder as having an infinite length.

In Fig. 6.3, measurements obtained using the source position at d_s =0.5 m are compared to measurements obtained with d_s =0.75 m. Results are shown here for the measurements excluding the diffraction effects for frequencies from 10 Hz to 6000 Hz.
For the two positions of microphone considered here, the correspondence between the two sets of data is good. This proves that the measured amplification factors are valid. If deviations were observed, this could be due to a measurement performed in the near–field of the source or to vibrations of the cylindrical shell contributing to the pressure field.

Finally, the measured amplification factors are typical of the horn effect. The amplification increases with frequency up to a maximum level around 900 Hz and shows interferences at higher frequencies, which in the present case, are not strongly pronounced. To the contrary, above around

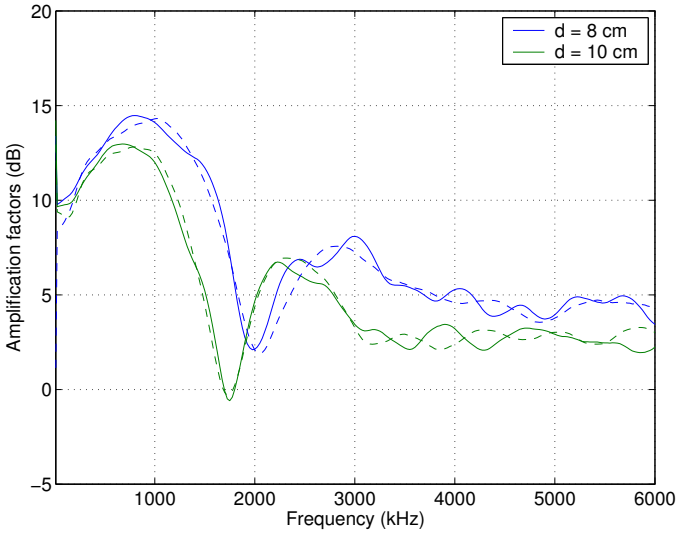

Figure 6.3: *Horn effect for a cylinder over a rigid surface : comparison of the different measurement positions. Full lines : d_s =0.5 m ; broken lines : d_s =0.75 m.*

3000 Hz, the amplification levels out to around 3-5 dB depending on the position of the microphone inside the horn. This level appears to be higher if the microphone is closer to the horn centre. Moreover, as expected, the level of maximum amplification decreases if the microphone is moved away from the horn centre, falling from around 15 dB for d =8 cm to 13 dB for d =10 cm.

6.3 Comparison to *2D* tyre model predictions

In this section, the measured amplification factors presented above are compared to predictions obtained using the *2D* model for the tyre radiation of [3] (see also [11] for further details on the model functionning).

6.3.1 Model implementation

The model, two–dimensional, assumes a infinite rigid cylinder. The sound field is reproduced by a multipole source. The presence of an infinite rigid plane is accounted for by introducing the mirror image of the multipole source. For sound field predictions, the amplitude of the multipole is tuned according to a boundary condition given on the tyre surface. Once this is done, the pressure field can be calculated at any point outside the tyre body and above the road surface.

For the simulations shown below, the model is implemented using a 64-th order multipole. The cylinder diameter is the tyres' diameter plus the thickness of the envelop, giving the structure a diameter of 0.2738 m.
The model uses the real locations of the source and of the microphone. The source is placed at the 1/15-th pass–by scaled position in front of the tyre. The microphone is placed inside the horn at 3.2 mm above the surface, height which corresponds to the half the diameter of the microphone capsule.
The boundary condition is given as the velocity distribution due to a two–dimensional monopole

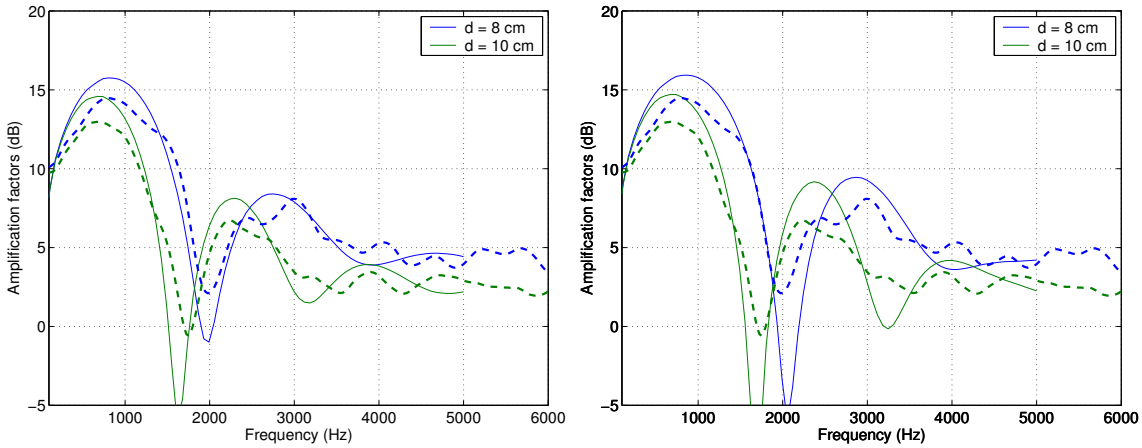

(a) Circular cylinder

(b) Deformed cylinder

Figure 6.4: *Comparison between measurements and predictions of horn amplification for an infinite cylinder over a rigid surface. Measurements : broken lines ; model predictions : thin lines.*

source placed in front of the tyre at the position of the noise source. The collocation method is used, which means that the number of points used to discretised the tyre surface equals the number of modes which can be described by the multipole, namely $2N_{max} + 1$.
The gap between the tyre and the road surface is set to 1 mm.

In addition, the model is implemented for a circular tyre or a deformed tyre (see §*5.3*). The value of the contact length was estimated on the real cylinder structure during the measurement campaign. For a deformed tyre, the model uses a 2.5 cm contact length.

6.3.2 Comparison results

Measurements are compared to results from the multipole model in Fig. 6.4(a) for a circular tyre and in Fig. 6.4(b) for a deformed tyre.

As expected, the two implementations of the model give very similar results in the low frequency range up to around 1000 Hz. At higher frequencies, the model with the deformed tyre predicts interferences which are more pronounced. In this case indeed, the tyre curvature in the contact zone is more important than for a circular tyre. This leads to more rapid interferences than when the sound waves are smeared out inside the horn. At these frequencies, the curvature of the circular tyre may be more realistic.

However, for the two models, the interference pattern is correctly reproduced and the levels in the high frequency range are correctly estimated. The shift in frequency which can be observed may be due to an error in measurement of the microphone position. Moreover, the two models does not succeed to predict the correct maximum level of amplification. This is due to the two–dimensional simplifications of the model, leading to an over–estimation of the amplification at low frequencies.

In total, the deviations observed are acceptable, and the overall agreement is satisfactory for the two models on the whole frequency range examined.

6.4 Summary

This chapter presents measurement performed using an acoustically rigid cylinder placed over a rigid surface.

The finite length of the cylinder leads to diffraction effects at the edges of the cylinder. These effects can be removed by an adapted filtering.
Measurements shown here are typical for the horn effect over a rigid surface. The amplification increases with frequency up to a maximum level, around 15 dB in the present case. At higher frequencies, the amplification presents interferences and levels out at around 3 to 5 dB depending on the position of the microphone inside the horn.

Measurements are also compared to predictions obtained with a two–dimensional model for the tyre radiation. The model was implemented for a circular and a deformed tyre. Results obtained with the two models are in good correspondence with measurements as the maximum deviation is 2 dB on the whole frequency range.

Finally, this structure could not be used for measurements of horn amplifications over an absorbing surface. Because the absorbing materials used in the present work have a surface, the properties of which may be affected by the load of the cylinder.

7 – Single wheel over a rigid surface

In this chapter are presented measurements of horn amplifications for a single wheel placed over a rigid plane. The measurement procedure is first described. Measurement results are given in a second part and compared to model predictions in a third part.

7.1 Principle of the measurements

Figure 7.1: *Global view of measurement for a single wheel over a rigid surface.*

For this experiment, the floor of the laboratory is used as the rigid plane (see §*3.3.1* and [14] for more details).

The tyre is a passenger car tyre with a smooth belt. Its dimensions are 155/70 R13 75S. This means that the width is 155 mm and the diameter is 0.2736 m.
The tyre is held from above using a metallic frame as shown in Fig. 7.1. Doing so, the tyre oscillations in the rolling direction are avoided to a large extent. Moreover, the holders are adjusted so that the tyre sidewalls are vertical.
This frame is finally used in the last part of the experiment to suspend the tyre and to adjust the gap between the tyre and the floor to the desired value. The value of the gap introduced corresponds to the estimated thickness of the mineral rockwool, namely 15 mm.

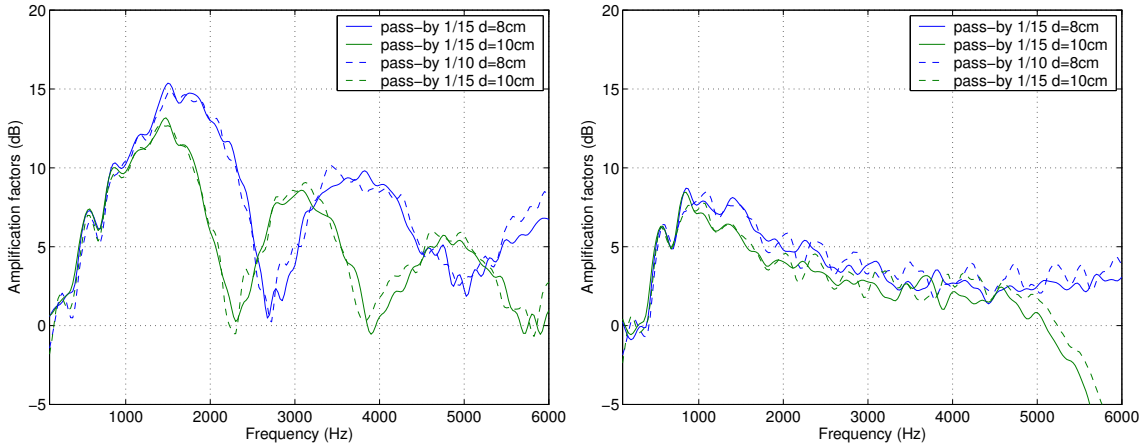

(a) Tyre in contact

(b) Tyre 15 mm above the surface

Figure 7.2: *In–plane measurements of horn effect amplifications for a single wheel over a rigid surface.*

Both in–plane and directivity measurements are performed. Fig. 7.1 shows for instance a picture of the measurement for 90° of incidence.

7.2 Measurements results

Measurements are presented in this section for a tyre in contact with the surface and for a tyre 15 mm above the surface. Both in–plane (Fig. 7.2) and directivity measurements (Fig. 7.3) are shown and discussed.

7.2.1 In–plane measurements

The observation of the two situations of Fig. 7.2 reveals that the correspondence between the two scaled pass–by positions at high frequencies is not as good as for the cylinder. Deviations of around 1 dB are observed for frequencies beyond 4000 Hz. For a 15 mm gap, deviations are observed for frequencies as low as 2000 Hz. This may be due to the fact that the microphone positions are not exactly the same between the two measures.

For the tyre in contact (see Fig. 7.2(a)), the measurements are very similar to those shown in [3] or in [7]. At very low frequency, the tyre width is small compared to the sound wavelength, yielding zero amplification factors. With increasing frequencies, the amplification increases up to a maximum level beyond which interferences are observed. The maximum amplification decreases and the frequency at which it occurs also decreases if the position of the microphone further away from the horn centre.
For the positions tested here, the maximum levels reach 15 dB for d =8 cm and 13 dB for d =10 cm. Moreover, the interferences occuring beyond this maximum level reach 10 dB and 8 dB for

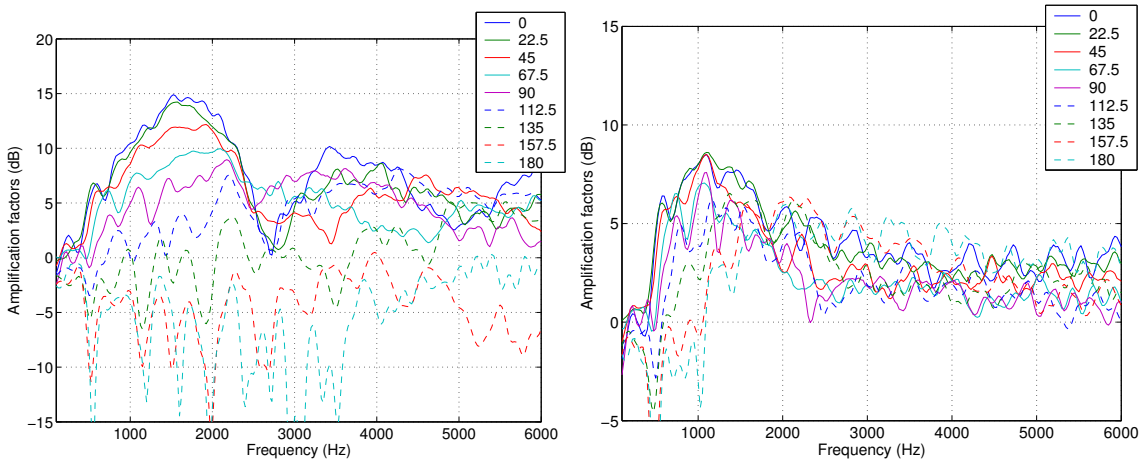

(a) Tyre in contact

(b) Tyre 15 mm above the surface

Figure 7.3: *Directivity measurements of horn effect amplifications for a single wheel over a rigid surface.*

the two positions of the microphone. In total, the horn effect is significant for frequencies from around 1000 Hz up to 4000 Hz.

If a 15 mm gap is introduced (Fig. 7.2(b)), the maximum amplifications are significantly lower than if the tyre is in contact, as expected. The maximum levels lie around 9 dB at around 900 Hz for the two positions of the microphone inside the horn. At higher frequencies, the amplitude of the interferences, at most 1 dB, are much smaller than in the previous case. The amplification decreases slowly to reach a minimum around 3 dB at 4500 Hz.
These measurement results will be discussed further in the presentation of the measurements over the mineral rockwool.

7.2.2 Directivity measurements

Results are shown in Fig. 7.3 for the directivity measurements performed with the tyre in contact or with a 15 mm gap. Results are presented for all azimutal positions from 0° to 180°.

For the tyre in contact, the maximum amplification factors are obtained for 0°, as expected. For larger azimutal positions, the maximum amplification level decreases and the frequency at which it occurs is shifted toward higher frequencies. At 90°, the maximum reaches almost 10 dB around 2000 Hz, which is quite substantial. In total, this gives amplification factors comprised between 15 and 10 dB in the frequency range of maximum contribution to A–weighted noise levels. It is thus expected that the horn effect contributes significantly to the measured pass–by noise.
For 157.5° and 180°, the amplification factors become negative on the entire frequency range. For these positions and if the tyre is in contact, the horn is closed forming thus a barrier between the microphone and the noise source. Finally, for all measurement positions, this gives amplification factors ranging from +15 dB to -15 dB. Therefore, the influence of the horn effect for these positions on pass–by noise levels is expected to be very small.

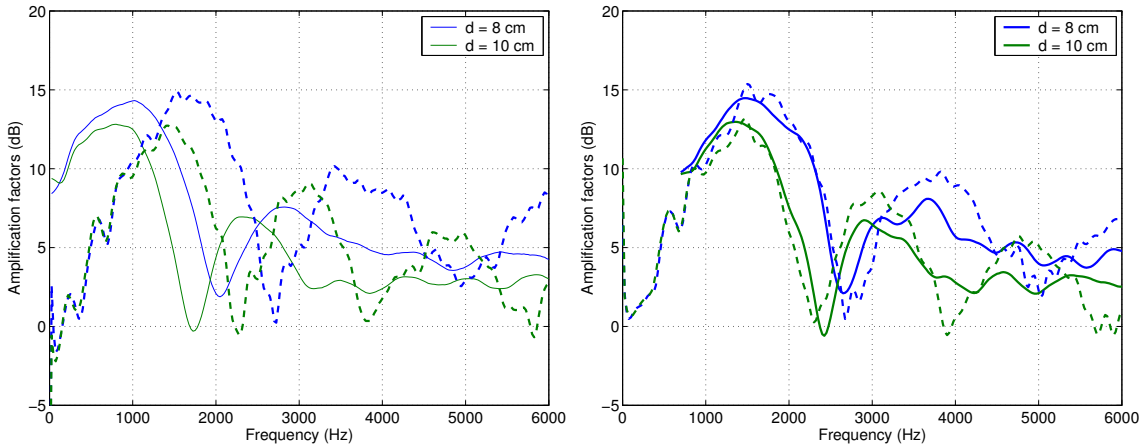

(a) Without correction

(b) With correction : f_{shift} =675 Hz

Figure 7.4: *Measurements for a cylinder corrected for comparisons with measurements for a single wheel. Single wheel : broken lines ; cylinder : full lines.*

The picture changes when the tyre is 15 mm above the surface. The maximum amplification, around 13 dB, is obtained for three positions : 0°, 22.5° and for 45°. In this case, except at low frequencies for 157.5° and 180°, the amplifications are always positive. This means that for all incidences, the presence of the tyre leads to a higher sound levels compared to when the tyre is removed. Moreover, at frequencies above 3000 Hz, the amplification factors for all positions have a value around 3 dB ±2 dB. These measurements are discussed further in §*8.2.3*.

7.3 Comparison to *2D* tyre model predictions

Since the model assumes a infinite cylinder, the sound pressure field can only be predicted in a plane which is perpendicular to the cylinder axis. Therefore, the measurements considered here for comparisons are in–plane measurements only for a 1/15-th scaled pass–by source position.

7.3.1 Correction 2D / 3D

As shown in Fig. 7.4(a), measurements for the cylinder must be corrected for comparisons with single wheel measurements. In particular, the maximum amplification is measured with the cylinder at lower frequency than that obtained for the tyre. This is due to the fact that the tyre has a finite width compared to the cylinder examined previously. This effect has been illustrated in [6] which quotes works from Ronneberger, and in [7]. In these works, the horn is formed by two planes, one of which is of finite width. It is shown that if the width of one plane decreases, the maximum amplification decreases and is shifted towards higher frequencies.

As an example of the application of this procedure, measurements for a single wheel are compared to measurements obtained using a long cylinder. For this, the frequency of maximum amplification is searched and the frequency shift is determined. Note that, in the present case, this is an

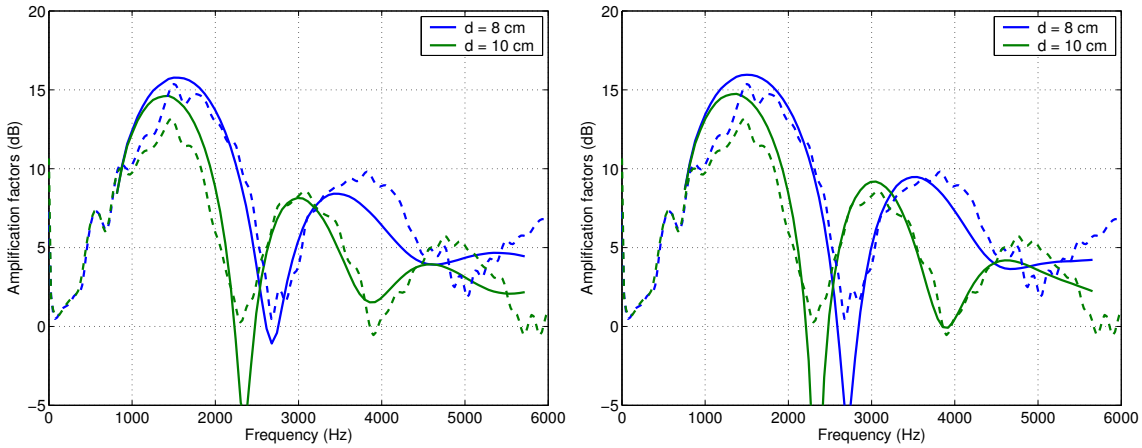

(a) Circular tyre : f_{shift} =717 Hz

(b) Deformed tyre : f_{shift} =655 Hz

Figure 7.5: *Comparisons between measurements for a single wheel and model predictions corrected for 2D simplifications. Surface is rigid. 2D model : lines ; single wheel : broken lines.*

approximation because the two structures have slightly different radii. Therefore, one cannot state definitely on the levels of maximum amplification.
Comparison results are presented in Fig. 7.4(b) where a frequency shift of 675 Hz has been applied on the measurements for the cylinder. Regarding the approximation due to the different structure radii, the correspondence is good for frequencies from 700 Hz to 2500 Hz, which coincides with the frequency range of interest for traffic and tyre noise. Therefore, this procedure is applied for the comparisons between model predictions and single wheel measurements.

7.3.2 Model implementation

Details on the implemented model can be found in [3] and in [11].

The parameter values for the present experiment are the same than for the implementation of *Section 6.3*, except for the cylinder radius.
In the present implementation, the cylinder has a diameter corresponding to the tyre radius, namely 0.2736 m. The tyre surface is discretised using $2N_{max} + 1$ =129 points and the gap between the cylinder and the surface is set to 1 mm. The model uses either a circular cylinder or a deformed cylinder. For this latter cylinder, the contact length is estimated to be 2.5 cm.
The model uses real positions of the source and of the receiver. This means that the source is placed in front of the tyre while the receiving point is located inside the horn region at 3.2 mm above the surface.

7.3.3 Comparison results

Results are compared in Fig. 7.5(a) for a circular tyre where a frequency shift of 717 Hz is applied. Fig. 7.5(b) shows the results obtained for a deformed tyre with a frequency shift of 655 Hz, which

is very close to the value of the frequency shift obtained previously for the cylinder of finite length, i.e. 675 Hz.

The two different model implementations give very similar results in the low frequency range up to around 2000 Hz. As expected, they predict a somewhat higher amplification than the one measured.
At higher frequencies, deviations are observed between the two model predictions. Particularly, the interference at 2500 Hz is more pronounced in the case of a deformed tyre. Moreover, this latter implementation gives correct predictions up to a frequency which is higher compared to the model using a circular tyre. The highest frequency of correct predictions is almost 5000 Hz for the model using a deformed tyre.
Therefore, in both cases, the levels are correctly predicted on the main frequency range of interest for traffic noise and the frequencies at which they occur are well estimated.

7.4 Summary

This chapter presents measurements of horn effect amplification for a single wheel placed over a rigid surface. Both in–plane and directivity measurements were performed.
For a tyre in contact with the surface, the amplification factors are very similar to those presented in [5] or in [3]. Maximum levels are obtained in the plane of the wheel and reach 15 dB at around 1500 Hz. For other incidences, the amplification factors are lower and becomes negative for measurements on the back of the tyre. This gives in total amplification factors from +15 dB to -15 dB for all incidences.

Measurements were also performed for a gap between the tyre and the surface, which corresponds to the thickness of the mineral rockwool. These measurements are mainly dedicated to comparisons with the measurements performed over the mineral rockwool.
In this case, there is lower disparity between the measurements for all incidences than in the previous situation. The maximum levels reach around 8 dB at 1000 Hz. At higher frequencies, the measured amplifications level out to around 3 dB for all incidences.

With a view to prediction purposes, it is shown that a frequency shift could be applied which give good correspondence between measurements using a cylinder and measurements using a single wheel. With this type of correction, predictions of horn effect using the model of [11] correspond well with the measurements for frequencies between 1000 Hz to 4000-5000 Hz.

8 – Single wheel over an absorbing surface

This chapter presents measurements performed over absorbing surfaces. The absorbing materials used for this are the fitted–carpet and the mineral rockwool presented in *Chapter 1*. Both in–plane and directivity measurements are performed for the two surfaces. Measurement results are presented and comparisons to model predictions are finally discussed.

8.1 Principle of the measurements

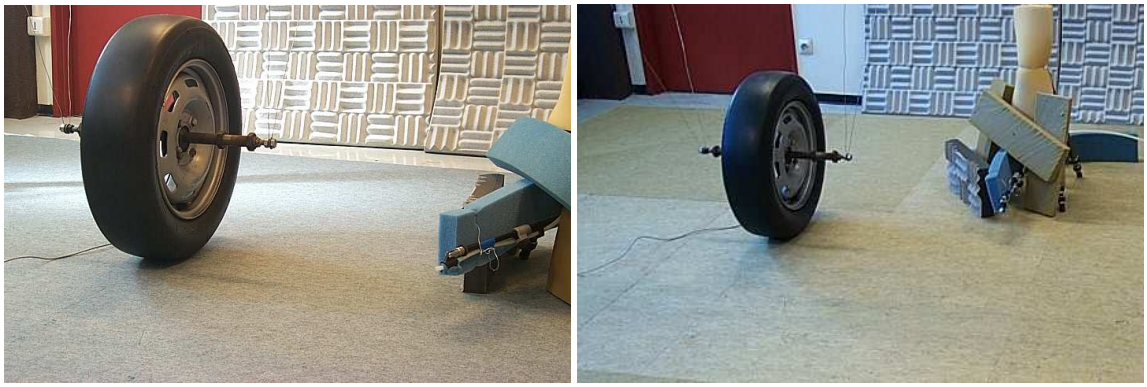

(a) Fitted–carpet (b) Mineral rockwool

Figure 8.1: *Picture of measurements over the absorbing surfaces.*

The same tyre as for horn effect over a rigid surface is used. Its dimension is 155/70 R13. The previous metallic frame is also used in this experiment to avoid that the tyre compresses the surface and changes the acoustic properties of the surface in this region. Calculations and measurements presented in [11]show that the surface impedance in this region controls to a large extent the measured sound pressure levels. Therefore, the contact length between the tyre and the ground is assumed to be very small.

The impedance surface consists of a layer of an absorbing material laid on top of an acoustically rigid surface. Two absorbing material are chosen to represent one rather low and one rather high absorbing surfaces. The material chosen to be of the first kind is a fitted–carpet and the material of the second kind is a mineral rockwool. The properties of the hardbacked surfaces obtained with this arrangement are given in §*3.3.1.*

The fitted–carpet is laid directly on the floor of the laboratory. The surface covered by the fitted–carpet has an area of 3×3 m^2. The mineral rockwool is laid on top of a wooden support, the

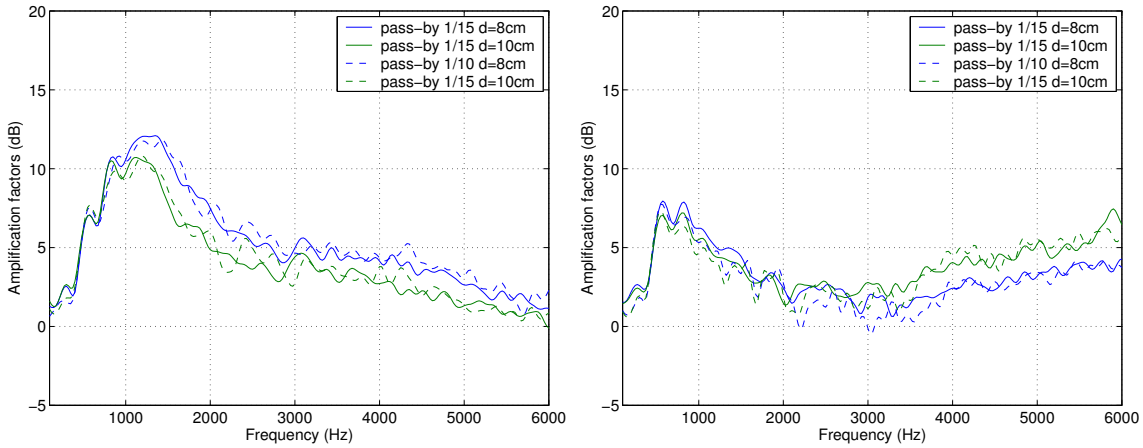

(a) Fitted–carpet

(b) Mineral rockwool

Figure 8.2: *In–plane measurements of horn effect amplification for a single wheel over an absorbing surface.*

surface of which has been tested to be acoustically rigid. The covered surface is 3.6×3 m^2. The properties of these hardbacking surfaces are given in §*3.3.1*.

Measurements are performed in the plane of and around the wheel for the tyre in contact with the impedance surface. An additional gap between the tyre and the surface does not present any interest in the case of an absorbing surface.

8.2 Measurements results

Fig. 8.2, respectively Fig. 8.3, presents the in–plane measurements, respectively the directivity measurements, for both the fitted–carpet and the mineral rockwool.

8.2.1 In–plane measurements

For the two absorbing materials, the correspondence between the two pass–by positions is good on a large frequency range. The deviations observed, which do not exceed 2 dB, are certainly due to slight changes in the measurements positions.

The horn effect amplifications for the fitted–carpet are similar to those obtained over a rigid surface for the tyre in contact. This could be expected regarding the very low absorption power of the material up to around 3000 Hz. However, the maximum levels are somewhat lower than for the rigid surface ; they reach 12 dB in the present case. The frequencies of maximum amplification are also shifted toward the low frequency range compared to the rigid case. They occur here at 1100 Hz to 13000 Hz depending on the microphone position inside the horn.
Beyond this frequency, the amplification decrease uniformly until almost zero amplification at 6000 Hz. In this frequency region, the absorption coefficient increases also uniformly from 0.05 to 0.15 at 6000 Hz, which still represents very low absorption properties.

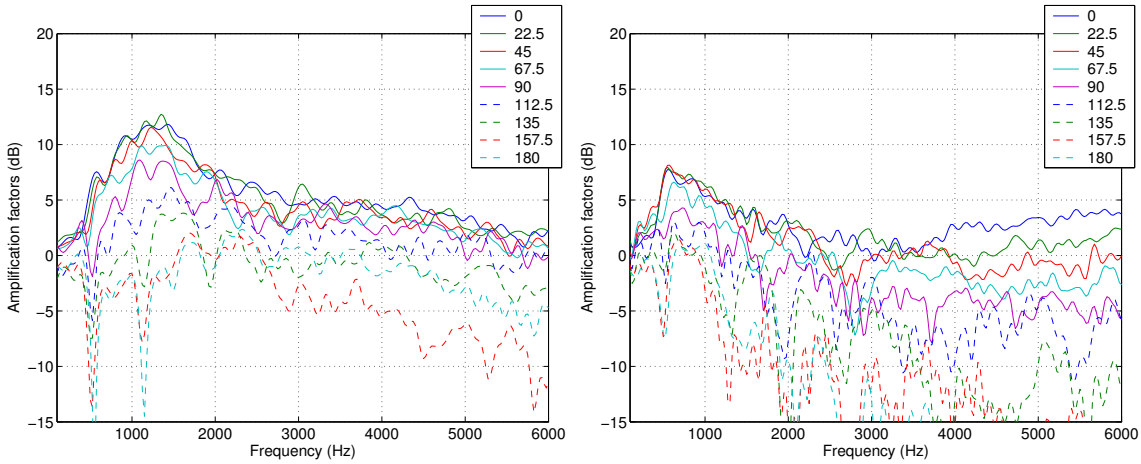

(a) Fitted–carpet

(b) Mineral rockwool

Figure 8.3: *Directivity measurements of horn effect amplification for a single wheel over an absorbing surface. 2D model : lines ; single wheel : broken lines.*

The horn effect amplifications over the mineral rockwool (see Fig. 8.2(b)) are very similar to those obtained in [11] for a similar surface. The maximum levels reached in this case are somewhat lower than those obtained for a rigid surface, i.e. 7 dB here against 8 dB for the rigid case. Compared to the rigid case, the frequency of maximum amplification is shifted toward lower frequencies, namely from 900 Hz for the rigid surface to 600-800 Hz in the present case.
As for the fitted–carpet, the amplifications at higher frequencies decrease to reach near to zero amplification at 3000 Hz. In frequency range, the absorption coefficient increases uniformly up to 0.8, which represents a high absorption. Above 3000 Hz, contrary to the fitted–carpet, the amplification levels increase again. At these frequencies, the absorption coefficient still increase, but slowlier than at lower frequencies, and finally levels out around 0.9 at 6000 Hz. This increase of horn amplification factors is fairly surprising. However, this is certainly a local interference effect and this is not expected to be representative of global quantities like the acoustic power.

8.2.2 Directivity measurements

Directivity measurements are shown in Fig. 8.3(a) for the fitted carpet and in Fig. 8.3(b) for the mineral rockwool.

For the fitted–carpet, the maximum level is found for 0° and for 22.5° of incidence at around 1200 Hz. For increasing incidences, the amplification levels decrease from 13 to 8 dB on the frequency range between 100 Hz up to 1500 Hz. This level of amplification, quite substantial, is expected as the absorption coefficient is less than 0.1 in this frequency range.
In the frequency range from 2500 Hz to 6000 Hz, the amplifications measured in the front side of the tyre are very similar for all incidences : they all decrease from 5 dB to almost zero amplification at 6000 Hz. Moreover, the lowest measured amplification is obtained not for 180° as expected but for 157.5°. In total, the measured amplification levels present less disparity in this case than for a tyre in contact with a rigid surface.

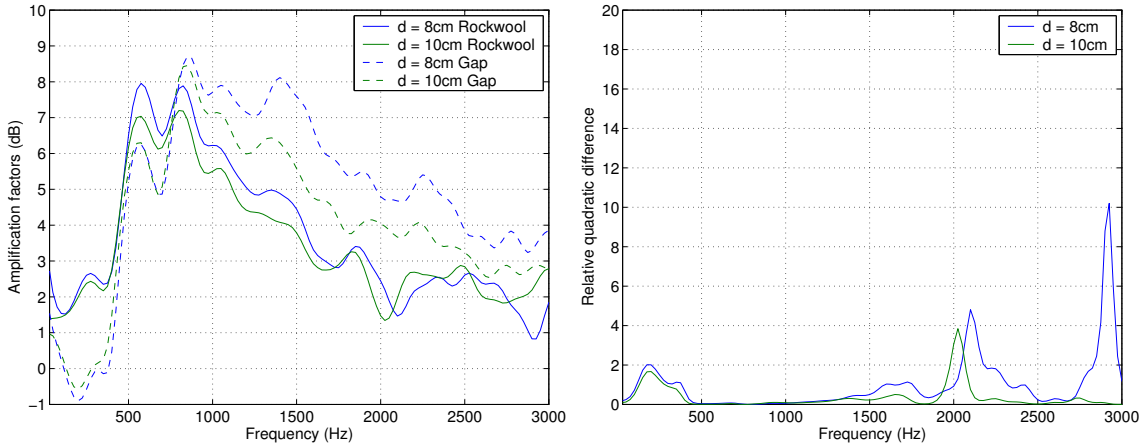

(a) Horn effect amplifications

(b) Relative quadratic difference

Figure 8.4: *Comparison between horn amplifications over mineral rockwool and for a tyre 15 mm above a rigid surface. In–plane measurements of Fig. 8.2(b) and Fig. 7.2(b) – 1/15-th source position.*

For the mineral rockwool, amplification levels for 0° to 45° of incidence are very similar for frequencies from 100 Hz to 2000 Hz. The maximum level, around 8 dB, is obtained simultaneously for these three positions at around 500 Hz. At 1000 Hz, the frequency of maximum contribution to A–weighted levels, the amplification factors still reach around 5 dB, while the absorption coefficient of the surface is around 0.4 at this frequency.
At higher frequencies, the amplification decreases with frequency to reach zero amplification at 2500 Hz. In the low frequency range, only measurement position in front of the tyre give positive amplification factors. For measurement positions on the back of the tyre, the amplification is always negative.

In conclusion, meanwhile the maximum of amplification decreases for an absorbing surface, the relative contribution from incidences out of the plane of the wheel increases with increasing absorption of the road surface.

8.2.3 Effect of an absorbing material on the horn amplification

From an academic point of view, it is of interest to compare measurements performed for a tyre in contact with the surface of rockwool and for a tyre 15 mm above a rigid surface. The second situation corresponds to the first situation where the layer of absorbing is removed, leaving thus the hardbacking surface with a gap corresponding to the material thickness. By doing so, the effect of the absorption due to the material can be estimated.

Comparisons of horn effect amplification factors are shown in Fig. 8.4(a). At frequencies below 500 Hz, the amplification obtained over the rockwool are larger than those obtained if the material layer is removed. This illustrates the fact that the absorption power of the rockwool is very low at these frequencies. In the high frequency range, the situation is reversed and the amplification

measured with the rockwool are lower than those obtained if the rockwool layer is removed. The cross–over frequency between these two situations is around 800 Hz.

In Fig. 8.4(b) are shown the quadratic differences relative to the value of the horn amplifications measured over the rockwool, obtained for the two positions of the microphone inside the horn. Besides the isolated peaks which are certainly due to changes in the interference pattern, the differences are very small on most of the frequency range examined here. On this frequency range, the absorption coefficient increases rapidly from 0.05 up to 0.8 at 3000 Hz. This means that the surface absorption has a linear effect on the horn effect measured in the plane of the wheel. This further implies that the estimation of the influence of an absorbing surface on the horn effect from the knowledge of its absorption properties is possible. However, the exact determination of the procedure would require further work and is not discussed further.

8.3 Comparison to *2D* tyre model predictions

8.3.1 Correction *2D* / *3D*

As for the tyre radiating over a rigid surface, a correction has to be applied to correct for the finite width of the tyre in the measurements.

In the model used here [11], the calculation of the tyre radiation is separated from the calculation of the radiation from the ground sources, which represent the reflected sound field. To fit with the measurements, only the field radiated by the tyre has to be corrected ; the field from the ground sources does not need to be corrected because the surface is assumed to be sufficiently long in the direction of the tyre width.
For different absorbing surfaces, this gives a tyre radiation which is corrected in the same way. However, the contribution from the ground sources increases with increasing absorption properties. In total, this gives a correction term which is expected to be smaller for surfaces having larger absorption properties.

Therefore, the value of the frequency shift is estimated visually to give an acceptable fit with the measurements. For the fitted–carpet, a frequency shift of 500 Hz is applied and for the mineral rockwool, a frequency shift of 100 Hz is applied.

8.3.2 Model implementation

The model used for the prediction of the tyre radiation over an absorbing surface is described in [11]. This model uses the model for the tyre radiation over a rigid surface described in [3] and used previously. Since the tyre used for this experiments is the same as for the rigid surface, this part of the model is implemented using the same parameters values as in *Section 7.3*.
A 64-th order multipole is placed at the centre of the infinite cylinder, having a diameter of 0.2736 m. The tyre surface is discretised into $2N_{max} + 1$ =129 points. For the present simulations, the tyre is assumed to be circular. A gap of 1 mm is set between the tyre surface and the ground.

The source is placed at the 1/15-th scaled pass-by position and the sound pressure levels are calculated for the microphone at d =8 cm and d =10 cm from the horn centre.

The ground is discretised from 0.2736 m on the back side of tyre to 0.6 m ahead of the source location. As recommended in [11], the length of the surface element should be at most equal to the value of the gap between the tyre and the road. Therefore, all elements have the same length,

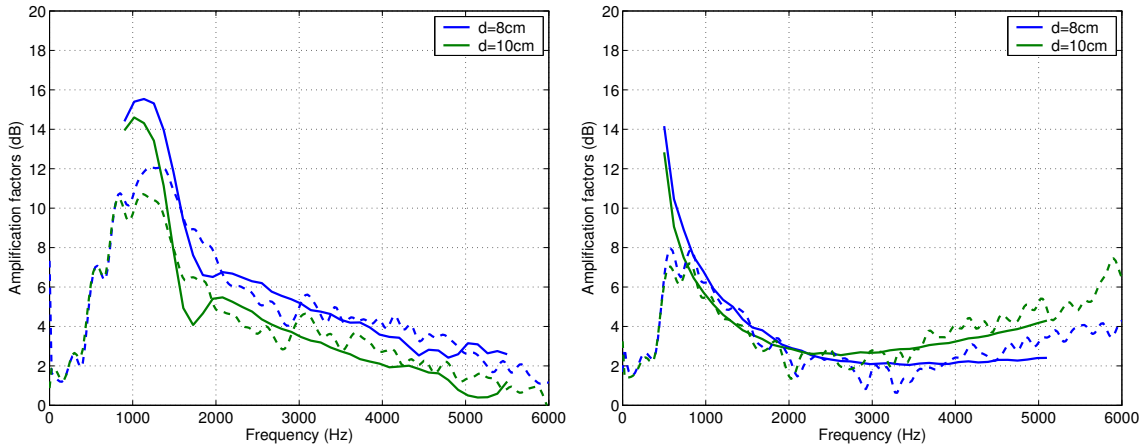

(a) Fitted–carpet : f_{shift} =500 Hz

(b) Mineral rockwool : f_{shift} =100 Hz

Figure 8.5: *Comparison between measurements for a single wheel and model predictions corrected for 2D simplifications. Surface is absorbing. 2D model : lines ; single wheel : broken lines.*

i.e. 1 mm.
The ground impedance is given by the model used for level difference measurements [15]. The input values of thickness and flow resistivity are the mean values found for tube measurements and level difference measurements given in *Chapter 4*. For the fitted–carpet, t =2.20 mm and σ =12.25 kNs/m^4. For the mineral rockwool, t =16.6 mm and σ =123 kNs/m^4.

Finally, the calculations are performed for frequencies from 400 Hz to 5000 Hz.

8.3.3 Comparison results

Comparisons between measurements and predictions are shown in Fig. 8.5(a) for the fitted-carpet. A 500 Hz frequency shift has been applied to the model predictions.
The model overestimates the level of maximum amplification at 1000 Hz. This frequency corresponds to the limit of validity of the two–dimensional simplifications of the model. With the applied frequency shift, the correspondence between measurements and predictions is good at frequencies above 1500 Hz. In this frequency range, the maximum deviation is less than 1 dB.

For the horn effect over the mineral rockwool, measurements and predictions are compared in Fig. 8.5(b), where a 100 Hz frequency shift has been applied to the model simulations. In the low frequency range up to 900 Hz, the model clearly overestimates the amplification factors. At frequencies where the *2D* simplifications of the model are valid, measurements and predictions lie within 1 dB on the entire frequency range examined.

8.4 Summary

Measurements of horn effect amplifications were performed for a tyre placed above an absorbing surface. The acoustical properties of the surfaces used in the experiments are described in *Part I*

of this document. They have been chosen to represent a rather low absorbing surface and a highly absorbing surface.

Both in–plane and directivity measurements were performed. Amplification levels present a maximum level which is lower for higher surface absorbing properties. For the low absorbing surface for instance, at 1000 Hz, the absorption coefficient is less than 0.05 but the decrease in the maximum sound amplification is about 3 dB. At the same time, the frequency of maximum is shifted toward the low frequency range. At higher frequencies, the amplification levels decrease uniformly to reach zero amplification at a frequency which depends on the absorbing surface. For instance, for the highly absorbing surface, amplifications are close to zero at 3000 Hz.
When examining the directivity measurements, it is found that the maximum level found in the plane of the tyre, can also be obtained for positions outside the plane of the wheel. This means that the influence of the horn effect over absorbing surfaces is significant for larger azimutal positions compared to the horn effect over rigid surfaces.

Measurements were also compared to the predictions obtained with the two–dimensional model of [11]. The correction term between *2D* predictions and *3D* measurements is found to be smaller for absorbing surfaces than for rigid surfaces. The exact determination of this correction term is still an open question. Provided this correction is valid, measurements and predictions lie within 1 dB on the frequency range of validity of the two–dimensional simplifications of the model.

9 – Double wheels over a rigid surface

This chapter presents measurements of horn effect amplification factors for a double wheel structure placed over a rigid surface. The structure is a scaled twin–wheels structure which can be found on heavy trucks. Details on the structure are first given ; measurement results are then presented and discussed.
The measurements presented in this chapter can also be found in [16]

9.1 Principle of the measurements

This section presents details on the mounting of the twin wheels and the measurement configurations tested using this structure.

9.1.1 Mounting of the twin wheels

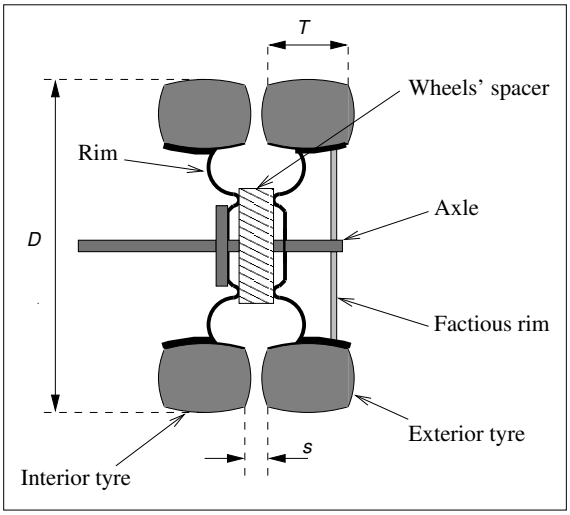

Figure 9.1: *Schematic view of the twin wheels' mounting.*

Measurements are performed over the linoleum floor, the properties of which are given in §*3.3.1.*

For practical reasons, the twin wheel system is built with two passenger car tyres. Tyres of dimensions 155/70 R13 are chosen to have the same ratio diameter / tread width as truck tyres. The geometry is thus scaled by a factor 0.56. This has for consequence that the actual frequencies of the measurement correspond to twice the frequencies for a real scale structure.

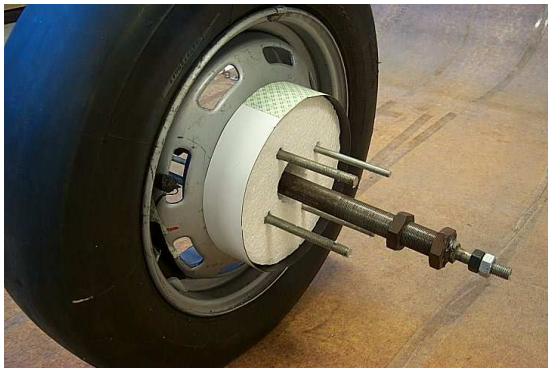

(a) Inside gauge

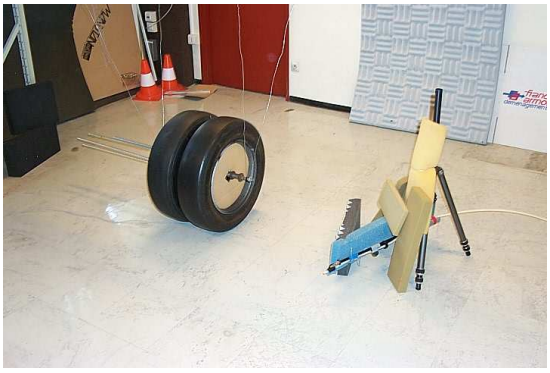

(b) Global view

Figure 9.2: *Pictures of the twin wheels.*

The value of the distance between the two wheels is set according to two parameters. The first parameter is the ratio between the distance s between the treads of the twin wheels and the tyre diameter D (see Fig. 9.1). The second parameter is the ratio between s and the tread width T. Experimentally, the first parameter gives s =4.15 cm and the second one gives s =4.2 cm. Therefore, a distance of 4.2 cm is set between the tyres of the scaled system by using a gauge especially made for this use (see Fig. 9.2(a)). The surface of the gauge is acoustically rigid, as in the case of twin wheels for trucks.
The two rims face symmetrically as in a mirror, leaving their hollow parts towards the outside. Since the hollow part of truck wheels is "filled" by the wheel hub, an acoustically rigid protection is installed as indicated in Fig. 9.1 (factious rim) and which can be seen in Fig. 9.2(b).
Finally, the metallic frame previously presented is used to avoid back and forth displacements and to keep the sidewalls vertical.

9.1.2 Measurement configurations

Using this structure, both in–plane and directivity measurements are performed using the acoustic reciprocity. The positions of the source and of the receivers are given in *Section 5.4*.

For directivity measurements using twin tyres, two measurements situations are possible. One can measure the influence of the exterior tyre on the noise radiated by the interior tyre or vice–versa. These two situations, respectively called "masked" and "baffled", are depicted in Fig. 9.3. In the first situation, the second tyre has the effect of masking the sound recorded by the microphone, and in the second one the tyre acts as a baffle for the first tyre.

The origin of the coordinate system is taken at the centre of the contact zone of the tyre under which the microphone is placed, as indicated in Fig. 9.3. By doing so, the influence of the second tyre can be determined in both the masked and the baffled situation by comparisons with measurements using a single wheel.

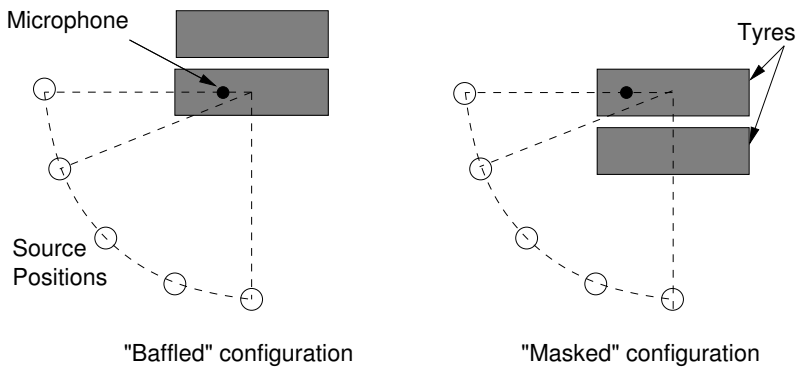

Figure 9.3: *Possible situations for directivity measurements using twin wheels.*

9.2 Measurement results

In–plane and for directivity measurements are presented and discussed using the real scale frequency axis.

9.2.1 In–plane measurements

In–plane measurements are presented in Fig. 9.4 for the baffled and the masked situations.

The correspondence between the two scaled pass–by positions is good on the low frequency range up to 2000 Hz. Beyond this frequency, deviations of at most 2 dB are observed. Since the source is not in the middle of the twin wheels, the horn amplifications are not expected to be the same at the two scaled pass–by positions, at least in the high frequency range.

Moreover, the baffled and the masked situation give very similar results at low frequencies up to around 2000 Hz. In this region, between 300 Hz and 600 Hz, three peaks are clearly visible for the two source positions and for the two measurement configurations. This phenomenon, not observed with a single tyre, seems associated with tyres mounted as twin wheels.

For the two measurement configurations, the maximum amplification is reached at 900 Hz to 1000 Hz depending on the position of the microphone inside the horn. It reaches 13 to 12 dB, which is somewhat lower than for a single wheel. Above this maximum frequency, a sharp interference is seen at a frequency which is much lower to that for a single wheel. At higher frequencies, amplification levels become very chaotic. For certain measurement positions, the maximum amplification in this region may exceed 10 dB, which is as high as the 1000 Hz peak. In total, in–plane measurements are very similar for the baffled and for the masked configurations in the main frequency range of interest of traffic noise.

9.2.2 Directivity measurements

Directivity measurements are presented in Fig. 9.5 for the real scale frequency axis. For each azimutal position, measurement results for the baffled configuration are plotted against measurements for the masked situation. To see the specificities of the twin wheels better, the measurements previously presented for a single wheel are also reported on the same plot using the real scale frequency axis.

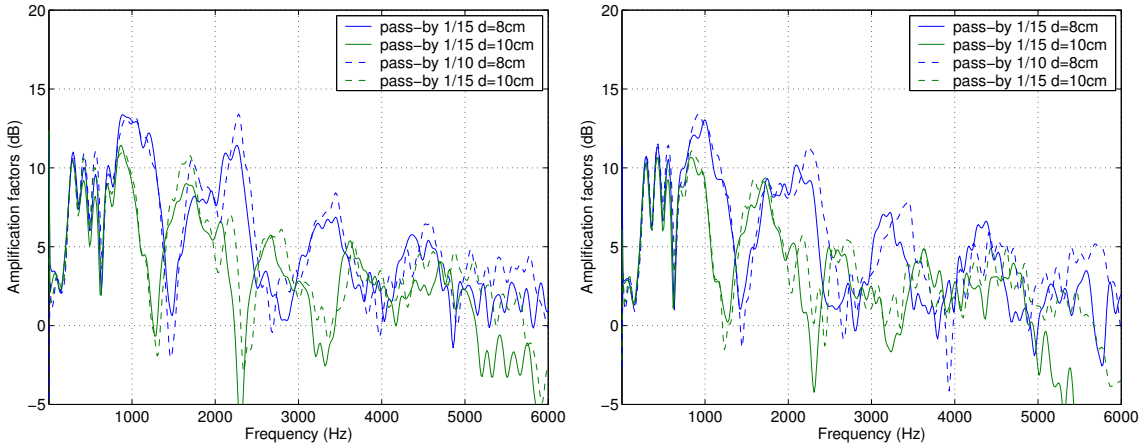

(a) Baffled configuration

(b) Masked configuration

Figure 9.4: *In–plane measurements of horn effect amplification for twin wheels over a rigid surface. Real scale frequency axis.*

Contrary to a single wheel, the maximum amplification level considering all incidences is obtained in this case for 22.5° and for 45° at 1000 Hz. This frequency corresponds to the maximum contribution to A-weighted noise levels.

For larger azimutal positions, the amplification decrease more rapidly for the masked configuration than for the baffled configuration. As a matter of fact, for incidences from 22.5° to 67.5°, the amplification factors obtained for the baffled situation are larger than for a single wheel.

At 90° of incidence, amplification factors for the baffled situation are very similar to that measured with a single tyre ; there is not significant influence of the second wheel. Amplification levels reach 10 dB and are almost always positive up to 10 kHz. On the other hand, amplifications for the masked situation are almost always negative on the same frequency range. As could be expected, the masking tyre has a maximum influence on the measurements at this position. A similar observation may be made for 112.5°.

At 135°, measurements for the baffled configuration show a series of large interferences which are not observed for the masked situation nor in the case of a single wheel. The periodicity of these peaks is about 2000 Hz in terms of scaled frequencies. At this frequency, the quarter wavelength corresponds to the distance s between the wheels. It should also be noted that the maximum amplifications reach 8 dB at 1000 Hz and 9 dB around 2500 Hz.

For both 157.5° and 180°, the amplification factors for twin wheels are positive at frequencies below 1000 Hz. They reach 5 dB to 7 dB at these two azimutal positions. This is quite different from single wheel measurements for which the amplification factors are negative on the entire frequency range.

9.3 Summary

A twin wheel structure has been built, the dimensions of which are scaled compared to twin wheels for trucks. Using this structure, horn effect amplification factors could be measured both in the plane of the tyre and around the tyre. Particularities of the twin wheels were thus identified.

It is found that the maximum amplification is somewhat lower than that obtained for a single wheel. However, the frequency at which it occurs, 1000 Hz, coincides with the region of maximum contribution to A-weighted noise levels. Furthermore, the maximum amplification is not found in front of the twin wheels, but somewhere between 22.5° and 45° of incidence, which enhance its contribution to pass–by noise levels.

Is is also observed a series of three peaks at frequencies between 300 Hz and 600 Hz clearly associated with twin wheels. Moreover, the horn amplifications measured on the back side of the wheel are much larger than for a single wheel.

In conclusion, horn effect for twin wheels appears to differ in many ways from horn effect for a single tyre. Since most of these deviations occur in the frequency range around 1000 Hz, the previous observations deserve to be confirmed by measurements on real twin truck tyres.

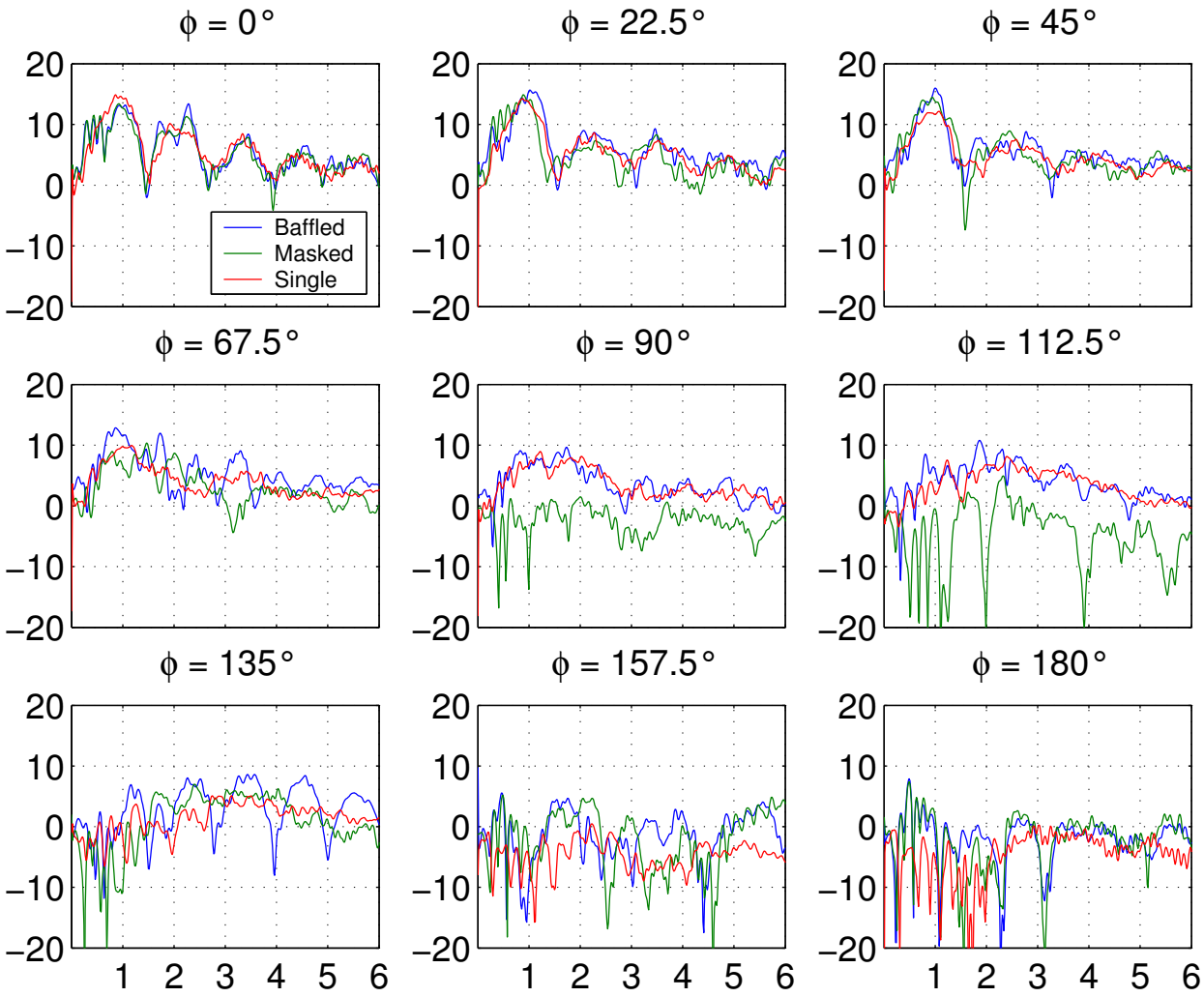

Figure 9.5: *All directivity measurements for twin wheels. Real scale frequency axis in kHz. Baffled : blue ; Masked : green ; Single wheel : red.*

10 – Summary and Discussion

This part presents measurements of amplification factors due to the horn effect for a long cylinder, for a single tyre and for twin wheels. The surface of the ground was either rigid or absorbing.

Using a systematic experimental protocol, a large number of measurements have been performed. Together with the knowledge of the material absorbing properties collected previously, this constitutes a valuable database for the estimation of the influence of absorption on pass–by noise levels. Measurements were performed for a low absorbing surface and for a high absorbing surface. It is shown that, for substantial absorption properties, the horn amplifications are significant for positions out of the plane of the tyre. Contrary to the amplification factors measured over a rigid surface, the amplifications measured on the back side of the tyre may be significant for absorbing surfaces.

The set of collected data is also very interesting for the validation of the modelling tools. Measurements were compared here to predictions obtained two–dimensional models for rigid and for absorbing surfaces. It is shown that a frequency shift could be applied to compare *3D* measurements to *2D* measurements or predictions. By With this correction, the predictions correspond well with measurements in the domain of validity of the two–dimensional simplifications. Provided the correction is valid, which would require further work, the present work show that the *2D* models could be used to include the absorption in the traffic noise predictions.

Finally, a twin wheels system was built, the dimensions of which are scaled regarding twin wheels for trucks. The structure allowed to examined the specificities of twin wheels for the horn amplification. It is shown that the maximum amplification for twin wheels is obtained for incidences between 22.5° and 45°, at 1000 Hz. This corresponds to the region of maximum contribution to A–weighted noise levels, enhancing the importance of this effect. Moreover, amplifications measured on the back side of twin wheels could be significantly larger than the amplification measured for a single wheel.

References for Part III

[1] K. Schaaf D. Ronneberger. *Noise radiation from rolling tires – Sound amplification by the "horn effect"*. In *Proceedings of inter.noise 1982, San Fransisco, USA*, 1982.

[2] P. Klein. *Modélisation du contact pneumatique - chaussée - Etude de la démarche de Kropp*. Report MMA n°9807, Institut National de Recherche sur les Transports et leur Sécurité, august 1998.

[3] W. Kropp F-X. Bécot S. Barrelet. *On the sound radiation from tyres*. Acustica - Acta Acustica, 86(5):769–779, 2000.

[4] J. W. S. Rayleigh. *Theory of sound*. Dover publications, 1945.

[5] D. Ronneberger. *Towards quantitative prediction of tire/road noise, a workshop on rolling noise generation*. In *Proceedings of Workshop on Rolling Noise, Newport Beach, USA*, October 1989.

[6] C. Deffayet J-C. Clairet. *Phénomènes d'effet dièdre dans le bruit de contact pneumatique / chaussée*. Report INRETS n°147, Institut National de Recherche sur les Transports et leur Sécurité, 1991.

[7] R. A. Graf C.-Y. Kuo A. P. Dowling W. R. Graham. *On the horn effect of a tyre / road interface, Part I : Experiment and computation*. *Journal of Sound and Vibration*, 256(3):417–431, 2002.

[8] W. Kropp. *Ein Model zur Beschreibung des Rollgeräusches eines unprofilierten Guertlreifens auf rauher Strassenoberfläche*. PhD thesis, Institut für Technische Akustik, Berlin, Germany, 1992.

[9] F. Anfosso-Lédée. *Application de la méthode des équations intégrales à la modélisation du bruit aux abords des routes – Interaction chaussée / écran antibruit*. PhD thesis, Ecole Nationale des Ponts et Chaussées, Paris, France, 1997.

[10] A. Fadavi. *Modélisation numérique des vibrations d'un pneumatique et de la propagation du bruit de contact*. PhD thesis, Ecole Nationale des Ponts et Chaussées, Paris, France, 2002.

[11] F-X. Bécot. *Tyre noise over impedance surfaces – Efficient application of the Equivalent Sources method*. PhD thesis, Chalmers university of technology & Insa–Lyon, 2003.

[12] Martin Ochmann. *The source simulation technique for acoustic radiation problems*. Acustica - Acta Acustica, 81:512–527, 1995.

[13] F-X. Bécot P. J. Thorsson W. Kropp. *An efficient application of equivalent sources to noise propagation over inhomogeneous ground*. *Acustica - Acta Acustica*, 88(6):853–860, 2002.

[14] J-M. Clairet F-X. Bécot. *Effet dièdre sur plan réflecteur et sur surface absorbante – Descriptif des mesures.* Report LTE n°0414, Institut National de Recherche sur les Transports et leur Sécurité, june 2004.

[15] E. Delany E. N. Bazley. *Acoustical properties of fibrous absorbent materials.* Journal of the Acoustical Society of America, 3:105–116, 1970.

[16] F-X. Bécot J-M. Clairet. *Twin wheels horn effect and pass–by noise.* In *Proceedings of CFA / DAGA 2004, Strasbourg, France*, 2004.

Part IV

Conclusions and perspectives

Conclusions and perspectives

The objective of the present work is to contribute to the design of a procedure for introducing the effect of the road absorption in the hybrid traffic noise prediction methods. Two milestones have been fulfilled : the determination of the material acoustic properties and the experimental characterization of the horn effect over absorbing surfaces.

Two complementary methods for the determination of the material acoustic properties have been implemented. These methods are complementary as one is a laboratory technique and the second one can be implemented outdoors. The present work records litterature informations and experiences concerning the principle, the limitations and the application of the methods. In this respect, the applications of the present work cover a domain which is larger than traffic noise predictions.

The experimental characterization of the horn effect amplification was conducted using the laboratory facilities. For this, an accurate, omni–directional point source has been built on the basis of previous works. Various structures, i.e. a cylinder, a single wheel and twin wheels, have been examined for different impedance surfaces. This resulted in a large set of measurements, which represents a valuable database for the continuation of the SilVia project.

Finally, it was shown that two–dimensional models could be used to predict the effect of the absorption on the horn amplifications. Besides the present work leaves some open questions concerning the comparisons of *2D* predictions or measurements to *3D* measurements. Since these models use an approximate description of the tyre / road interface, they are mainly dedicated to be used with simpler models for traffic noise predictions. By doing so, it is expected that a correction procedure to account for the road absorption in the predictions of hybrid models could be designed.

Part V

Appendices

11 – Optimisation process

This appendix presents the optimisation process used for impedance tube measurements and for level difference measurements. It consists in finding a pair of parameters that give the best fit between some measured datas to the prediction obtained with a given propagation model.

11.1 Principle

The method is based on fitting some measured data to some predictions obtained from a given impedance model. The optimal input parameters for the impedance model are those giving the best correspondence between the two sets of data. To find the best fit between the two set of datas, a numerical optimisation is performed. In fact, the optimisation consists in minimizing a "cost" function which gives a measure of the correspondence between the predictions and the measurements. Therefore, the optimal parameter values give a minimum value of the cost function.

For the optimisation process, it was chosen to use an existing, robust algorithm, which is available in the "optimisation toolbox" of the calculation software Matlab©, through the built–in function `fminsearch.m`. Basically, this function performs an unconstrained, non–linear optimisation. It finds the minimum of a given function based on successive evaluations of the function values. It starts from a given initial value and stops when the error made falls under a given threshold value.

The cost function is set to give the cumulated absolute difference between the measured and predicted values :

$$F_{cost} \;=\; \sum_{f} \mid q_{meas}(f) - q_{pred}(f) \mid \tag{11.1}$$

where q is the acoustical quantity upon which the optimisation is performed ; it is of course a function of the frequency f.

This algorithm can thus handle possible discontinuities in the function to be optimised ; however in our case, it is very unlikely to happen for "standard" measurements. In addition, the algorithm of the optimisation is not accurate for functions of more than two variables. For instance, if an impedance model, which requires three or four parameters, is used, either some parameter values must be fixed while the others are optimised, or another optimisation algorithm must be thought of.

11.2 Limitations and precautions of use

The main limitation is that the algorithm is able to find only a local minimum of the function, which may not be the global minimum. This situation occurs if the function to be minimized has several minima and/or the global minimum is not well marked compared to the local ones. It may also happen if the initial values are too far from the optimal values.

As a rule of thumb, if the values of some parameters can be easily guessed or, better, measured (material thickness for instance), these values should be input as initial values. In addition, the experience of the user and the study of related works may help for the choice of the initial values.

There is no rule for the choice of the quantity to be optimised ; only some general considerations may be outlined. In particular, the function to be fitted with the predictions will preferably not have large extremum values nor present rapid variations. When this is the case indeed, the function estimations in the regions of sudden changes is very delicate. As a consequence, the convergence may not be reached or the optimal values may be only approached.

An alternative may consist in avoiding the frequency regions where these difficulties (or others) appear. This results in considering a narrow frequency range where the optimisation could be performed. Because some difficulties like resonances of the tested sample are very local, the solution could be to consider a series of narrow frequency ranges, not forcely contiguous. The final optimal values could be then taken to be the average of the values found for the different frequency bands.

11.3 Examples of tube measurements data

The functionning of the minimisation search is illustrated below.

For this, initial values of the material thickness and of the flow resistivity are given and the quantities of interest for tube measurements are computed, namely the absorption coefficient, the acoustical impedance, the reflexion coefficient and the transfer function. The model for the sound propagation inside the tube is that of *Section 2.1.* Then, the same quantities are computed using the values of thickness and flow resistivity with $\pm 10\%$ deviation. Finally, the cost function as defined in the equation below is calculated using these two set of data, the exact values and the corrupted ones.

$$F_{cost} \;=\; \Big[\sum_{f} \mid q_{meas}(f) - q_{pred}(f) \mid^2 \Big]^{1/2} / N_f \tag{11.2}$$

where N_f is the number of frequency points examined.

The exact values of the absorption coefficient are shown in Fig. 11.1(a). The possible values are t =0.005 m and 0.03 m and σ =2 kNs/m^4 and 50 kNs/m^4. These values represent four different types of absorption, from very low to high absorption properties, which are not meant to be realistic.

The cost function values for the different quantities are shown in Fig. 11.1(a), (b) and (c) respectively for the absorption coefficient, the acoustical impedance and the reflexion coefficient. The values of the cost function for the transfer function are shown in Fig. 11.2(a) for the large tube and in Fig. 11.2(b) for the small tube.

The shape of the cost functions reveals that in certain cases, it may be very difficult to find a global minimum on the scanned region. For instance, for the highest absorption (t =0.03 m and σ =50 kNs/m^4), the optimisation performed upon the absorption values may be difficult as the region of minimum is large and not clearly bounded. A similar situation is the optimisation upon absorption coefficient for the mineral rockwool. As a matter of fact, the results of Fig. 12.10 predict a material thickness which is larger than the measured one, indicating a failure of the optimisation.

11.4 Conclusion

In all cases, it is recommended that several runs with different initial values are performed to ensure that the resulting values correspond to a global minimum. In final, the resulting optimal value should not deviate much from the measured or guessed value of the input parameter. If this is the case though, three reasons may be invoked : the minimum is not global, the optimisation algorithm is not adapted to the shape of the function to be fitted or the propagation model is not adapted to the material. If the optimisation process inevitably fails, it may be of interest to examine more in details the values of the cost function as shown above. This could help to determine new input parameter values or to bound the domain of the minimisation search.

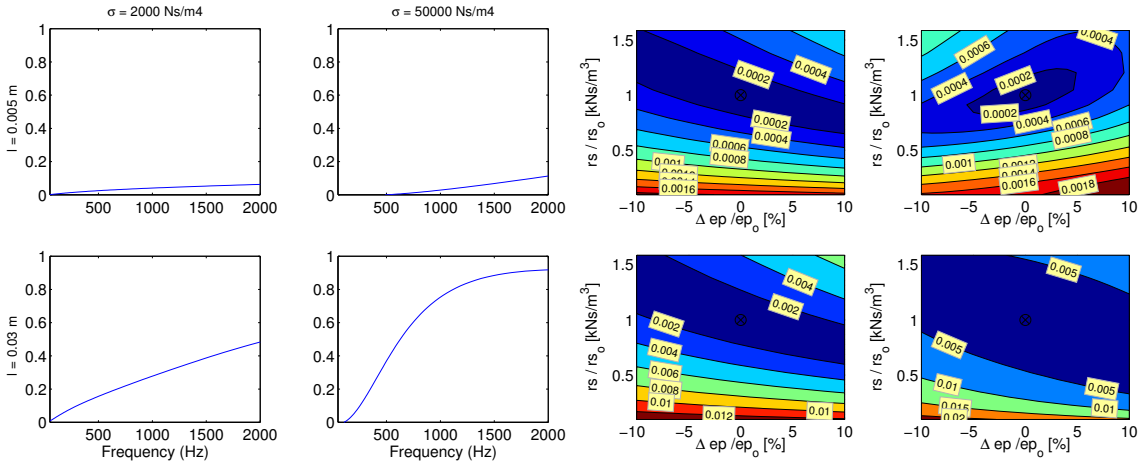

(a) Initial absorption coefficient

(b) Error on absorption coefficient

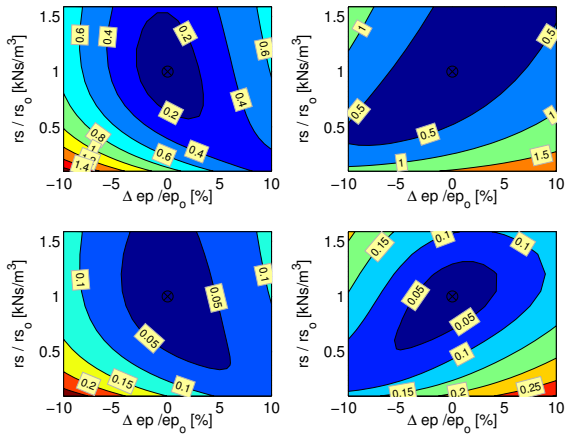

(c) Error on acoustical impedance

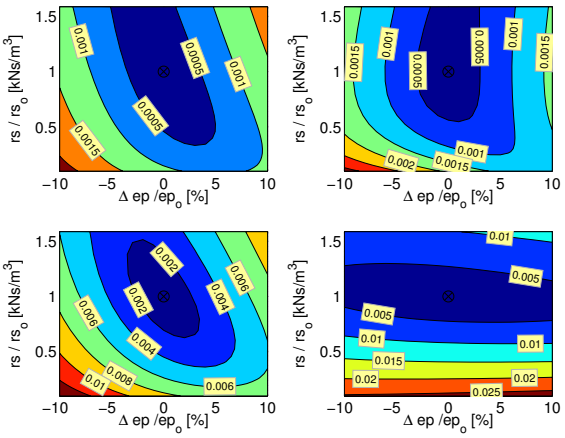

(d) Error on reflexion coefficient

Figure 11.1: *Error estimate for tube measurements. Initial values of thickness and flow resistivity are indicated in the top of figure (a).*

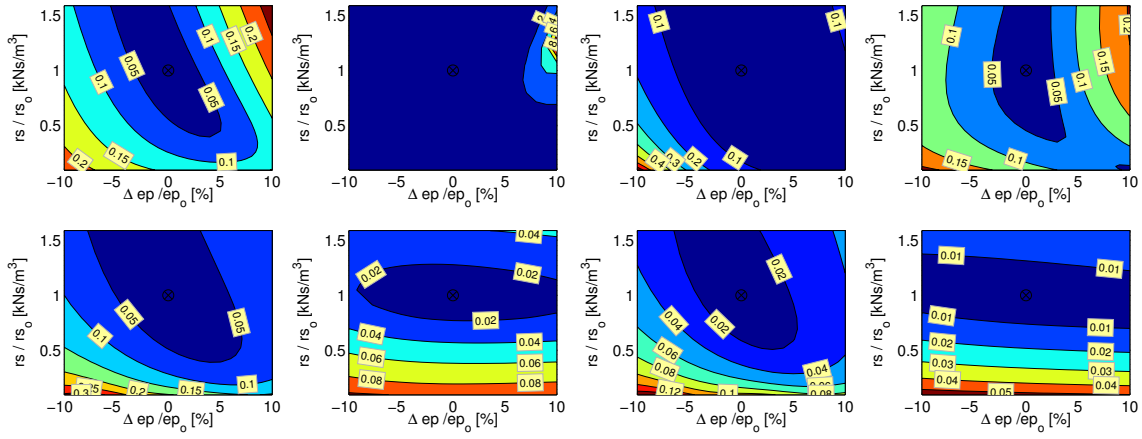

(a) Error on transfer function : large tube

(b) Error on transfer function : small tube

Figure 11.2: *Error estimate on transfer function for large and small tube measurements. Initial values of thickness and flow resistivity are indicated in Fig. 11.1(a).*

12 – Results of optimisation upon impedance tube measurements

For all following plots, the optimisation was performed for the quantity shown. For example, for the plot the legend of which is "transfer function", the best correspondence was searched for transfer function values. As a result, predicted and measured values of the transfer function are compared in the same display. For this given configuration, the resulting optimal parameters are given in the legend.

The frequency range of optimisation is indicated with a gray strip. For small tube measurements, the range examined spans from 200 Hz to 1000 Hz and for large tube measurements, the range spans from 1000 Hz to 5000 Hz.

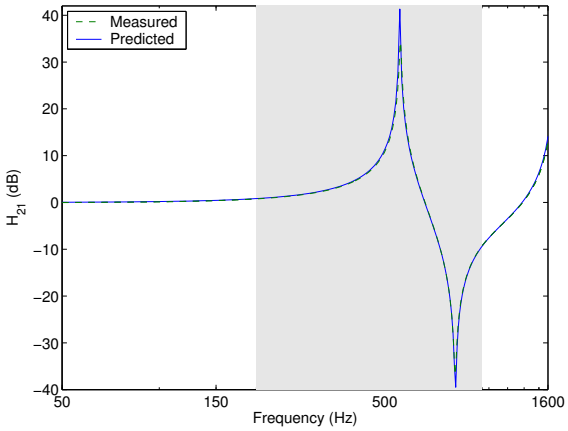

(a) Transfer function

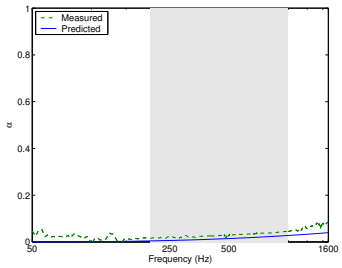

(b) Absorption coefficient

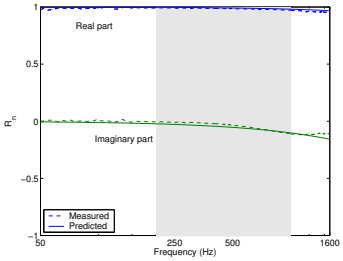

(c) Reflection coefficient

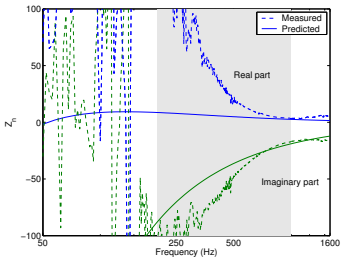

(d) Acoustical impedance

Figure 12.1: *Tested surface is fitted–carpet. Large impedance tube measurements. Optimised quantity is transfer function : $L(mm) = 2.50$; $\sigma(kNsm^{-4}) = 4.9$.*

12.1 Fitted–carpet – Large tube measurements

Results are shown in Fig. 12.1,Fig. 12.2, Fig. 12.3, Fig. 12.4.

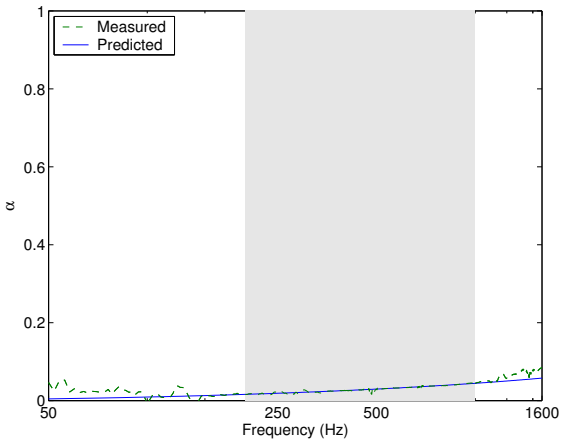

(a) Absorption coefficient

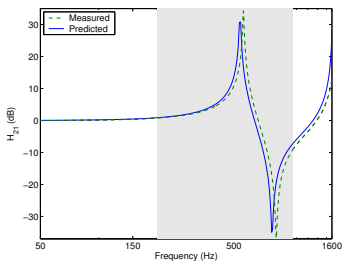

(b) Transfer function

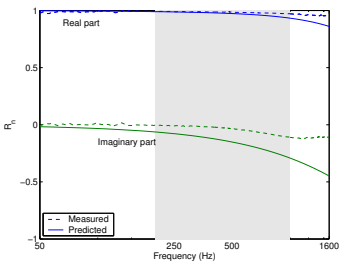

(c) Reflection coefficient

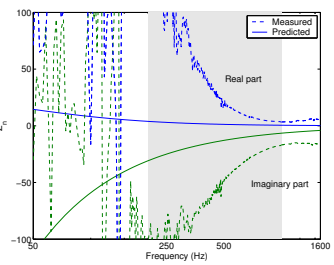

(d) Acoustical impedance

Figure 12.2: *Tested surface is fitted–carpet. Large impedance tube measurements. Optimised quantity is absorption coefficient : $L(mm) = 7.94$; $\sigma(kNsm^{-4}) = 0.6$.*

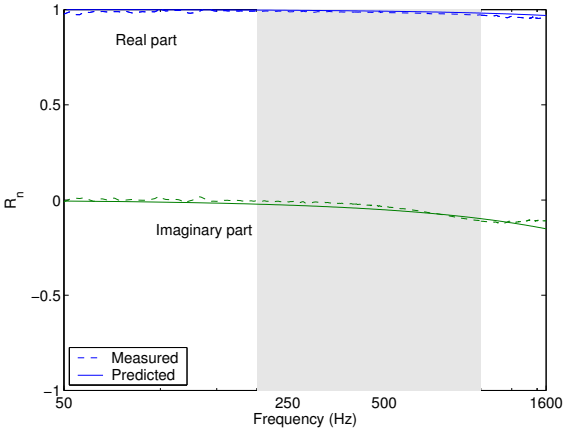

(a) Reflection coefficient

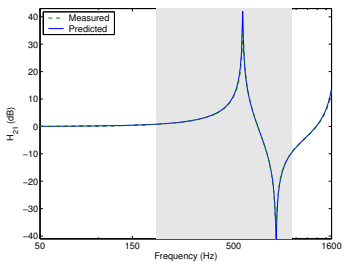

(b) Transfer function

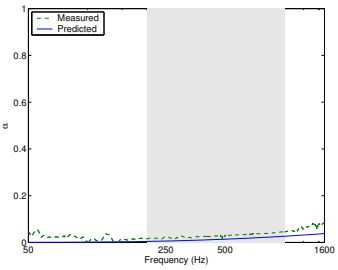

(c) Absorption coefficient

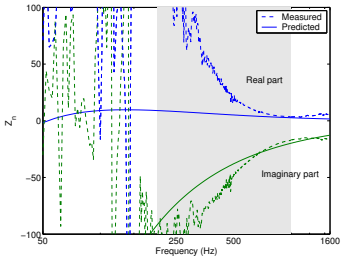

(d) Acoustical impedance

Figure 12.3: *Tested surface is fitted–carpet. Large impedance tube measurements. Optimised quantity is reflection coefficient : $L(mm) = 2.41$; $\sigma(kNsm^{-4}) = 4.9$.*

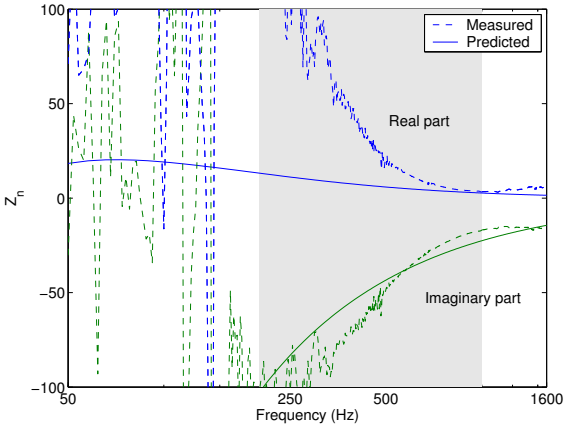

(a) Acoustical impedance

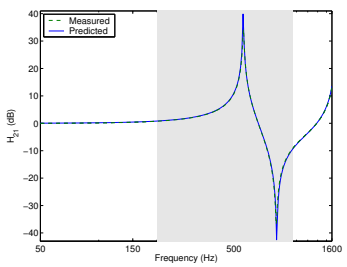

(b) Transfer function

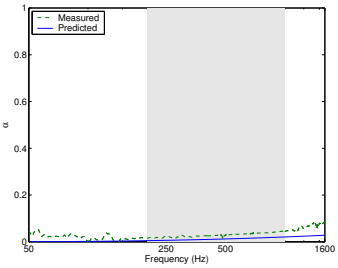

(c) Absorption coefficient

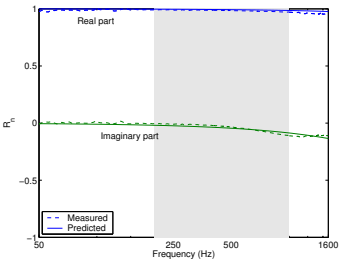

(d) Reflection coefficient

Figure 12.4: *Tested surface is fitted–carpet. Large impedance tube measurements. Optimised quantity is acoustical impedance : $L(mm) = 2.20$; $\sigma(kNsm^{-4}) = 2.6$.*

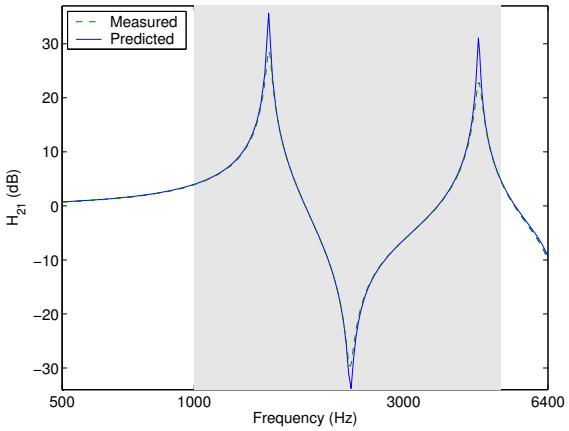

(a) Transfer function

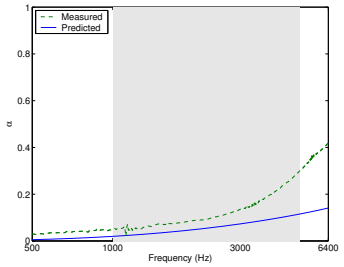

(b) Absorption coefficient

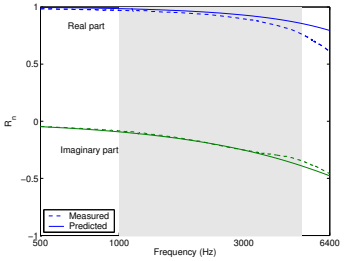

(c) Reflection coefficient

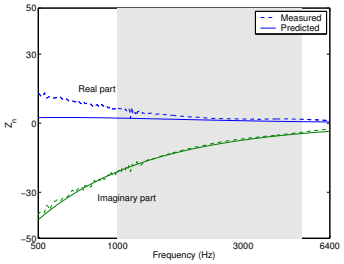

(d) Acoustical impedance

Figure 12.5: *Tested surface is fitted–carpet. Small impedance tube measurements. Optimised quantity is transfer function : $L(mm) = 2.09$; $\sigma(kNsm^{-4}) = 22$.*

12.2 Fitted–carpet – Small tube measurements

Results are shown in Fig. 12.5,Fig. 12.6, Fig. 12.7, Fig. 12.8.

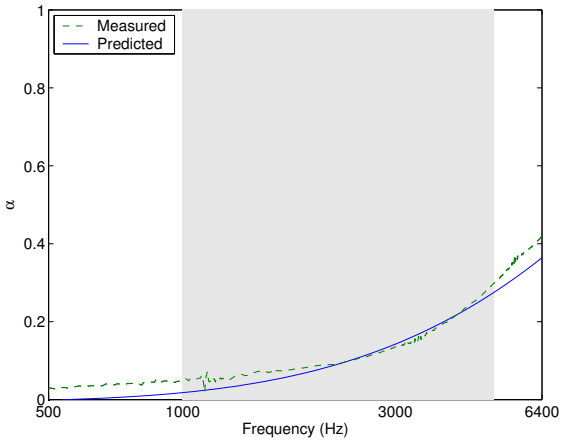

(a) Absorption coefficient

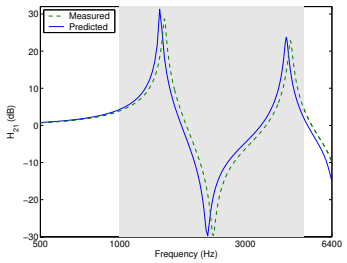

(b) Transfer function

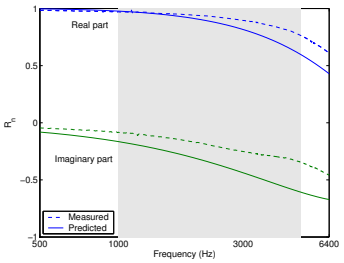

(c) Reflection coefficient

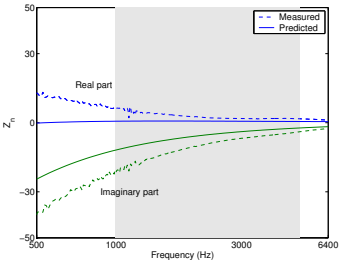

(d) Acoustical impedance

Figure 12.6: *Tested surface is fitted–carpet. Small impedance tube measurements. Optimised quantity is absorption coefficient : $L(mm) = 3.69$; $\sigma(kNsm^{-4}) = 56$.*

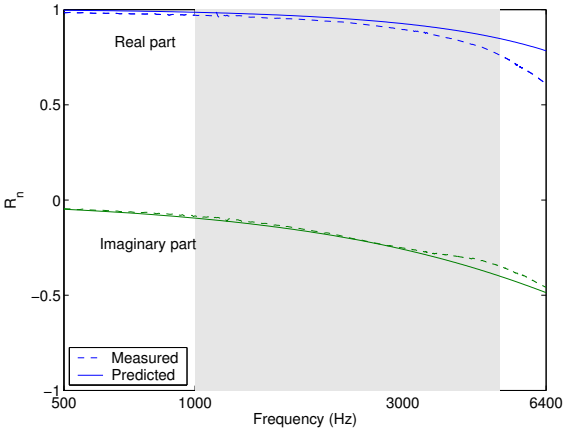

(a) Reflection coefficient

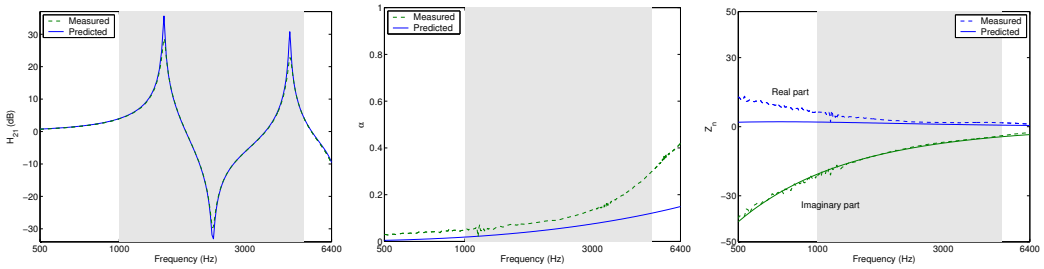

(b) Transfer function (c) Absorption coefficient (d) Acoustical impedance

Figure 12.7: *Tested surface is fitted–carpet. Small impedance tube measurements. Optimised quantity is reflection coefficient : $L(mm) = 2.13$; $\sigma(kNsm^{-4}) = 26$.*

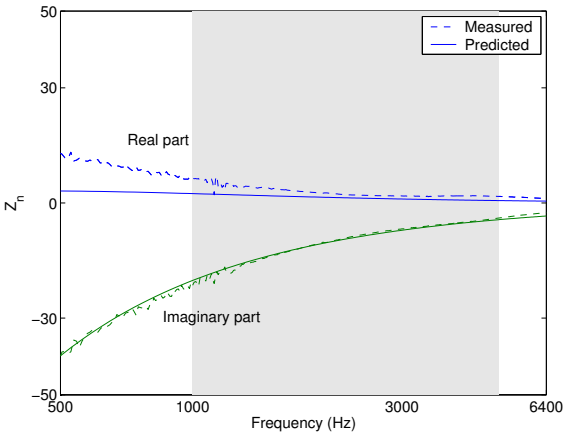

(a) Acoustical impedance

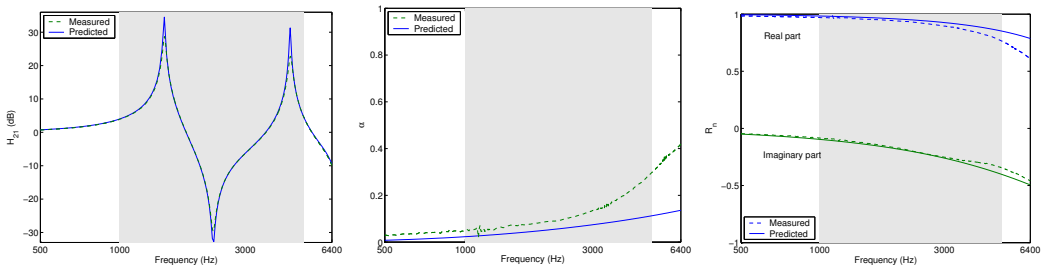

(b) Transfer function (c) Absorption coefficient (d) Reflection coefficient

Figure 12.8: *Tested surface is fitted–carpet. Small impedance tube measurements. Optimised quantity is acoustical impedance : $L(mm) = 2.20$; $\sigma(kNsm^{-4}) = 17$.*

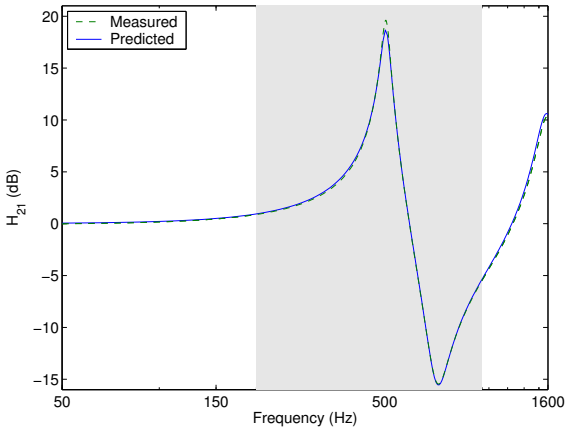

(a) Transfer function

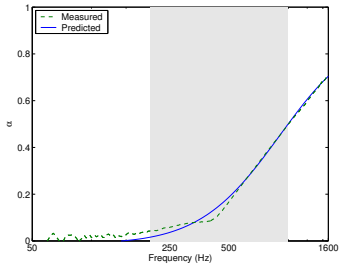

(b) Absorption coefficient

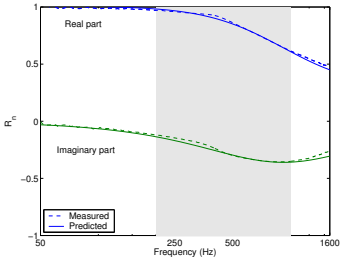

(c) Reflection coefficient

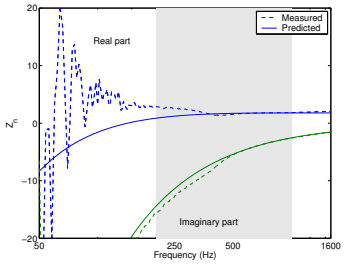

(d) Acoustical impedance

Figure 12.9: *Tested surface is mineral rockwool. Large impedance tube measurements. Optimised quantity is transfer function : $L(mm) = 17.8$; $\sigma(kNsm^{-4}) = 115$.*

12.3 Mineral rockwool – Large tube measurements

Results are shown in Fig. 12.9,Fig. 12.10, Fig. 12.11, Fig. 12.12.

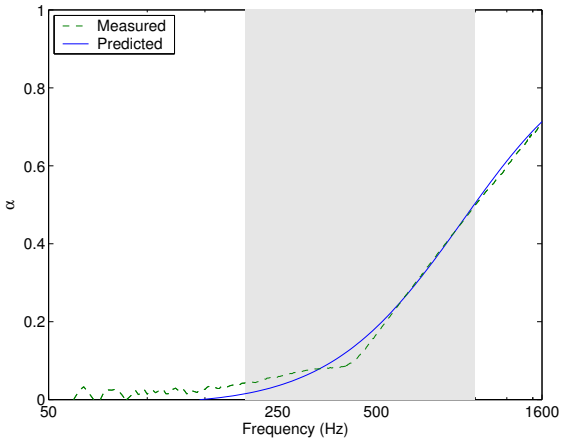

(a) Absorption coefficient

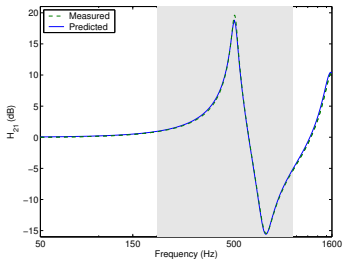

(b) Transfer function

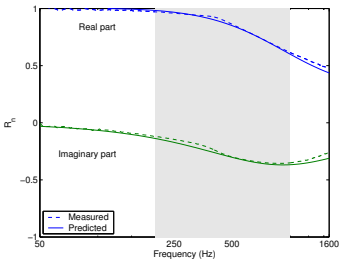

(c) Reflection coefficient

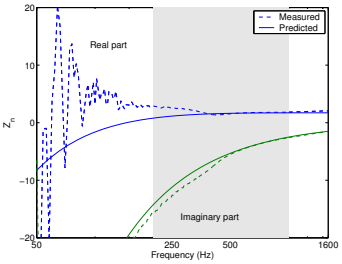

(d) Acoustical impedance

Figure 12.10: *Tested surface is mineral rockwool. Large impedance tube measurements. Optimised quantity is absorption coefficient : $L(mm) = 17.9$; $\sigma(kNsm^{-4}) = 110$.*

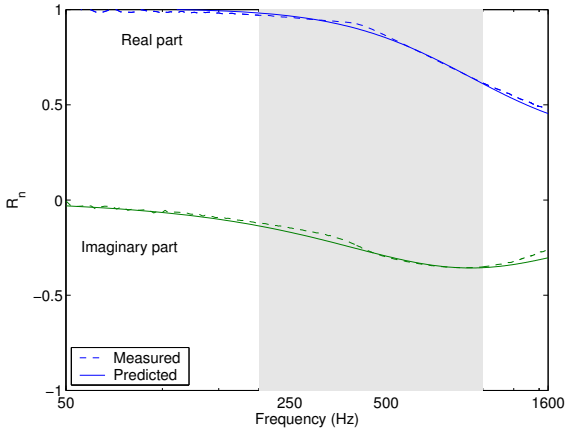

(a) Reflection coefficient

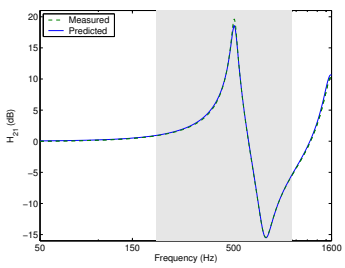

(b) Transfer function

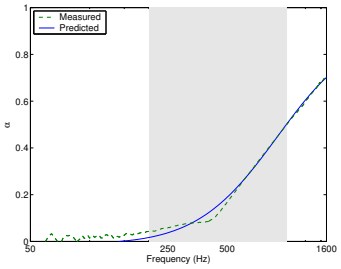

(c) Absorption coefficient

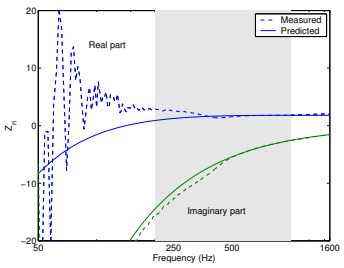

(d) Acoustical impedance

Figure 12.11: *Tested surface is mineral rockwool. Large impedance tube measurements. Optimised quantity is reflection coefficient : $L(mm) = 17.7$; $\sigma(kNsm^{-4}) = 117$.*

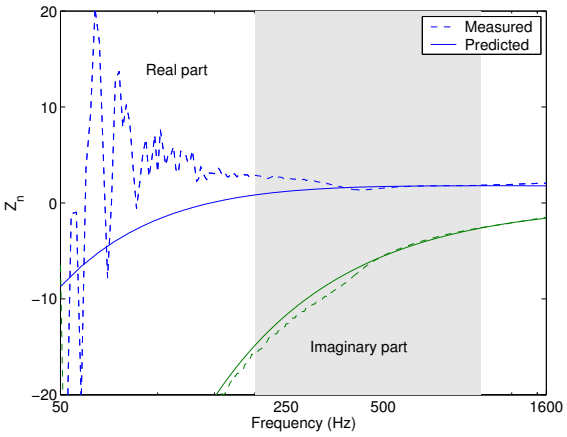

(a) Acoustical impedance

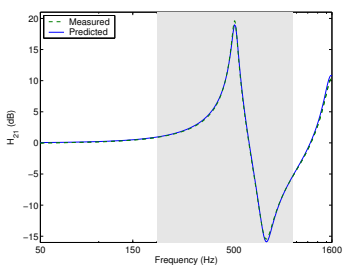

(b) Transfer function

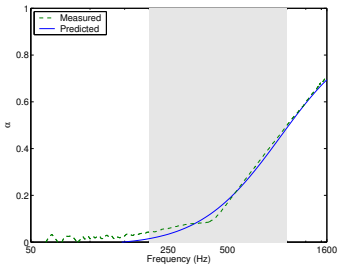

(c) Absorption coefficient

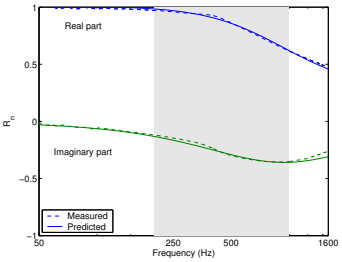

(d) Reflection coefficient

Figure 12.12: *Tested surface is mineral rockwool. Large impedance tube measurements. Optimised quantity is acoustical impedance : $L(mm) = 17.3$; $\sigma(kNsm^{-4}) = 119$.*

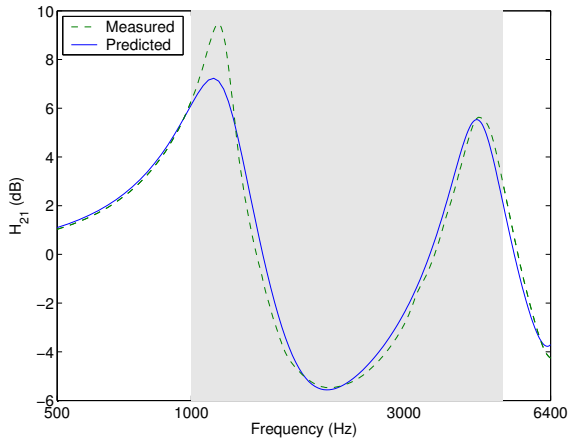

(a) Transfer function

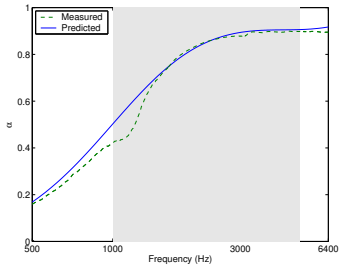

(b) Absorption coefficient

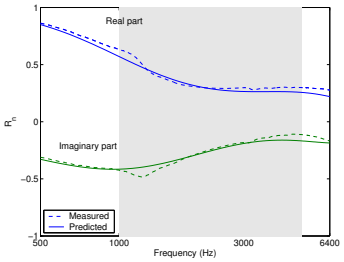

(c) Reflection coefficient

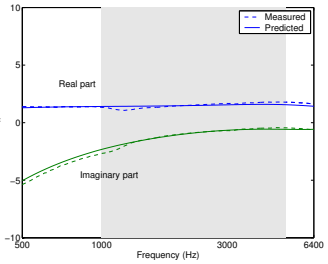

(d) Acoustical impedance

Figure 12.13: *Tested surface is mineral rockwool. Small impedance tube measurements. Optimised quantity is transfer function : $L(mm) = 18.3$; $\sigma(kNsm^{-4}) = 88$.*

12.4 Mineral rockwool – Small tube measurements

Results are shown in Fig. 12.13,Fig. 12.14, Fig. 12.15, Fig. 12.16.

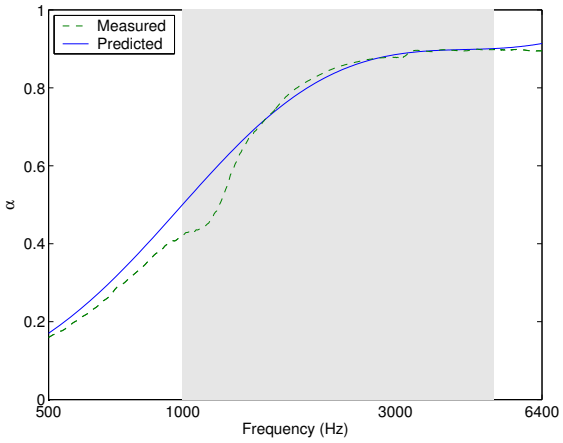

(a) Absorption coefficient

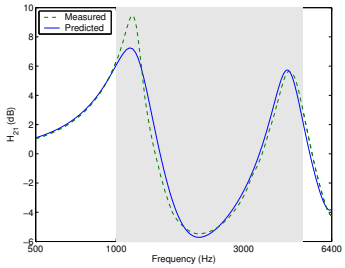

(b) Transfer function

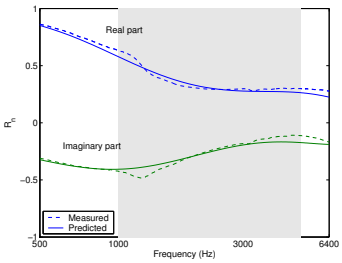

(c) Reflection coefficient

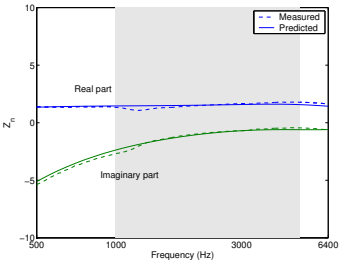

(d) Acoustical impedance

Figure 12.14: *Tested surface is mineral rockwool. Small impedance tube measurements. Optimised quantity is absorption coefficient : $L(mm) = 18.1$; $\sigma(kNsm^{-4}) = 92$.*

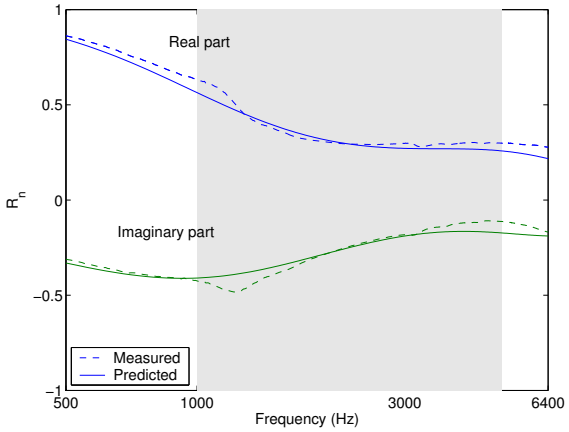

(a) Reflection coefficient

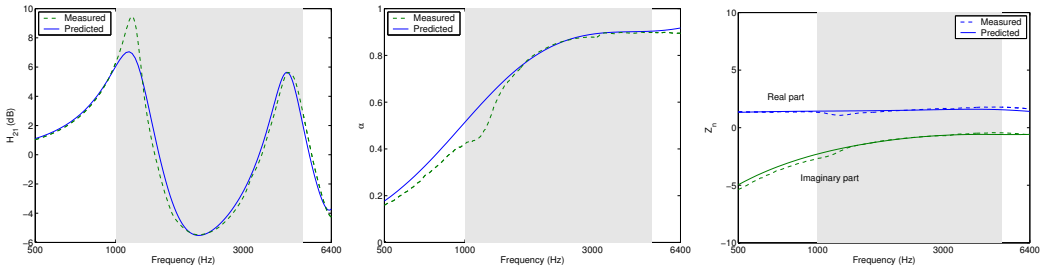

(b) Transfer function (c) Absorption coefficient (d) Acoustical impedance

Figure 12.15: *Tested surface is mineral rockwool. Small impedance tube measurements. Optimised quantity is reflection coefficient : $L(mm) = 18.6$; $\sigma(kNsm^{-4}) = 88$.*

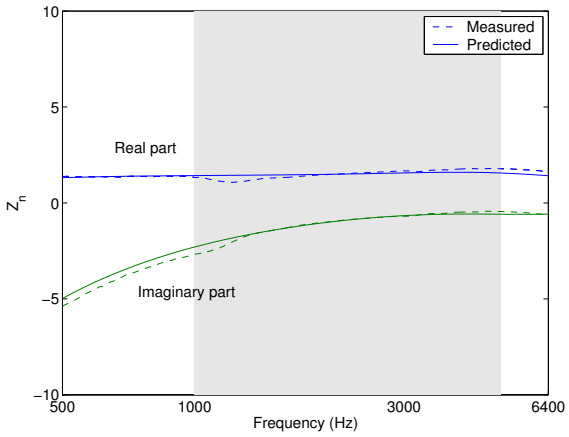

(a) Acoustical impedance

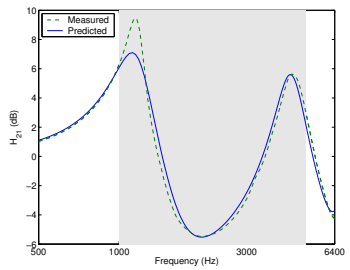

(b) Transfer function

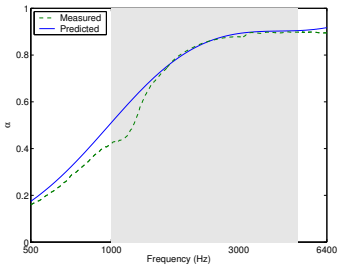

(c) Absorption coefficient

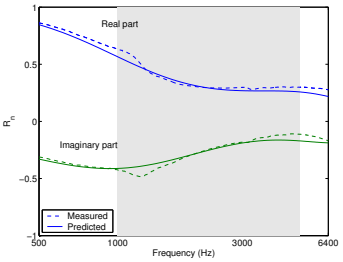

(d) Reflection coefficient

Figure 12.16: *Tested surface is mineral rockwool. Small impedance tube measurements. Optimised quantity is acoustical impedance : $L(mm) = 18.5$; $\sigma(kNsm^{-4}) = 88$.*

13 – Results of optimisation upon level difference measurements

In this appendix, results of the optimisation upon level difference measurements are presented.

The frequency range of optimisation is indicated with a gray strip. For all optimisation shown below, frequencies from 800 Hz to 2500 Hz are considered for the optimisation.

13.1 Fitted–carpet

Results are shown for a recorded signal corresponding to an averaged spectrum (SU signals) in Fig. 13.1 and in Fig. 13.2.

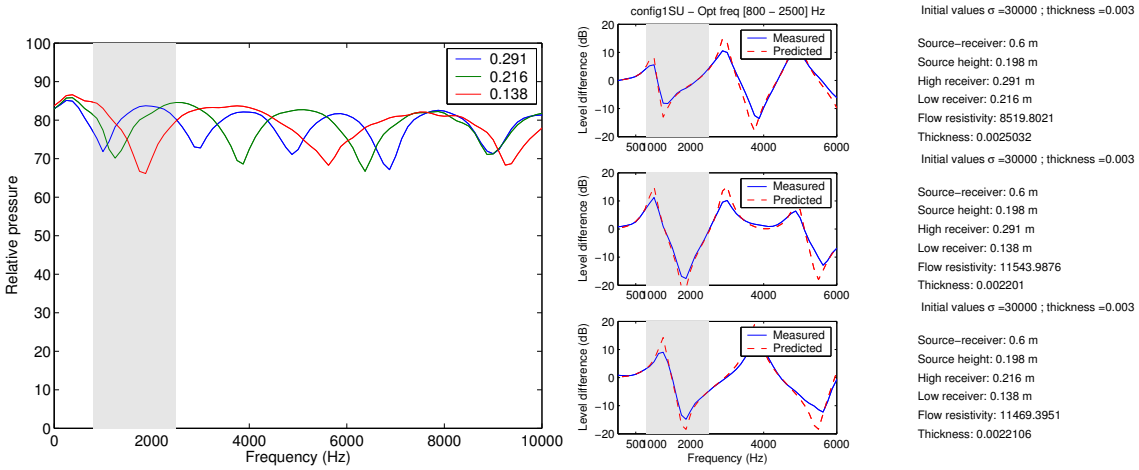

(a) Measurement data (b) Optimisation results

Figure 13.1: *Results of optimisation upon level difference measurements. Surface is fitted–carpet – Signal is averaged spectrum.*

Results of optimisation upon averaged time signals (AV signals) are shown in Fig. 13.3 and Fig. 13.4.

Results of optimisation upon spectra calculated from averaged time signals (SC signals) are shown in Fig. 13.5 and Fig. 13.6.

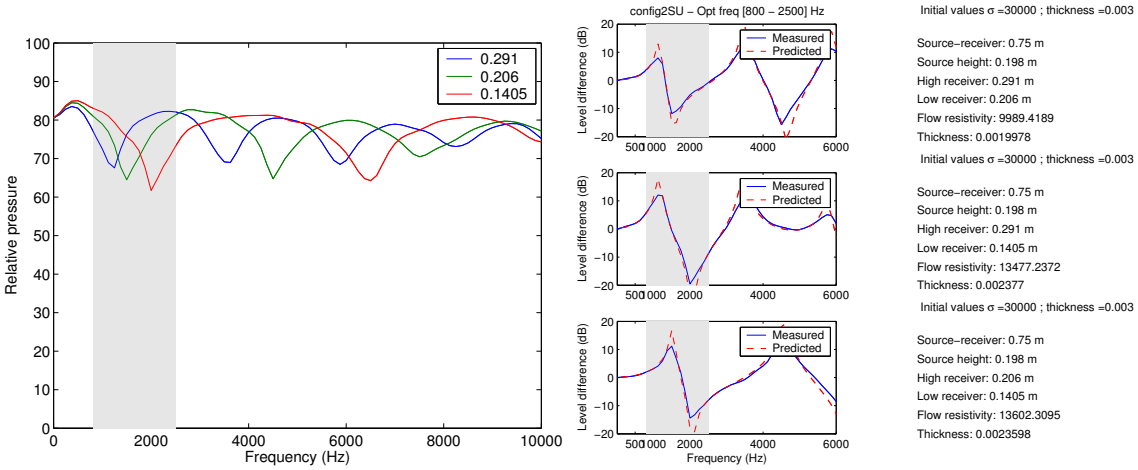

(a) Measurement data (b) Optimisation results

Figure 13.2: *Results of optimisation upon level difference measurements. Surface is fitted–carpet – Signal is averaged spectrum.*

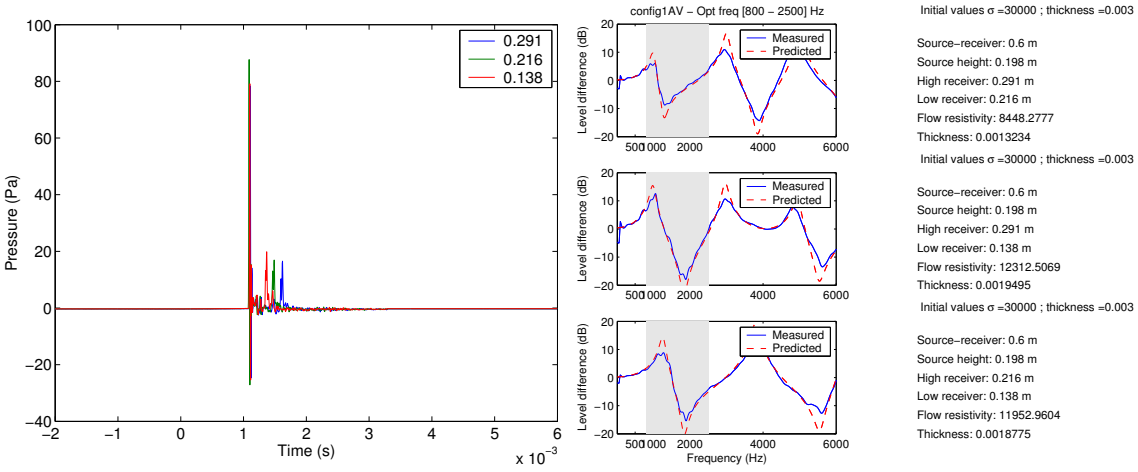

(a) Measurement data (b) Optimisation results

Figure 13.3: *Results of optimisation upon level difference measurements. Surface is fitted–carpet – Signal is averaged time signal.*

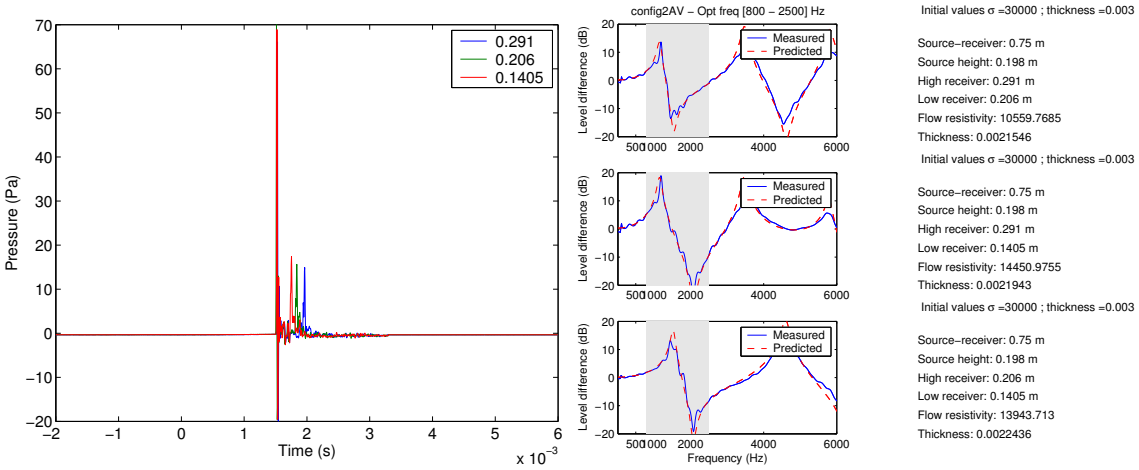

(a) Measurement data (b) Optimisation results

Figure 13.4: *Results of optimisation upon level difference measurements. Surface is fitted–carpet – Signal is averaged time signal.*

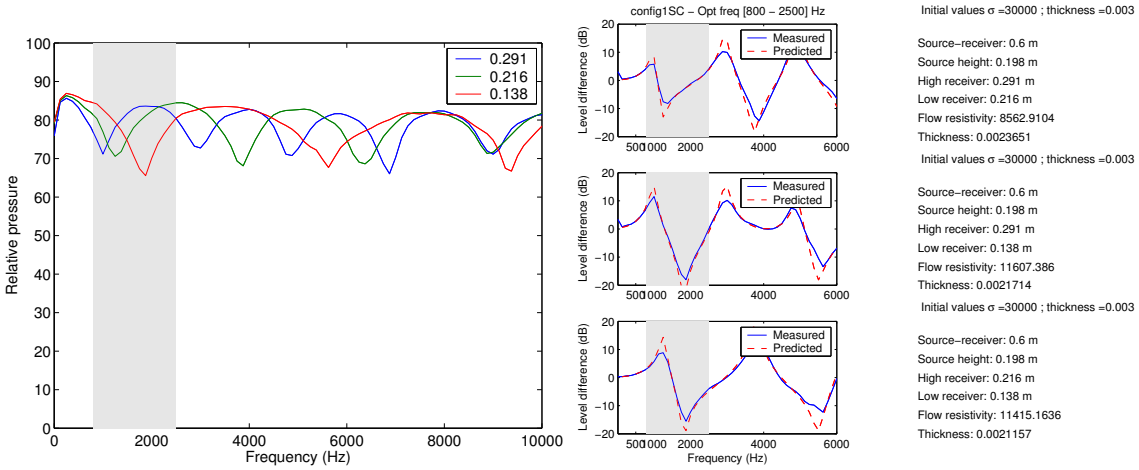

(a) Measurement data (b) Optimisation results

Figure 13.5: *Results of optimisation upon level difference measurements. Surface is fitted–carpet – Signal is spectrum computed from averaged time signal.*

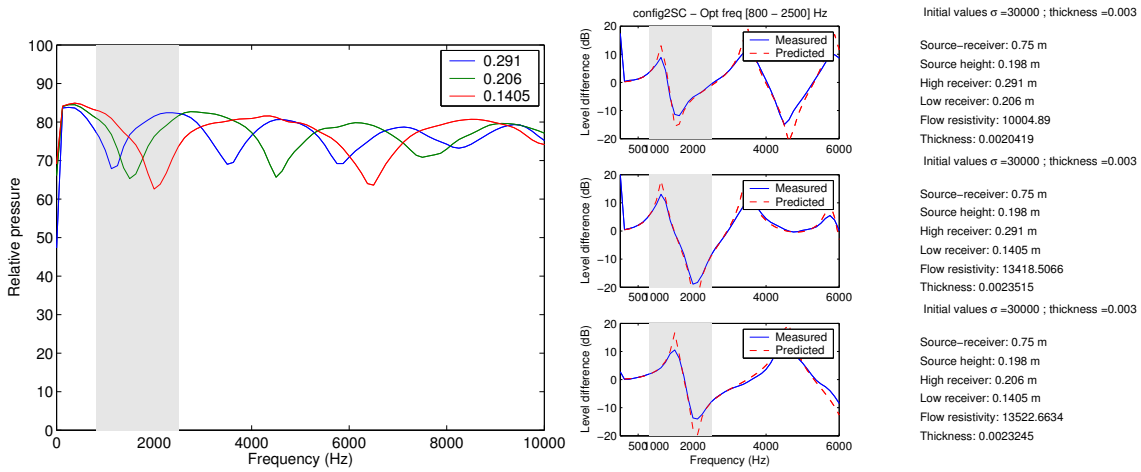

(a) Measurement data (b) Optimisation results

Figure 13.6: *Results of optimisation upon level difference measurements. Surface is fitted–carpet – Signal is spectrum computed from averaged time signal.*

13.2 Mineral rockwool

Results are shown for a recorded signal corresponding to an averaged spectrum (SU signals) Fig. 13.7.

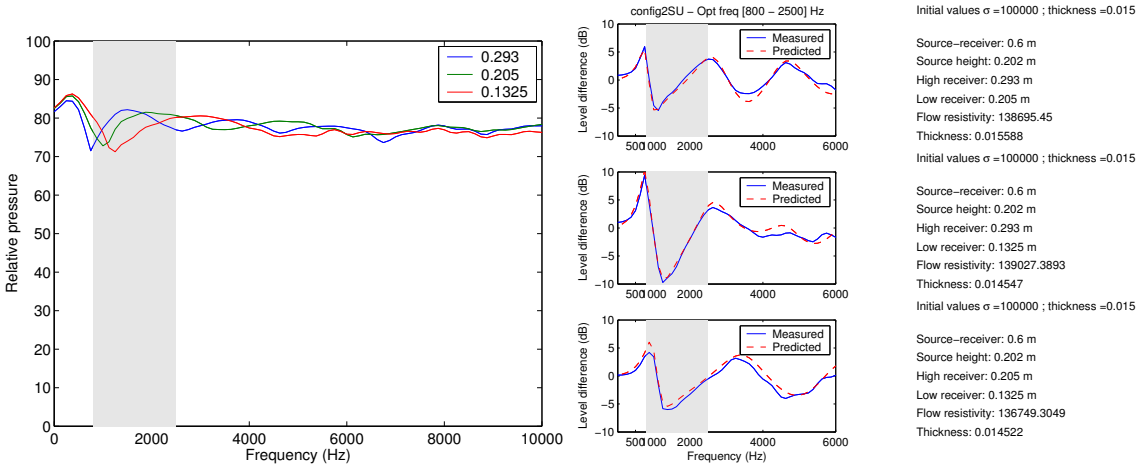

(a) Measurement data (b) Optimisation results

Figure 13.7: *Results of optimisation upon level difference measurements. Surface is mineral rockwool – Signal is averaged spectrum.*

Results of optimisation upon averaged time signals (AV signals) are shown in Fig. 13.8.

Results of optimisation upon spectra calculated from averaged time signals (SC signals) are shown in Fig. 13.9.

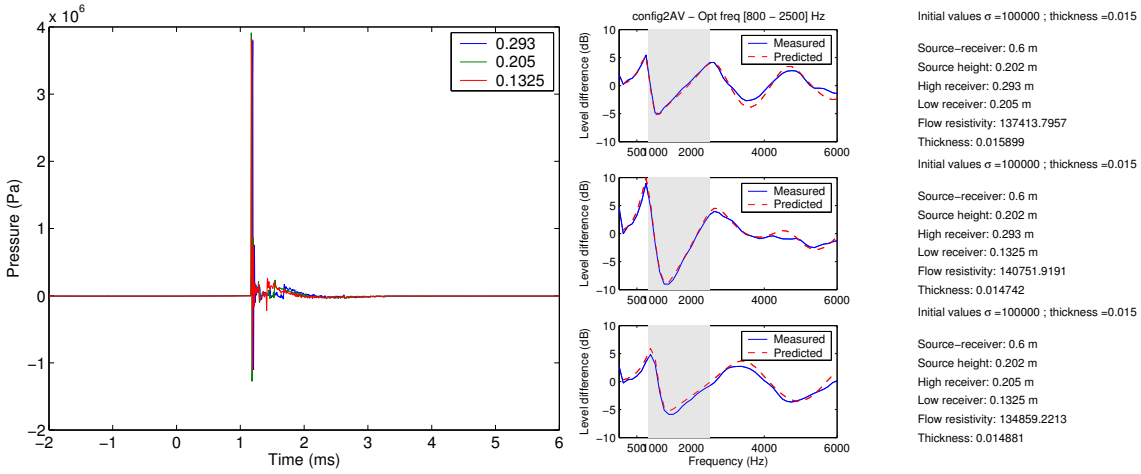

(a) Measurement data (b) Optimisation results

Figure 13.8: *Results of optimisation upon level difference measurements. Surface is mineral rockwool – Signal is averaged time signal.*

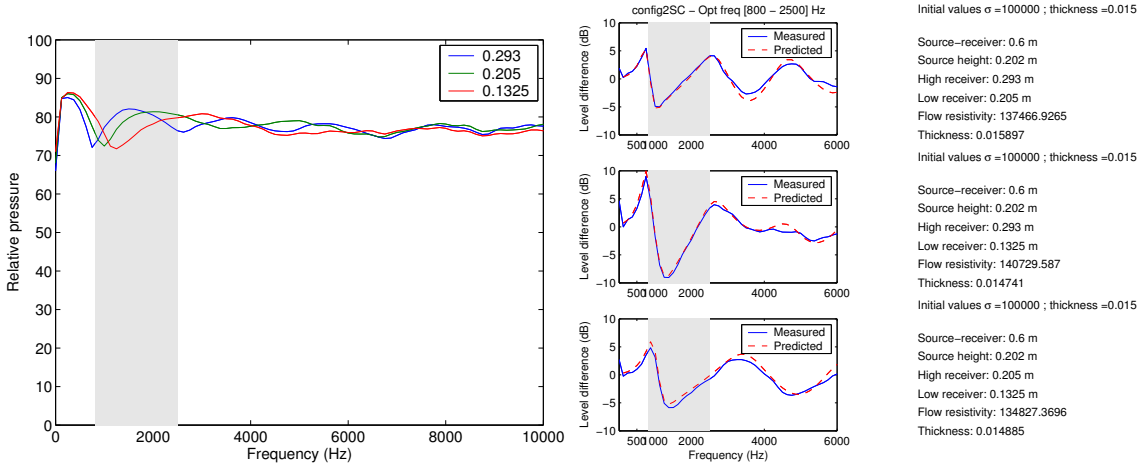

(a) Measurement data (b) Optimisation results

Figure 13.9: *Results of optimisation upon level difference measurements. Surface is mineral rockwool – Signal is spectrum computed from averaged time signal.*

14 – Acoustic impulse source

This appendix describes the noise source used in the level difference measurements and for horn effect measurements. This source, an omnidirectional, impulse point source, was designed and perfected in the INRETS laboratory by the technical staff.

14.1 Principle

The setup is based on works presented by Schaaf[1]. A shock wave is created inside a tube by the sudden opening an electronically–driven valve, which release a volume of compressed air. The end of the tube is open on air, so that the wave impedance drops suddenly when the shock wave reaches the end of the tube. If the tube section is circular, the sound is radiated in the same manner in all directions of space (in front of the tube).

The acoustic impulse created in this way should be higly reproducible. This is achieved by keeping a constant valve opening time and a constant upstream pressure, that is before the valve.

14.2 Theoretical background

According to Liepmann and Roshko[2], for a fixed observer, the speed of sound in a fluid moving at u is

$$c(P) = c_0 \pm u$$

where c_0 is the sound speed measured if the the observed would move with the fluid. The '-' sign, respectively the '+', corresponds to a propagation opposite to the fluid motion.

Assuming the process is isentropic and that the processes are linear so that the acoustic laws apply, we have

$$\frac{\rho}{\rho_0} = \left(\frac{P}{P_0}\right)^{1/\gamma}$$

and thus, the speed of the moving fluid is expressed as a function of its density ρ as

$$u = \pm\frac{2c_0}{\gamma - 1}\left[\left(\frac{\rho}{\rho_0}\right)^{(\gamma-1)/2} - 1\right]$$

[1]Schaaf. *Messung der Schallabstrahlung von Lärmquellen am Kraftfahrzeugreifen mit Hilfe einer Impulsschallquelle. Diplomarbeit 1981, Drittes Physikalishes Institut, Göttingen.*

[2]H.W. Liepmann A. Roshko. *Elements of gasdynamics*. John Willey & sons, New York, 1967 - p. 76.

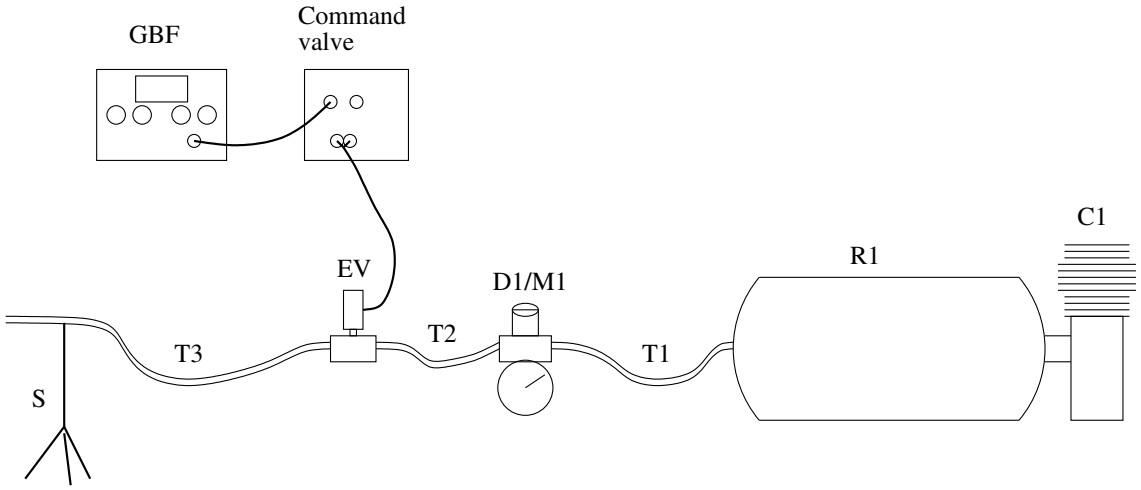

Figure 14.1: *General setup for the acoustic impulse source.*

where γ=1.4 for perfect gases. Hence, the sound speed for a fixed observer becomes

$$c(P) = c_0 \left\{ 1 + \frac{\gamma+1}{\gamma-1} \left[\left(\frac{P}{P_0} \right)^{(\gamma-1)/(2\gamma)} - 1 \right] \right\}$$

The rising of the pressure inside the tube takes a certain amount of time, which depends on the time necessary for the valve to open completely, say ΔT_v. During this time, the wave front has traveled a distance equal to $c_0 \Delta T_v$.

Finally, inside the tube, the first wave front travels at the speed c_0, followed by a second wave front travelling with the speed $c(p)$ larger than c_0. The shock wave is created when the second wave front reaches the first one. This further implies that the tube is long enough so that the shock wave is formed before the end of the tube. Hence, the shock wave is formed at a time ΔT_{shock} :

$$\Delta T_{shock}(P) = \frac{c_0 \Delta T_v}{c(P) - c_0} = \frac{\Delta T_v}{\frac{c(P)}{c_0} - 1}$$

or

$$\Delta T_{shock}(P) = \Delta T_v \frac{\gamma-1}{\gamma+1} \left[\frac{1}{\left(\frac{P}{P_0} \right)^{\frac{\gamma-1}{2\gamma}} - 1} \right]$$

ΔT_{shock} depends clearly on the pressure level released by the opening of the tube.

14.3 Experimental setup

The general setup for the acoustical source is shown in Fig. 14.1. A compressor (C1) supplies a tank (R1) with air at a pressure of approximately 4 bars. A regulator (D1/M1) is installed which allowed to maintain the pressure level around 2.4 bars at the entry of the electronic valve (EV).

Finally, the opening of the valve is controlled by an external trigger provided by a signal generator (GBF).

The valve has been chosen for its short time response of its opening, which is about $\Delta T_v = 4$ ms. The knowledge of the upstream pressure value gives an estimation of the necessary tube length :

$$L(P) = \Delta T_s \; c(P)$$

Some examples are given in the table below.

$P(bar)$	1.5	2	3	4	5	6
ΔT_{choc} (ms)	3.5	2.0	1.2	0.9	0.8	0.7
L (meter)	2.3	2.7	3.4	4.0	4.4	4.7

Table 14.1: Examples of necessary tube lengths according to the upstream pressure.

For the experiments, the upstream pressure is set to around 2.4 bars. For this value, ΔT_s is 5 ms. This imposes a necessary tube length of at least 3.08 m. Practically, a flexible hose of 4.5 m length is chosen for T3 (see Fig. 14.1).

To be able to record average signals, several successive acoustic impulses are needed. The impulses must be spaced enough so that the valve can open and close completely. For this, the valve is driven by a 20 Hz square signal which gives a 5 seconds period (the valve can handle a maximum of 30 cycles per second). This is large enough to consider that the system is ready again : the valve is totally closed and the upstream pressure has rised to the desired value.

A final but important point concerns the orientation of the source. Due to an important blow of air in front of the tube opening, it was chosen to direct the axis of the tube perpendicularly to the direct path to the microphone. Therefore, the sound field of interest is that contained in the plan which is perpendicular to the tube axis. The sound field in this plan is expected to be omnidirectional. The measurements shown below proove the validity of this hypothesis.

14.4 Examples of acoustic impulses

An example of the acoustic impulse is shown in Fig. 14.2. For this, a microphone is placed at 0.5 m distance from the opening of the tube, ahead of it. The duration of the impulse (including the negative feedback) is around 50 μs. It should be underlined here that the signal is highly reproducible, assuring a good correlation between the averaged signals.

The maximum recorded level reaches around 55 Pa on Fig. 14.2(a). When a lower sampling frequency is used Fig. 14.2(b), the maximum signal is truncated and reaches around 21 Pa. At the same time, using a lower sampling frequency increase the length of the recorded signal. By doing so, unwanted reflexions on the laboratory walls may be recorded. This may be overcome by applying a force window on the recorded time signal (see Fig. 14.2).

The resulting energy spectrum is shown in Fig. 14.3 for 8 ms force window[3]. It shows a fairly spectrum up to 10 kHz. On this frequency range, the level decrease do not exceed 5 decibels, which is satisfactory.

[3]The window starts at the same time of the pre–trigger of the analyser. With a 6 ms pre–trigger, 2 ms of "useful" signal.

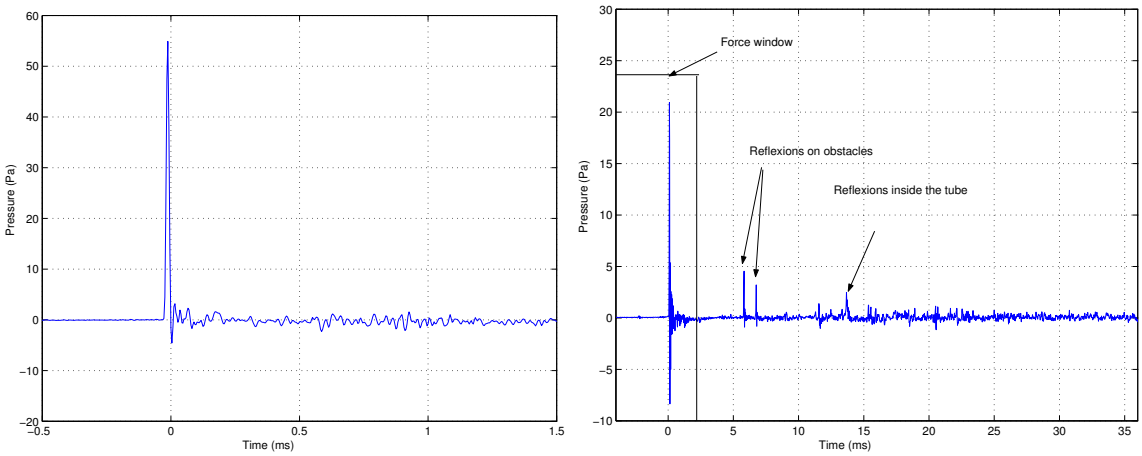

(a) Example of time signal : duration 8 ms sampled at 256 kHz.

(b) Example of time signal : duration 40 ms sampled at 51.2 kHz.

Figure 14.2: *Examples of two time signals with different sampling frequencies.*

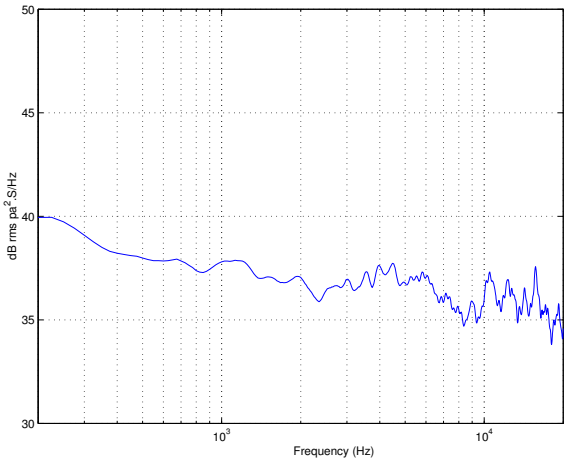

Figure 14.3: *Energy spectrum of the 40 ms signal Fig. 14.2 : force window of length 8 ms.*

Moreover, the directivity of the source was tested by measuring the transfer functions between two microphones, for different azimutal positions with respect to the axis of the source. The magnitudes of the measured data are shown in Fig. 14.4. The transfer function measured for a microphone at 22.5° with respect to 0°, the spectrum deviations do not exceed 1 decibel from 100 Hz to 10 kHz. For a measurement position at 67.5° and a reference microphone at 22.5°, the spectrum is not as flat as in the previous case. However, the deviations do not exceed 1 decibel up from 100 Hz up to 3 kHz, which gives a satisfactory frequency range of validity.

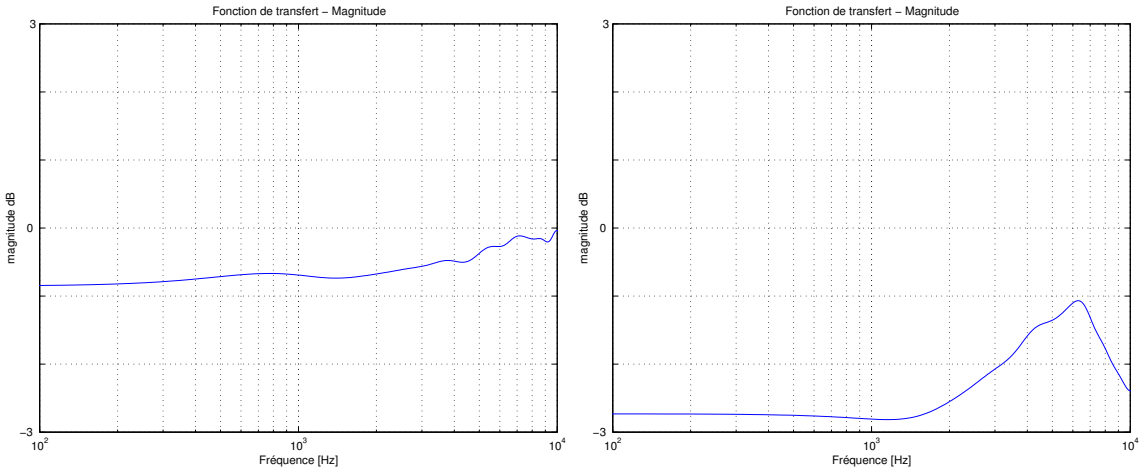

(a) Microphone at 22.5°, reference microphone at 0°.

(b) Microphone at 67.5°, reference microphone at 22.5°.

Figure 14.4: *Measured directivity of the source : magnitude of the transfer functions.*

It is usually agreed[4], that if the power of the source does not exceed 1 decibel for angles from -30° to +30°, the source can be considered as omnidirectional. Therefore, the present source can be said to be omnidirectional in the frequency range from 100 Hz to around 2000 Hz.

[4]M. Ögren H. Jonasson, *Measurement of the acoustic impedance of the ground*, SP, Swedish national testing and research institute, Technical report 1998:28

List of Figures